JOURNAL OF PETROLOGY

Journal of Petrology, 2015, Vol. 56, No. 1, 113–159
doi: 10.1093/petrology/egu073
Original Article

OXFORD

Concentration of Particulate Platinum-Group Minerals during Magma Emplacement; a Case Study from the Merensky Reef, Bushveld Complex

David Hutchinson[1]*, Jeffrey Foster[2], Hazel Prichard[3] and Sarah Gilbert[1]

[1]Codes, Arc Centre of Excellence in Ore Deposits, University of Tasmania, Private Bag 126, Hobart, TAS 7001, Australia, [2]Sirius Resources, PO Box 1011, Balcatta, WA 6914, Australia and [3]School of Earth and Ocean Sciences, University of Cardiff, Main College, Cardiff CF10 3AT, UK

*Corresponding author. mineralforensicservices@gmail.com

Received March 25, 2013; Accepted December 3, 2014

ABSTRACT

The petrology, mineralogy and geochemistry of a section of the Merensky Reef at Bafokeng Rasimone Platinum Mine (BRPM) are described. A model for the formation of platinum-group minerals (PGM), sulphide and chromitite is proposed that explains the stratigraphic relationships observed in the Merensky Reef, both at BRPM and at other locations in the Bushveld Complex. To achieve this it is necessary to understand platinum-group element (PGE) behaviour in naturally occurring mafic systems and for this reason comparisons are drawn from core TN207 through the Platreef at Tweefontein. The common link between the Platreef and Merensky Reef is the presence of unusually high concentrations of As, Sb, Bi and Te that promote the crystallisation of semi-metal bearing PGM from sulphide liquids. Under conditions of increasing semi-metal contamination, Pt is the first PGE to be extracted from a sulphide liquid followed by Rh, Ru, Os and Ir. While some Pd is released to form Pd-PGM much of it remains within the Ni-rich sulphide phase that crystallizes to form pentlandite. A critical aspect is the timing of their introduction into the magmatic system. For the Merensky magmas, contamination occurred predominantly within a staging chamber owing to wall-rock interaction with Transvaal sediments. This led to the formation of sulphide liquids that captured PGE and, ultimately, the crystallization of Pt- and Ru-PGM. The extreme enrichment in PGE and the high Pt/Pd ratios in the Merensky chromitites are attributed to density-driven concentration of PGM transported by magmas displaced from a staging chamber. Emplacement of these magmas into the Bushveld Complex resulted in thermo-mechanical erosion of the floor and deposition of chromites + sulphides + PGM. In places, these assemblages collected in sedimentary-like scour channels. In the Platreef, contamination occurred largely after magma emplacement owing to interaction with the local Transvaal sediments. As a result, mechanical separation of PGM did not occur and most PGM remain spatially associated with their original sulphide hosts.The Merensky Reef is a prime example of highly efficient PGE concentration resulting from mechanical processes, whereas the Platreef is a prime example of highly efficient PGE removal from sulphide liquids in response to extreme contamination by semi-metals.

Key words: Merensky Reef; Platreef; staging chamber; thermo–mechanical erosion; PGM; chromitite; LA–ICP–MS mapping

INTRODUCTION

Since its discovery the Bushveld Complex in South Africa has attracted unprecedented interest owing to its ranking as the world's largest layered intrusion, hosting the world's largest resources of platinum-group elements (PGE) and Cr (Vermaak, 1995; Cawthorn, 1999*a*; Naldrett, 2004). New ideas are still being generated to answer even the most fundamental questions about the origin of this intrusive complex and its mineralized layers, and fierce debates continue over the validity of existing models.

Three broad categories of model have been proposed to explain the origins of PGE mineralization: (1) collection by sulphide liquids (e.g. Campbell *et al.*, 1983; Naldrett, 1989); (2) direct crystallization from a silicate magma (e.g. Tredoux *et al.*, 1995; Cawthorn, 1999*c*; Ballhaus & Sylvester, 2000); (3) concentration by hydrothermal–hydromagmatic fluids (e.g. Lauder, 1970; Boudreau *et al.*, 1986; Nicholson & Mathez, 1991; Mathez, 1995; Boudreau & Meurer, 1999; Willmore *et al.*, 2000; Boudreau, 2008). However, mechanisms that explain the PGE mineralization need to be placed into context, as models need to account for a range of coexisting features over scales from microns to kilometres. Our approach was to study in detail a sample of the Merensky Reef from Bafokeng Rasimone Platinum Mine (BRPM) together with Platreef samples from drillhole TN207 from Tweefontein. These were used to test existing models and develop a new one that can be extrapolated across the Merensky Reef using observations documented in literature.

Geology of the Bushveld Complex

The 2·06 Ga magmatic event recorded in southern Africa led to the formation of several layered intrusions, the largest and most well-known of which is the Bushveld Complex (Von Gruenewaldt, 1977; Walraven *et al.*, 1990; Scoates & Friedman, 2008; Coggon *et al.*, 2012). Spatially and temporally associated intrusions include the Molopa Farms Complex, which lies 150 km west of the Bushveld (Coetzee & Kruger, 1989; Reichhardt, 1994; Cawthorn & Walraven, 1998), and the Uitkomst Complex, which hosts the Nkomati deposit, located *c.* 50 km to the east of the South Eastern Bethal Limb (De Waal *et al.*, 2001; Li *et al.*, 2002; Maier *et al.*, 2004; Eales & Costin, 2012; Fig. 1). Magmatism in the Bushveld was centred along a major 500 km ENE–WSW-trending crustal lineament, which marks a major crustal suture zone located at the northern margin of the Kaapvaal Craton [Thabazimbi–Murchison Lineament (TML); Reichhardt, 1994; Cawthorn & Walraven, 1998]. This was active prior to, syn- and post-emplacement of the Bushveld (McCourt & Vearncombe, 1987; Kruger, 2005b; Good & de Wit, 1997). Present-day volumes for the Eastern and Western limbs of the Bushveld Complex are estimated at between 370 000 and 600 000 km^3, although this is likely to be a gross underestimate, owing in part to erosion and in part to the volume of magma required to crystallize the combined amount of chromitite (Cawthorn & Walraven, 1998). Revised estimates place the original volume of magma at 740 000 to $1{\cdot}2 \times 10^6$ km^3, which, at the time of emplacement, covered at least 62 000 km^2 and possibly as much as 100 000 km^2 (Cawthorn & Walraven, 1998). This magma was emplaced as laterally extensive, but vertically restricted, sill-like bodies into upper crust largely composed of Transvaal sediments and basement granite gneiss (e.g. Pitra & de Waal, 2001). This may have occurred in less than 75 000 years (Cawthorn & Walraven, 1998). Notably absent from the Bushveld Complex are the extrusive equivalents of the mafic magmas; this characteristic, combined with the scale of the magmatism, has led some researchers to propose that the Bushveld may be a failed flood basalt province (Daly & Molengraaff, 1924; Hatton, 1995; Cawthorn & Walraven, 1998).

The Bushveld Complex comprises five distinct sub-regions referred to as lobes or limbs (Fig. 1). Early attempts to establish the stratigraphy of the Bushveld Complex by Hall (1932) have been revised many times (e.g. Willemse, 1964; Kruger & Marsh, 1982; Cawthorn, 2013). The mafic and ultramafic portions of the Complex (the Rustenburg Layered Suite; RLS) have been subdivided into five discrete packages, which from bottom to top are: (1) 'Marginal Zone' comprising pre- and syn-emplacement sills and dykes; (2) 'Lower Zone' of ultramafic cumulates; (3) 'Critical Zone' (Lower and Upper) predominantly of layered pyroxenites and anorthosites, which also contains most of the Ni–Cu–PGE and chromite mineralization; (4) 'Main Zone' comprising a thick package of unlayered mafic units (norites, gabbronorites); (5) 'Upper Zone' of more evolved rocks, which include ferrogabbros, ferrodiorites and diorites famed for their magnetite layers (e.g. Von Gruenewaldt, 1973; Molyneux, 1974). Most stratigraphic sections show the RLS overlain by felsic volcanic rocks of the Rooiberg Group (the Rooiberg Felsites and Rashoop Granophyres), followed by a thick succession of late-stage granites (Lebowa Granite Suite; Fig. 1). However, a recent study by Cawthorn (2013) has challenged the perception that the Rooiberg Group formed after the Upper Zone, and it now seems likely that this reflects a phase of felsic volcanism that pre-dates the emplacement of the RLS.

Economic elements include precious and base metals (PGE, Cr, Ni and Cu) with Fe, Ti, V, Co, Mn and Sn also present in significant quantities (e.g. Willemse, 1969; Cawthorn, 1999*a*; Naldrett, 2004; Naldrett *et al.*, 2009). The discovery of platiniferous pipe-like bodies in 1924 led to the assumption that these were the source of the platinum group minerals (PGM) found in stream sediments. Subsequent field investigations by Dr Hans Merensky, prompted by the discovery of PGM in stream sediments on a property owned by Andries Lombaard, ultimately led to the discovery of what became known as the 'Merensky Reef' (Wager, 1923, 1925, 1929; Cawthorn, 2006).

Other significant PGE-producing 'reef' systems within the Bushveld Complex include the UG-2 chromitite layer and the Platreef. Stratigraphically, UG-2 occurs

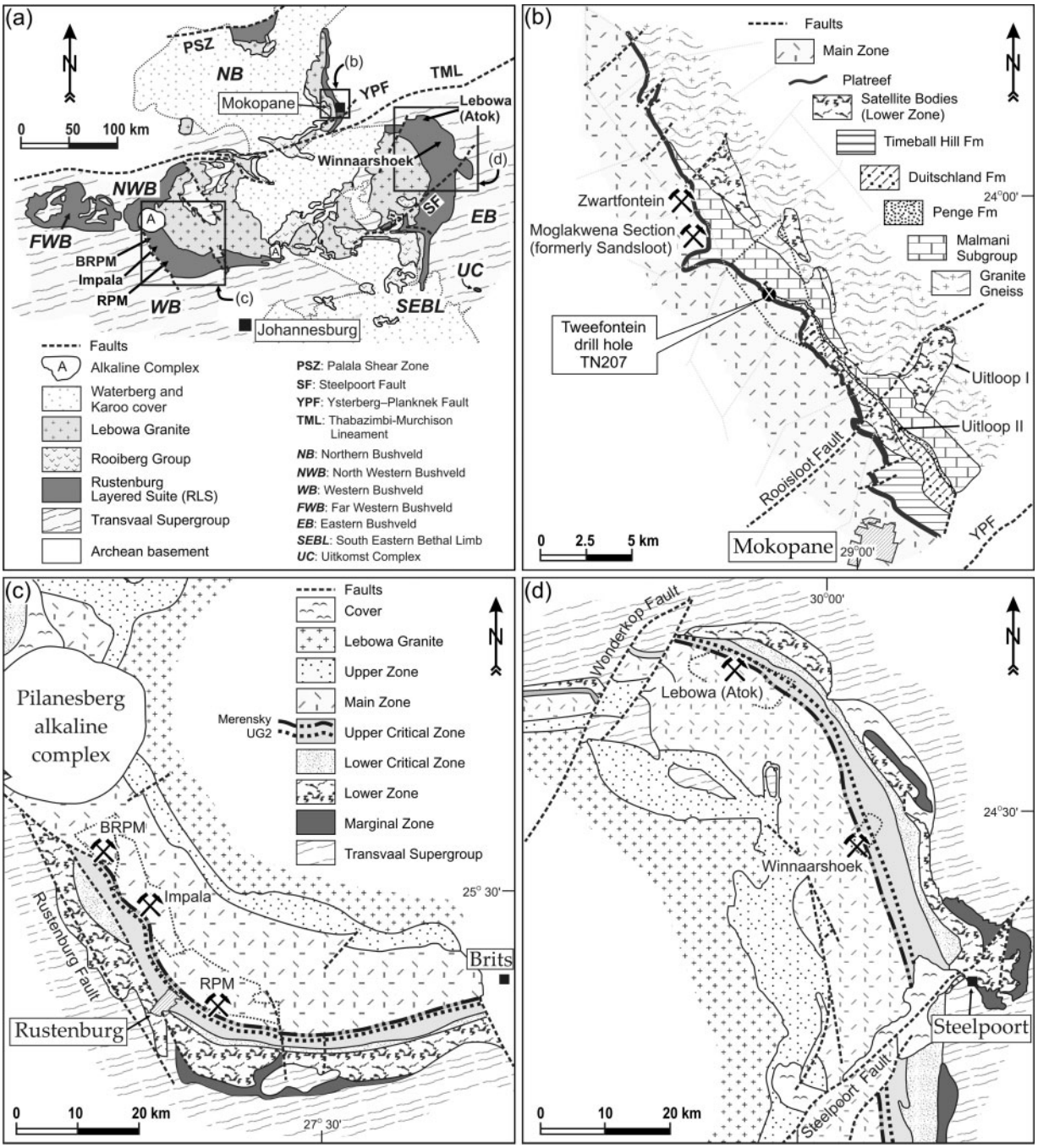

Fig. 1. Geology of the Bushveld Complex, modified after Van der Merwe (1976, 2008), Von Gruenewaldt *et al.* (1986), Ashwal *et al.* (2005), Kruger (2005b) and Cawthorn & Luvhimbe (2009). (a) Regional-scale map of the main recognized sub-regions. (b) Central portion of the Northern Bushveld showing the Platreef and location of drill-hole TN207 on Tweefontein. (c, d) Expanded portions of the Western and Eastern Bushveld showing the locations of the mines discussed in the text. Mines shown: Bafokeng Rasimone Platinum Mine (BRPM), Impala, Lebowa (Atok), Winnaarshoek and Rustenburg Platinum Mines (RPM), which includes Khuseleka 1 Shaft (formerly Townlands Shaft) and Siphumelele 2 Shaft (formerly Brakspruit Shaft).

below the Merensky Reef in the Eastern and Western limbs of the complex (Fig. 2), whereas the Platreef forms part of the Northern Limb succession of the Bushveld (Fig. 3). PGE grades and reserves in UG-2 are similar to those of the Merensky Reef, which as a combined resource are estimated to host 75% and 50% of the worlds of Pt and Pd, respectively, and almost all the world's Ru (Cawthorn, 1999*a*; Naldrett, 2004).

Geology of BRPM and Tweefontein

A comprehensive overview of the geology of the Merensky Reef at BRPM has been given by Moodley (2008). The stratigraphy of the Western Bushveld, together with a generalized stratigraphy from BRPM, is shown in Fig. 2.

Tweefontein is situated in the central portion of the Northern Limb (Fig. 1b). The Platreef occurs as a

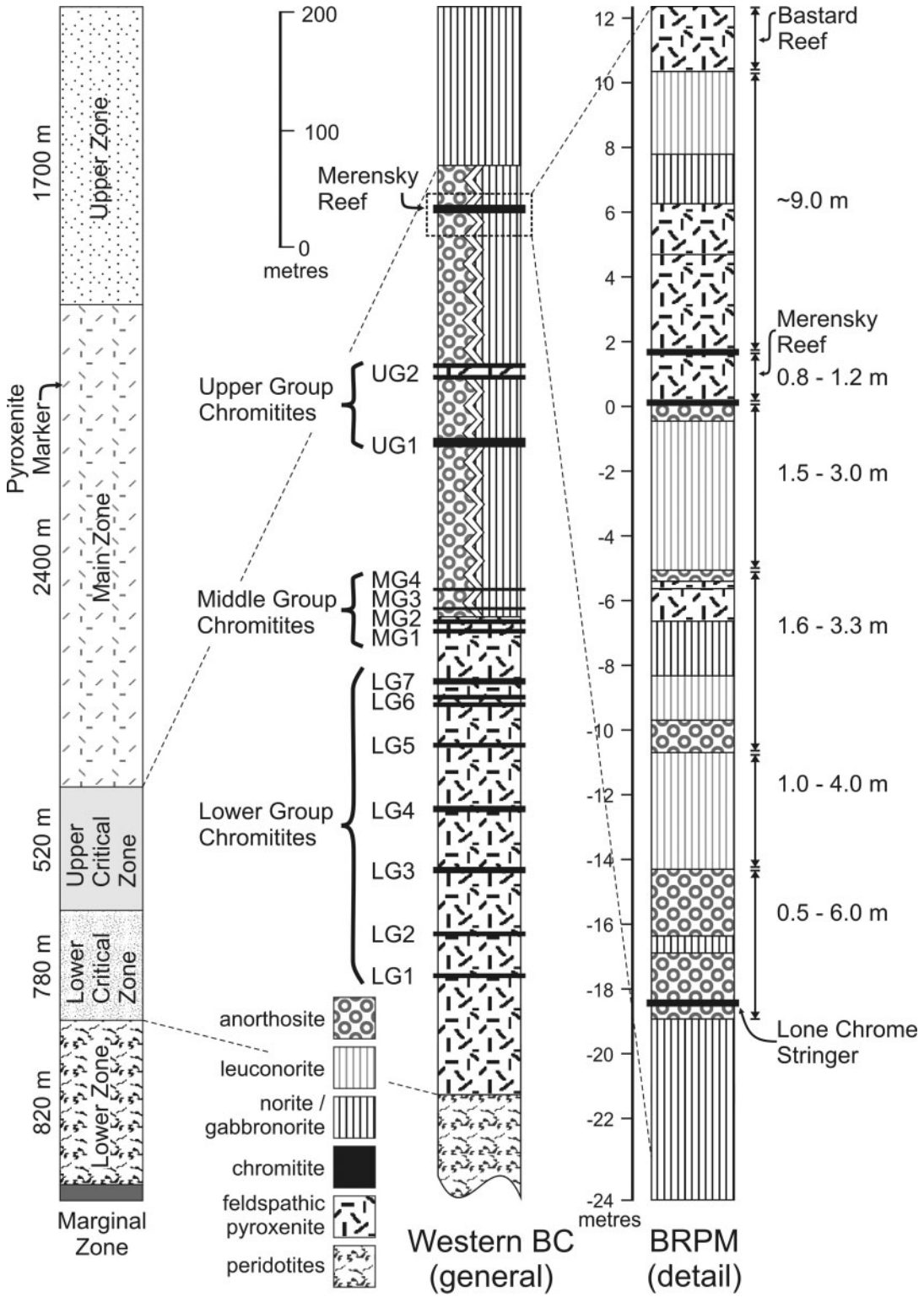

Fig. 2. Stratigraphy of the Western Bushveld together with a detailed log of the Merensky Reef at BRPM. Modified after Von Gruenewaldt *et al.* (1986), Cawthorn & Lee (1998) and Moodley (2008). BC, Bushveld Complex.

dominantly pyroxenitic package from the intrusion floor to the contact with the Main Zone and has been correlated with the Critical Zone of the Eastern and Western Bushveld (Gain & Mostert, 1982; Lee, 1996; Fig. 3). The presence of economic base-metal sulphides and PGE mineralization, together with its stratigraphic position below the Main Zone, has led to speculation that the Platreef is the Northern Limb equivalent of the Merensky Reef (Kruger, 2005*a*, 2005*b*, 2010). Nevertheless, in many areas it is significantly thicker, including at Tweefontein in drill-hole TN207 where the reef is 118 m thick compared with 1–10 m typical of the Merensky Reef;

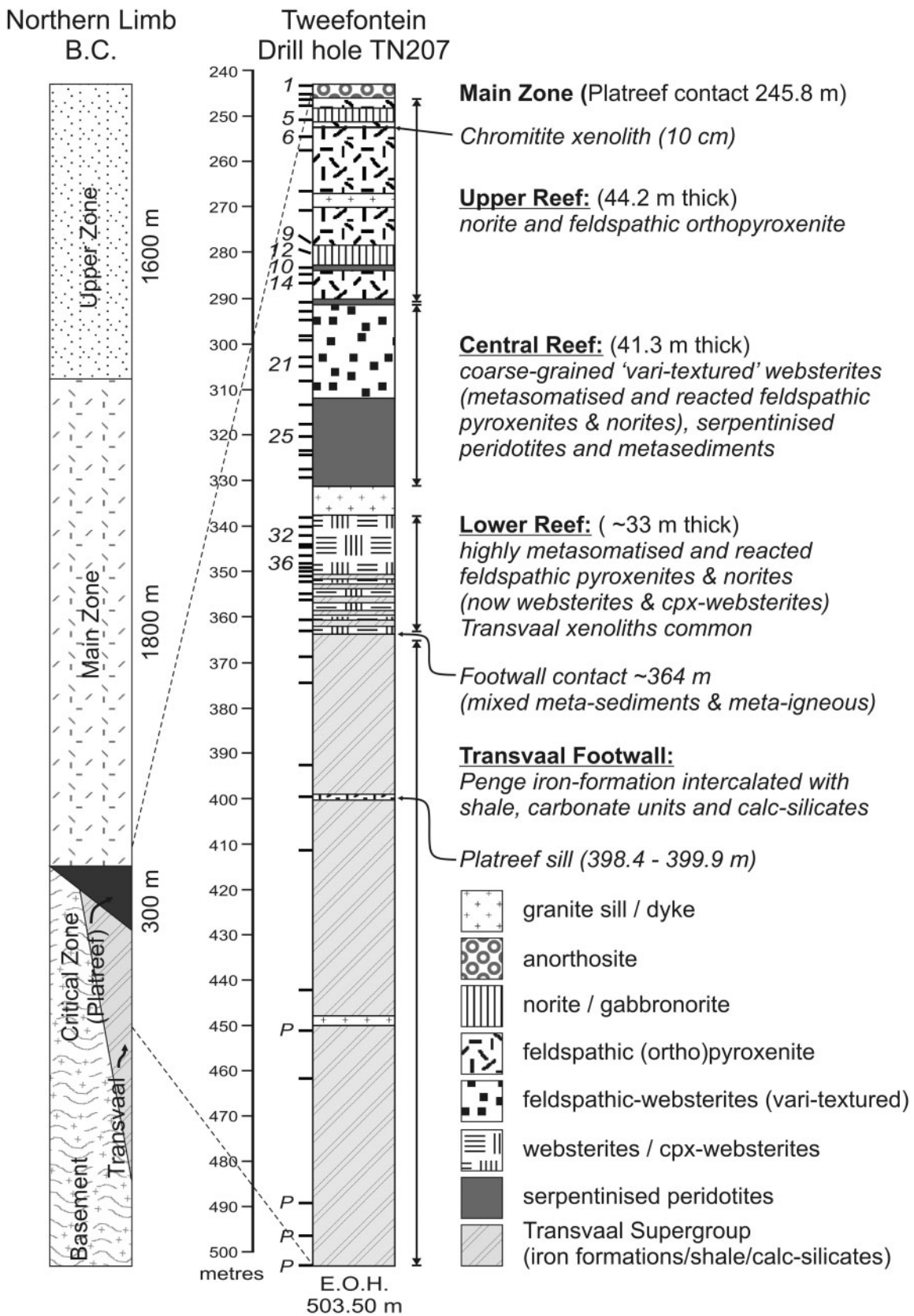

Fig. 3. Detailed section log of drill-hole TN207 from Tweefontein Hill, Platreef, Northern Bushveld. Numbered tick marks show the position of the samples discussed in the text. Unnumbered tick marks show the position of the full sample set. All samples include whole-rock data and petrographic sections unless indicated by '*P*', which denotes petrographic-only. Bushveld stratigraphy modified after Cawthorn & Lee (1998).

additionally, the Platreef does not contain persistent chromitite horizons (e.g. Gain & Mostert, 1982). Another important difference is that the Platreef magmas interacted with a reactive sedimentary footwall that resulted in substantial post-intrusion contamination and modification of the sulphide and PGM assemblages (Buchanan *et al.*, 1981; Gain & Mostert, 1982; Kinloch, 1982; Cawthorn *et al.*, 1985; Kinloch & Peyerl, 1990; Hutchinson & Kinnaird, 2005; Holwell & McDonald, 2006, 2007; Holwell *et al.*, 2006; Hutchinson & McDonald, 2008). A detailed review of the geological setting of Tweefontein Hill has been given by Nex (2005).

Samples studied

For Merensky Reef from BRPM, a hand specimen was sectioned into seven jigsaw-fit oriented blocks and two polished thin-sections that cover the lower portion of the reef from the footwall anorthosite to the lowermost portion of the Merensky melanorite. For the bulk-rock geochemical investigations, material was carefully extracted using a thin-bladed rock saw from each of the recognizable layers and then powdered in an agate mill.

For Platreef drill-core TN207, detailed core logging together with a sampling program was conducted along the entire length of the drill-hole. A total of 51 samples were collected that cover the upper 140 m of footwall stratigraphy (Transvaal sediments) through the Platreef and into the base of the Main Zone (Fig. 3). Careful examination of the geochemistry, mineralogy and petrology, together with observations from the core logs, led to the recognition of several discrete packages. From these, a subset of 11 representative samples from each of these packages were chosen for the detailed investigations presented here.

ANALYTICAL METHODS

A wide range of analytical techniques and configurations were used in the collection of the data presented. These include: (1) laser ablation inductively coupled plasma mass spectrometry (LA-ICP-MS) in spot and mapping modes to obtain *in situ* element concentrations and observe the distribution of key elements in the sulphides; (2) X-ray computed tomography (X-ray CT) on two samples of Merensky chromitite; (3) whole-rock geochemistry; (4) microprobe analyses of the main silicate minerals and chromite; (5) scanning electron microscopy (SEM) to document the textures and associations of the PGM, sulphide, chromite, silicate and trace minerals present in the samples. Full descriptions of the analytical techniques can be found in Supplementary Data Electronic Appendix 1 (supplementary data are available for downloading at http://www.petrology.oxfordjournals.org). The LA-ICP-MS work, together with the trace element geochemistry (by solution with an ICP finish), was conducted at CODES, University of Tasmania; the SEM and microprobe data were obtained at the Central Sciences Laboratory (CSL) at the University of Tasmania; the X-ray CT work was done at CSIRO, co-ordinated by Steve Barnes and Belinda Godel. The whole-rock data for the Merensky samples were obtained from the GEO labs in Canada, whereas the Platreef samples were analysed at ACME labs in Canada as they form part of a broader research project funded by Anglo American.

PETROGRAPHIC OBSERVATIONS: MERENSKY SAMPLE

The sample of Merensky Reef from BRPM can be subdivided into five distinct layers (Fig. 4b). From base to top these are: (1) footwall comprising mottled anorthosite (Mer-Ano); (2) lower chromitite (Mer-ChL); (3) upper chromitite (Mer-ChU); (4) coarse-grained to pegmatitic melanorite (Mer-Peg); (5) medium-grained melanorite (Mer-Nor) that forms the majority of the Merensky succession at BRPM.

Layer 1: mottled anorthosite

At outcrop scale the anorthosite contains dark-coloured bands defined by pyroxene oikocrysts, which are cut by, and terminate against, the base of the Merensky chromitites (Fig. 5). Single pyroxene oikocrysts also appear to be truncated by the chromitite, as similarly observed in a sample from Impala (Fig. 4).

The anorthosite is a moderately seriate-textured plagioclase adcumulate to mesocumulate that contains *c.* 5% intergranular cpx and opx (i.e. an ophimottled texture). The contact against the overlying chromitite is sharp with little evidence for crystal realignment of the plagioclase (Fig. 4a). Although the general degree of alteration is extremely low some of the larger orthopyroxene oikocrysts show alteration to serpentine and amphibole. Accessory minerals include small intergranular patches of quartz, titanite (up to 200 μm), apatite sometimes associated with titanite, zircon containing U, Th and Pb (up to 7·5 μm), oxides (magnetite, rutile and laths of ilmenite), and sulphides. The sulphides are commonly associated with the interstitial pyroxene and occur as small, highly disseminated, granular to intergranular, monomineralic or composite, chalcopyrite, pentlandite and pyrrhotite, together with occasional galena and sphalerite. PGM occur as extremely small (0·5–2 μm) grains dominated by Pd-phases (91%) that are typically hosted within silicate but are spatially associated with sulphides (Table 1). The Pd-minerals include naldretteite (Pd_2Sb), stibiopalladinite (Pd_5Sb_2), sobolevskite (PdBi) and an unnamed phase [IMA2004-020, $Pd_4(SbTeAsBi)_3$], whereas the Pt-minerals are sperrylite (Fig. 6; Table 1).

Layers 2 and 3: Merensky chromitites

The basal chromitite at BRPM comprises two distinct layers: (1) lower chromitite comprising 0·5–2·0 mm, subhedral to highly irregular grains; (2) upper chromitite composed of finer grained, closely packed, 0·2–0·4 mm, equant chromites with occasional larger (0·5–2·0 mm) single grains and clusters (Fig. 7). The chromites in both

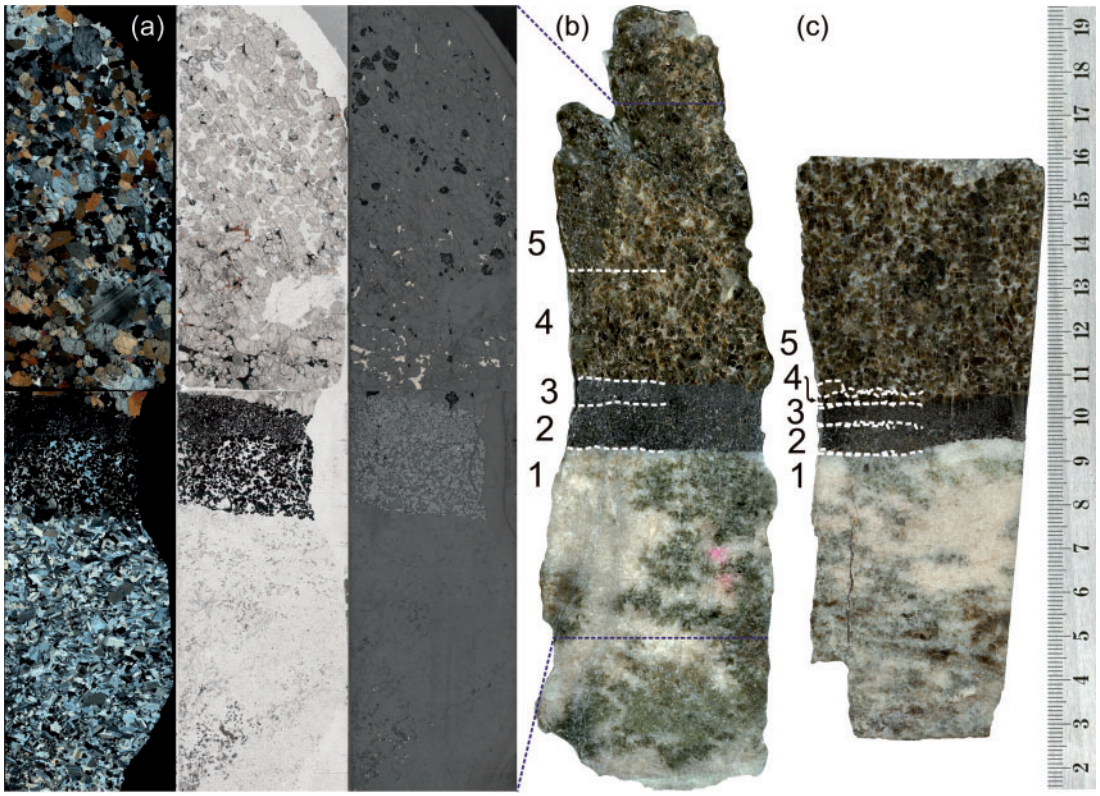

Fig. 4. Sample of Merensky Reef from BRPM together with a comparison sample from Impala. (a) Thin-section views through BRPM sample (cross-polarized, plane-polarized and reflected light, from left to right respectively). (b) BRPM sample with the five main stratigraphic units. (c) Impala sample with the same identifiable layers as the sample from BRPM. 1, mottled anorthosite (Mer-Ano); 2, lower chromitite (Mer-ChL); 3, upper chromitite (Mer-ChU); 4, pegmatite (Mer-Peg); 5, melanorite (Mer-Nor).

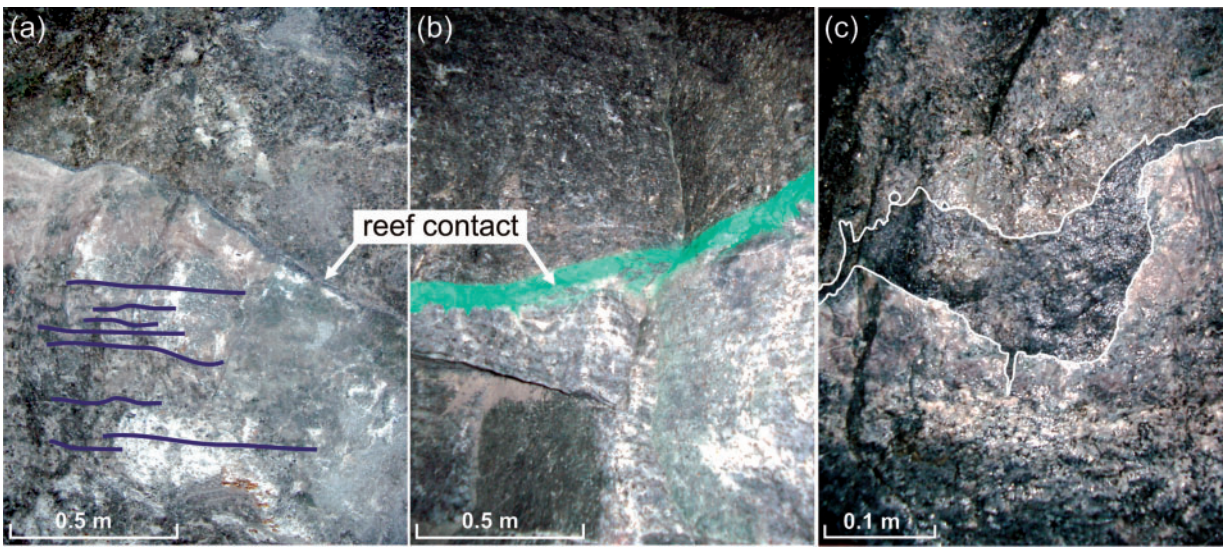

Fig. 5. Underground exposure at BRPM showing the contact relationships of the Merensky Reef against the anorthosite footwall. (a) 'Contact reef' type within an erosional angular unconformity relationship between the basal Merensky chromitite and underlying anorthosite (blue lines depict layering within the anorthosite). (b) Termination of anorthosite layering against the chromitite (highlighted in green). (c) Erosional 'scour' within the footwall anorthosite filled with chromite. It should be noted that a second chromitite stringer lies above the field of view in the silicates that would define this as a 'thick reef' (Naldrett *et al.*, 2009).

layers are enclosed by large oikocrysts of plagioclase and orthopyroxene with optical continuities that persist across both layers. Ghost outlines of relict, euhedral, plagioclase crystals were observed within the poikilitic feldspar in the lower chromitite that are comparable in size and morphology with plagioclase in the footwall anorthosite. Sulphides in both layers account for *c.* 0·7% of the mineralogy and occur as small (<0·5 mm),

Table 1. PGM statistics for the Merensky samples

Sample	PGM no.	PGM category			PGM broad associations (%)				PGM size statistics (μm)		
		Pt minerals no. (% of total)	Pd minerals no. (% of total)	IPGE minerals no. (% of total)	Chromite (no sulphide association)	Silicate (unaltered; no sulphide or chromite assoc.)	Sulphide (incl. spatial, pre- & post-alteration association)	Total	Pt-PGM range	Pd-PGM range	IPGE–PGM range
Mer-Nor	27	25 (95·0)	2 (5·0)	–	3·7	–	96·3	100	0·5–200·0	6·0–30·0	–
Mer-Peg	37	34 (91·9)	3 (8·1)	–	2·7	–	97·3	100	1·0–35·0	2·0–4·0	–
Mer-ChU	113	94 (83·2)	4 (3·5)	15 (13·3)	9·0	6·3	84·7	100	1·0–20·0	1·0–8·0	1·0–12·0
Mer-ChL	123	106 (86·2)	4 (3·2)	13 (10·6)	6·5	1·6	91·9	100	0·5–38·0	1·0–18·0	1·0–45·0
Mer-Ano	22	2 (9·1)	20 (90·9)	–	–	–	100	100	0·8–1·0	0·5–2·0	–

Sample	PGM no.	PGM detailed associations* (%)								PGM size statistics (μm)		
		1	2	3	4	5	6	7	Total	Pt-PGM median (average)	Pd-PGM median (average)	IPGE–PGM median (average)
Mer-Nor	27	18·5	40·7	–	–	3·7	–	37·0	100	3·0 (19·9)	18·0 (18·0)	–
Mer-Peg	37	13·5	5·4	–	32·4	2·7	–	45·9	100	3·5 (5·5)	4·0 (3·3)	–
Mer-ChU	113	45·0	3·6	5·4	21·6	9·0	6·3	9·0	100	4·5 (5·9)	1·3 (2·9)	7·0 (6·2)
Mer-ChL	123	30·1	0·8	35·0	15·4	6·5	1·6	10·6	100	5·3 (8·2)	5·5 (7·5)	6·5 (10·6)
Mer-Ano	22	4·5	9·1	–	–	–	–	86·4	100	0·9 (0·9)	1·0 (1·4)	–

Sample	PGM No.	% Pt arsenides	% Pt antimonides	% Pt tellurides	% Pt bismuthides	% Pt sulphides	% Pt sulfarsenides	% Pd bismuthides	% Pd antimonides	% Pd tellurides	% IPGE sulphides	% other
Mer-Nor	27	22·2	14·8	55·6	–	–	–	3·7	–	3·7	–	–
Mer-Peg	37	24·3	24·3	24·3	–	2·7	16·2	2·7	2·7	2·7	–	–
Mer-ChU	113	22·1	7·1	1·8	0·9	42·5	13·3	–	3·5	–	8·8	–
Mer-ChL	123	–	0·8	8·9	–	74·0	2·4	–	–	–	11·4	2·4
Mer-Ano	22	9·1	–	–	–	–	–	9·1	81·8	–	–	–

*PGM associations: 1, minerals in direct contact with sulphide; 2, minerals that occur in sulphide alteration haloes; 3, minerals that occur as inclusions associated with sulphide in chromite; 4, minerals in contact with sulphide and chromite; 5, minerals in contact with chromite without sulphide; 6, minerals in unaltered silicate not in contact with sulphide or chromite; 7, minerals in unaltered silicate that have a close spatial association with sulphide.

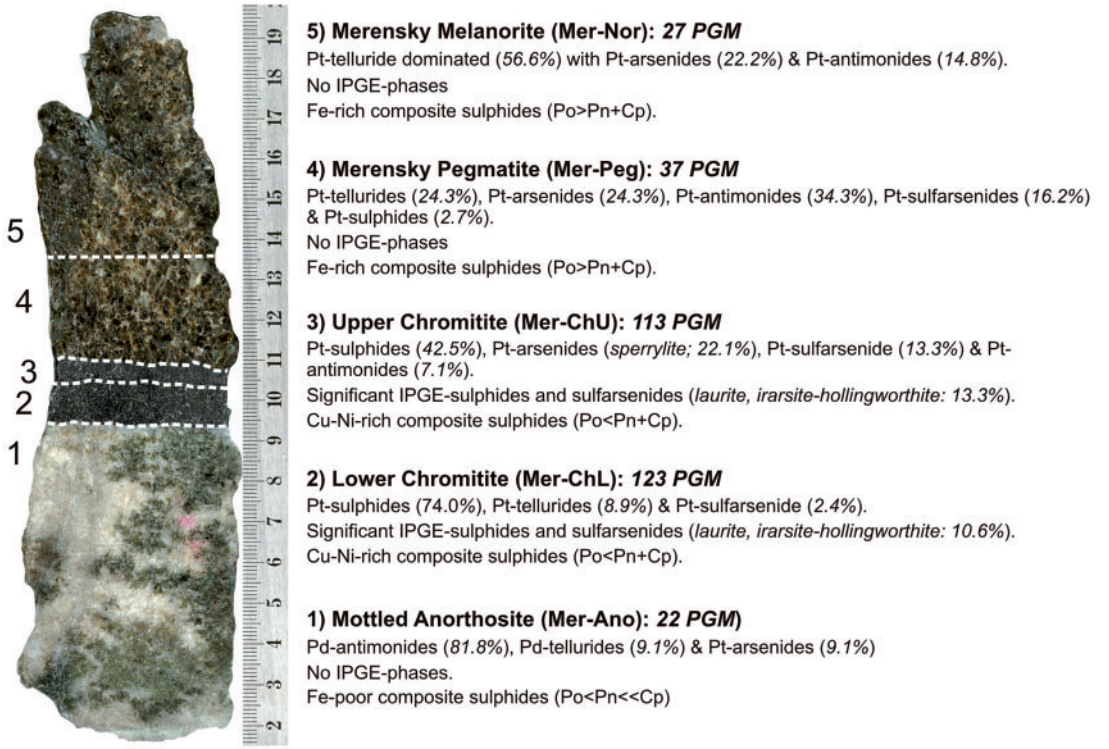

Fig. 6. Summary of the various sulphide and PGM assemblages present in the BRPM sample in each of the five main stratigraphic units.

granular, pyrrhotite-poor composite grains composed of pentlandite, chalcopyrite, pyrrhotite and minor pyrite (Table 2).

Many of the larger chromites from the lower layer contain apparent inclusions of silicates, although these are of the same type as, and are in optical continuity with, the silicate oikocrysts that enclose them. X-ray 3D tomography of the lower layer chromitite revealed that, in most cases, the silicate inclusions are artefacts generated by 2D sections cut through complex, highly irregular, chromite grains (Fig. 8). Micron-sized silicate inclusions are commonly present around the larger silicate inclusions as rings (e.g. Fig. 9c) or as random clusters (e.g. Fig. 9e). Minor minerals in the lower and upper chromitites include small grains of biotite (which are typically in contact with chromite), zircon, and occasional ilmenite, apatite and (possible) oliveiraite ($Zr_3Ti_2O_{10}.2H_2O$). Zircons (up to 30 μm), associated with ilmenite, are common within both the larger and smaller inclusions in the lower chromitite.

The footwall contact is sharp (Figs 4, 5 and 7) and neither the sulphides nor their associated PGM show any indication of migration below the contact. Instead, the sulphides and PGM typically occur in close proximity to the chromites (Fig. 9a) or as apparent inclusions within them (Fig. 9c–f; Table 1). In some cases, the sulphide inclusions take the negative crystal form of their chromite hosts (Fig. 9c–f). The PGM in the inclusions are the same as those present throughout the chromitite; however, the sulphide assemblages in some of the inclusions show replacement of pyrrhotite by pyrite

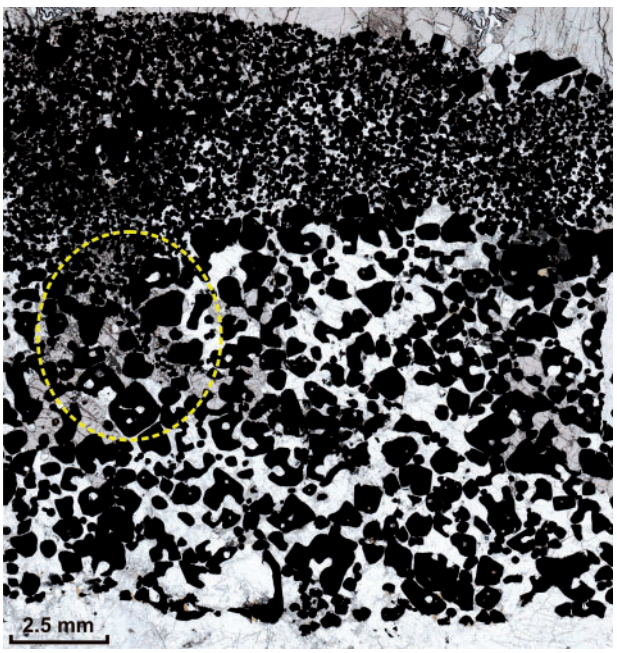

Fig. 7. Textures and contact relationships between the two chromitite layers. The presence of subvertical partings in the lower layer (circled) filled with chromite grains from the upper layer should be noted.

(Fig. 9d). In the upper chromitite the sulphides and PGM are similarly associated with chromite (Table 1), although no sulphide, PGM or silicate inclusions were observed in either the smaller or larger chromite grains.

Table 2. Major and trace element geochemistry of the Merensky and Platreef samples

Sample:	Mer-Ano	Mer-ChL	Mer-ChU	Mer-Peg	Mer-Nor	Platreef-1	Platreef-5	Platreef-6
Depth (from):*	–7·0 (cm)	0·0 (cm)	1·1 (cm)	1·6 (cm)	4·2 (cm)	243·05 (m)	250·42 (m)	254·17 (m)
Depth (to):*	0·0 (cm)	1·1 (cm)	1·6 (cm)	4·2 (cm)	9·4 (cm)	243·79 (m)	251·26 (m)	254·84 (m)
Lithology:	Anorthosite	Chromitite	Chromitite	Pegmatite	Melanorite	Anorthosite	Gabbronorite	Norite
wt %								
SiO_2	48·60	16·97	12·76	50·02	52·81	50·05	52·02	50·78
Al_2O_3	30·41	19·41	16·55	3·45	7·80	21·59	8·19	5·98
$FeO†_{(silicate+oxide)}$	0·78	20·94	25·08	10·18	9·40	5·69	9·16	10·05
$Fe†_{(sulphide)}$	0·09	0·27	0·29	3·22	0·69	0·06	0·30	1·48
MgO	0·84	8·25	10·13	23·08	21·99	4·65	20·56	22·24
CaO	15·78	4·35	2·42	4·36	4·72	11·74	5·02	4·02
Cr_2O_3	0·02	25·26	30·01	0·41	0·35	0·02	0·29	0·39
MnO	0·02	0·18	0·23	0·21	0·20	0·10	0·20	0·21
TiO_2	0·06	0·92	0·85	0·25	0·18	0·38	0·20	0·19
K_2O	0·19	0·13	0·09	0·09	0·09	0·73	0·24	0·19
Na_2O	2·47	0·66	0·14	0·24	0·58	2·61	0·81	0·56
P_2O_5	0·01	0·01	0·01	0·01	0·00	0·06	0·02	0·03
S	0·07	0·24	0·26	2·54	0·58	0·04	0·26	1·25
LOI	1·00	–0·92	–1·30	1·34	0·37	1·50	1·50	1·30
Total	100·37	97·14	98·06	100·78	100·29	99·25	99·04	99·53
Ppb								
Au	27	106·6	134	437	192	1	181	697
Ir	24	1244	876	202	14	n.a.	n.a.	n.a.
Pd	705	4303	3025	8242	1325	<10	79	1961
Pt	964	46 305	33 460	24 320	497	5	276	2506
Rh	97	4391	2902	783	49	n.a.	n.a.	n.a.
Ru	130	6630	4619	1146	78	n.a.	n.a.	n.a.
Ag	67	380	513	1003	516	15	259	1025
Ppm								
Cu	133	897	1082	3164	1417	28	753	2738
$Ni_{(silicate+oxide)}$	45	1158	1473	786	642	68	389	382
$Ni_{(sulphide)}$	192	824	873	8736	2176	30	999	4843
Ba	73·1	54	25·6	24·3	27·2	155	56·6	45·3
Cd	0·04	0·38	0·13	0·39	0·18	0·1	0·1	0·2
Ce	4·42	2·54	1·96	5·04	3·51	21·74	8·84	6·65
Co	8·74	248·06	274·97	247·11	126·82	31	101	157
Cs	0·11	0·05	0·05	0·09	0·06	1·21	0·69	0·83
Dy	0·28	0·13	0·10	1·22	0·62	2·20	0·977	0·782
Er	0·15	0·08	0·08	0·83	0·46	1·25	0·639	0·510
Eu	0·42	0·16	0·10	0·16	0·17	0·836	0·281	0·212
Gd	0·32	0·14	0·09	1·01	0·46	2·18	0·870	0·704
Hf	0·15	0·28	0·19	0·55	0·27	1·23	0·56	0·45
Ho	0·06	0·03	0·02	0·26	0·14	0·452	0·214	0·171
La	2·49	1·41	1·09	2·35	1·86	11·17	4·96	3·52
Li	1·5	2	2	4·1	4·1	6·80	6·37	7·22
Lu	0·02	0·02	0·02	0·13	0·08	0·170	0·105	0·087
Mo	<0·08	0·23	0·24	1·07	0·26	0·2	0·2	0·2
Nb	0·16	0·51	0·31	0·48	0·26	2·6	1·3	1·3
Nd	1·89	1·09	0·69	3·11	1·6	10·66	3·95	3·23
Pb	1·7	4	4·9	5·8	4·8	5·40	3·29	6·29
Pr	0·49	0·3	0·21	0·69	0·4	2·69	1·04	0·818
Rb	2·56	4·01	2·36	3·25	1·99	34·96	9·09	7·91
Sc	3·7	9·5	9·9	33·7	25·2	21·62	30·55	31·6
Sm	0·36	0·19	0·11	0·88	0·39	2·31	0·855	0·701
Sn	<0·16	0·36	0·4	0·42	0·34	0·6	0·4	0·6
Sr	464·2	124·9	74·6	38·2	111·3	306·1	88·5	63·9
Ta	<0·02	<0·02	<0·02	<0·02	<0·02	0·23	0·12	0·11
Tb	0·05	0·02	0·01	0·18	0·09	0·368	0·152	0·121
Th	0·13	0·15	0·08	0·42	0·33	1·54	1·15	0·84
Ti	385	3849	4841	1468	1002	1668	1081	978
Tl	0·01	0·02	0·02	0·10	0·03	0·145	0·117	0·217
Tm	0·02	0·01	0·01	0·13	0·08	0·182	0·099	0·082
U	0·04	0·04	0·02	0·24	0·12	0·40	0·30	0·22
V	19·3	1257·94	1445·65	140·20	104·1	130	144	128
W	<0·05	<0·05	0·27	0·06	<0·05	0·181	0·093	0·181
Y	1·59	0·82	0·72	7·53	4·27	11·69	5·51	4·36
Yb	0·12	0·10	0·10	0·85	0·54	1·144	0·661	0·546
Zn	7	593	731	80	80	50·06	73·12	77·45
Zr	6	9	<6	20	10	47·5	20·1	15·7
Sb	0·17	2·64	8·46	4·98	0·89	0·1	0·1	0·1
As	<0·70	6·87	30·47	32·32	4·08	0·8	0·5	0·4

(continued)

Table 2. (continued)

Sample:	Mer-Ano	Mer-ChL	Mer-ChU	Mer-Peg	Mer-Nor	Platreef-1	Platreef-5	Platreef-6
Depth (from):*	–7·0 (cm)	0·0 (cm)	1·1 (cm)	1·6 (cm)	4·2 (cm)	243·05 (m)	250·42 (m)	254·17 (m)
Depth (to):*	0·0 (cm)	1·1 (cm)	1·6 (cm)	4·2 (cm)	9·4 (cm)	243·79 (m)	251·26 (m)	254·84 (m)
Lithology:	Anorthosite	Chromitite	Chromitite	Pegmatite	Melanorite	Anorthosite	Gabbronorite	Norite
Bi	<0·15	0·28	0·23	1·58	0·59	0·02	0·12	0·80
Te	0·10	0·30	0·33	4·41	1·01	<0·01	0·5	2·4
Se	<0·10	0·45	0·45	13·45	2·95	<0·10	1·60	7·60
La/Sm	7·0	7·3	10·2	2·7	4·7	4·8	5·8	5·0
Nb/La	0·1	0·4	0·3	0·2	0·1	0·2	0·3	0·4
Zr/Y	3·8	11·0	–	2·7	2·3	4·1	3·6	3·6
Nb/Th	1·3	3·5	4·2	1·1	0·8	1·7	1·1	1·6
Sr/Y	292·0	152·3	103·6	5·1	26·1	26·2	16·1	14·6
Zr/TiO_2	93·4	14·0	–	81·7	59·8	170·7	111·4	96·1
Ce/Sm	12·4	13·2	18·3	5·7	9·0	9·4	10·3	9·5
Th/Y	0·1	0·2	0·1	0·1	0·1	0·1	0·2	0·2
Th/Yb	1·0	1·4	0·8	0·5	0·6	1·3	1·7	1·5
Cu/Pd	166	192	328	381	937	–	9231	1417
S/Se	–	5352	5808	1885	1966	–	1625	1645
Pt/Pd	1·4	10·8	11·1	3·0	0·4	–	3·5	1·3
Pt/Ir	39·8	37·2	38·2	120·5	36·7	–	–	–
Pd/Ir	29·1	3·5	3·6	40·8	97·9	–	–	–
Cp (wt %)	0·03	0·24	0·29	0·91	0·36	0·0	0·2	0·8
Pn (wt %)	0·06	0·26	0·27	2·73	0·68	0·0	0·3	1·5
Po (wt %)	0·10	0·18	0·17	3·30	0·58	0·1	0·2	1·2
$Sulphide_{(total)}$	0·19	0·68	0·73	6·94	1·62	0·1	0·7	3·5
Pt tenor (ppm)	506·7	6856·5	4559·7	350·2	30·8	4·7	37·8	71·7
Pd tenor (ppm)	370·6	637·2	412·2	118·7	82·0	0·0	10·8	56·2
Ni tenor (wt %)	10·1	12·2	11·9	12·6	13·5	2·9	13·7	13·9
Cu tenor (wt %)	6·1	12·3	13·5	4·6	7·7	2·4	9·9	8·0
$Mg\#_{(Fe2+=0·9Fet)}$	68·20	43·83	44·45	81·78	82·25	61·8	81·6	81·4

Sample:	Platreef-9	Platreef-12	Platreef-10	Platreef-14	Platreef-21	Platreef-25	Platreef-32	Platreef-36
Depth (from):*	277·38 (m)	279·66 (m)	282·90 (m)	286·34 (m)	304·40 (m)	320·14 (m)	341·66 (m)	347·5 (m)
Depth (to):*	278·48 (m)	280·96 (m)	284·00 (m)	287·37 (m)	305·42 (m)	320·77 (m)	342·54 (m)	348·57 (m)
Lithology:	Feld-pyrox	Feld-pyrox	Serp-perid	Feld-pyrox	Feld-webst	Feld-webst	Websterite	Websterite
wt %								
SiO_2	50·87	48·89	45·08	51·09	50·06	47·08	48·05	47·20
Al_2O_3	7·33	6·91	4·00	5·19	8·73	2·93	3·06	3·40
$FeO†_{(silcate+oxide)}$	9·47	9·10	12·13	10·09	10·76	15·08	12·61	18·00
$Fe†_{(sulphide)}$	0·19	0·45	1·54	0·34	0·51	1·15	1·58	2·89
MgO	22·06	20·75	26·61	23·94	19·86	22·27	12·75	15·38
CaO	6·23	5·79	2·97	4·73	5·25	6·06	16·47	6·18
Cr_2O_3	0·35	0·31	0·31	0·51	0·32	0·67	0·22	0·43
MnO	0·22	0·22	0·24	0·25	0·25	0·39	0·42	0·49
TiO_2	0·15	0·13	0·10	0·13	0·15	0·21	0·29	0·47
K_2O	0·12	0·11	0·05	0·07	0·36	0·25	0·18	0·21
Na_2O	0·54	0·53	0·15	0·38	0·64	0·20	0·43	0·36
P_2O_5	0·03	<0·10	<0·10	0·01	<0·10	<0·10	0·04	0·03
S	0·15	0·16	1·13	0·31	0·40	0·88	1·12	2·00
LOI	1·10	5·40	4·30	1·73	1·50	1·20	1·60	1·60
Total	99·01	99·44	98·90	99·12	99·06	98·83	99·12	99·02
ppb								
Au	72	234	180	174	79	68	77	52
Ir	n.a.	n.a.	n.a.	n.a.	n.a.	n.a.	n.a.	n.a.
Pd	54	271	1238	957	652	716	471	274
Pt	168	505	1272	921	803·4	133	349	215
Rh	n.a.	n.a.	n.a.	n.a.	n.a.	n.a.	n.a.	n.a.
Ru	n.a.	n.a.	n.a.	n.a.	n.a.	n.a.	n.a.	n.a.
Ag	123	837	328	369	350	678	308	246
ppm								
Cu	336	2296	796	1041	719	1260	812	717
$Ni_{(silicate+oxide)}$	515	380	400	381	347	400	400	400
$Ni_{(sulphide)}$	454	3588	1231	1359	1072	2415	1323	2141
Ba	25·8	12·1	27·5	17·6	51·5	40·5	33·5	40·7
Cd	0·1	0·2	0·1	0·1	0·1	0·2	0·2	0·2
Ce	3·07	1·59	3·02	2·17	4·83	6·32	15·43	14·31
Co	96	195	108	111	105	138	73	117
Cs	0·76	1·63	0·81	0·73	1·47	1·43	1·32	1·91
Dy	0·666	0·354	0·629	0·585	0·598	1·056	2·680	2·243
Er	0·454	0·269	0·437	0·423	0·437	0·700	1·485	1·394

(continued)

Table 2. (continued)

Sample:	Platreef-9	Platreef-12	Platreef-10	Platreef-14	Platreef-21	Platreef-25	Platreef-32	Platreef-36
Depth (from):*	277·38 (m)	279·66 (m)	282·90 (m)	286·34 (m)	304·40 (m)	320·14 (m)	341·66 (m)	347·5 (m)
Depth (to):*	278·48 (m)	280·96 (m)	284·00 (m)	287·37 (m)	305·42 (m)	320·77 (m)	342·54 (m)	348·57 (m)
Lithology:	Feld-pyrox	Feld-pyrox	Serp-perid	Feld-pyrox	Feld-webst	Feld-webst	Websterite	Websterite
Eu	0·165	0·091	0·173	0·123	0·202	0·210	0·540	0·368
Gd	0·527	0·262	0·499	0·436	0·477	0·903	2·602	2·021
Hf	0·23	0·14	0·23	0·21	0·31	0·54	1·29	0·77
Ho	0·150	0·086	0·143	0·132	0·138	0·234	0·539	0·480
La	1·53	0·85	1·48	1·04	2·65	3·22	6·47	6·33
Li	6·86	7·72	10·47	11·79	9·07	10·57	18·49	14·20
Lu	0·081	0·054	0·077	0·079	0·084	0·115	0·194	0·220
Mo	0·1	0·3	0·2	0·1	0·2	0·3	0·5	0·7
Nb	0·4	0·2	0·4	0·3	0·7	0·9	1·0	1·3
Nd	1·73	0·82	1·64	1·29	2·11	3·33	9·55	8·15
Pb	1·39	5·55	4·16	3·58	5·72	14·78	5·32	9·84
Pr	0·404	0·200	0·388	0·290	0·558	0·807	2·17	1·94
Rb	5·32	3·84	5·76	3·86	20·53	12·98	10·75	13·74
Sc	38·75	24·15	37·76	36·89	31·00	29·38	32·29	29·13
Sm	0·451	0·217	0·420	0·361	0·456	0·826	2·479	1·979
Sn	0·2	0·5	0·2	0·3	0·4	0·9	1·3	1·0
Sr	55·7	29·8	64·3	34·1	101·8	20·1	19·7	21·0
Ta	0·04	0·03	0·04	0·03	0·07	0·09	0·13	0·17
Tb	0·098	0·051	0·093	0·086	0·09	0·168	0·451	0·360
Th	0·33	0·14	0·31	0·23	0·74	0·84	1·25	1·25
Ti	829	547	1004	951	1051	1436	2040	2837
Tl	0·084	0·124	0·069	0·072	0·134	0·141	0·147	0·194
Tm	0·074	0·045	0·070	0·069	0·073	0·109	0·215	0·212
U	0·07	0·04	0·07	0·05	0·21	0·25	0·39	0·43
V	128	76	125	99	102	130	131	153
W	0·053	0·203	0·149	0·142	0·279	0·634	0·400	0·700
Y	3·80	2·15	3·60	3·45	3·63	6·10	13·84	12·23
Yb	0·502	0·321	0·485	0·483	0·519	0·733	1·309	1·429
Zn	70·13	91·49	73·63	79·35	83·07	95·91	43·32	94·96
Zr	6·9	4·0	7·4	6·13	10·4	18·1	39·0	22·5
Sb	0·1	0·1	0·1	0·1	0·3	0·3	0·2	0·4
As	0·4	0·5	0·5	0·5	1·0	2·2	0·9	2·6
Bi	0·08	0·59	0·20	0·38	0·49	0·93	0·55	0·47
Te	0·2	0·9	0·5	0·4	0·4	0·5	0·3	0·2
Se	0·90	1·45	4·70	1·83	1·70	2·90	2·50	3·80
La/Sm	3·4	3·9	3·5	2·9	5·8	3·9	2·6	3·2
Nb/La	0·2	0·2	0·3	0·2	0·3	0·3	0·2	0·2
Zr/Y	1·8	1·9	2·0	1·8	2·9	3·0	2·8	1·8
Nb/Th	1·1	1·1	1·3	1·1	0·9	1·0	0·8	1·1
Sr/Y	14·6	13·9	17·9	9·9	28·0	3·3	1·4	1·7
Zr/TiO_2	49·8	44·0	44·0	38·6	59·3	75·7	114·6	47·5
Ce/Sm	6·8	7·3	7·2	6·0	10·6	7·7	6·2	7·2
Th/Y	0·1	0·1	0·1	0·1	0·2	0·1	0·1	0·1
Th/Yb	0·7	0·4	0·6	0·5	1·4	1·1	1·0	0·9
Cu/Pd	5577	2595	1513	1080	1170	1598	1830	2881
S/Se	1667	1103	2404	1691	2353	3034	4480	5263
Pt/Pd	3·1	1·9	1·0	1·0	1·2	0·2	0·7	0·8
Pt/Ir	–	–	–	–	–	–	–	–
Pd/Ir	–	–	–	–	–	–	–	–
Cp (wt %)	0·1	0·2	0·5	0·3	0·2	0·3	0·2	0·2
Pn (wt %)	0·1	1·1	0·4	0·4	0·3	0·8	0·4	0·7
Po (wt %)	0·2	0·0	2·1	0·2	0·5	1·3	2·3	4·3
$Sulphide_{(total)}$	0·4	1·3	3·0	0·9	1·1	2·4	2·9	5·2
Pt tenor (ppm)	40·7	38·1	42·7	103·9	73·8	5·6	11·9	4·1
Pd tenor (ppm)	13·1	20·5	41·6	108·0	59·8	30·1	16·1	5·3
Ni tenor (wt %)	11·0	27·1	4·1	15·3	9·8	10·1	4·5	4·1
Cu tenor (wt %)	7·3	5·3	6·3	11·7	7·0	4·8	2·9	1·5
$Mg\#_{(Fe2+=0·9Fet)}$	82·2	81·9	81·3	82·5	78·5	74·5	66·7	62·9

*Depth (from) and Depth (to) in the Merensky samples denote height relative to the anorthosite-chromitite contact. Sample intervals were chosen to avoid cross-contamination and be representative of the key petrological zones shown in Figs 2 and 3.

†Fe originally reported as Fe_2O_3 wt % (total). This was converted to FeO (silicate and oxide) and Fe (sulphide) using the S wt % data together with calculated or estimated silicate Ni and Cu contents and modal mineral proportions derived from thin-sections. For the Merensky samples, Ni and Cu contents in oxides and silicates were measured using LA-ICP-MS. For the Platreef samples, partial aqua regia digestion values were used for silicate Ni and Cu. Samples 10, 25, 32 and 36 gave anomalously low Ni contents and a value of 400 ppm was used. This was based on the results from the other samples in this dataset, which range from 347 to 515 ppm (average 399).

n.a., not analysed. A table of the standards used can be found in Supplementary Data Electronic Appendix 1.

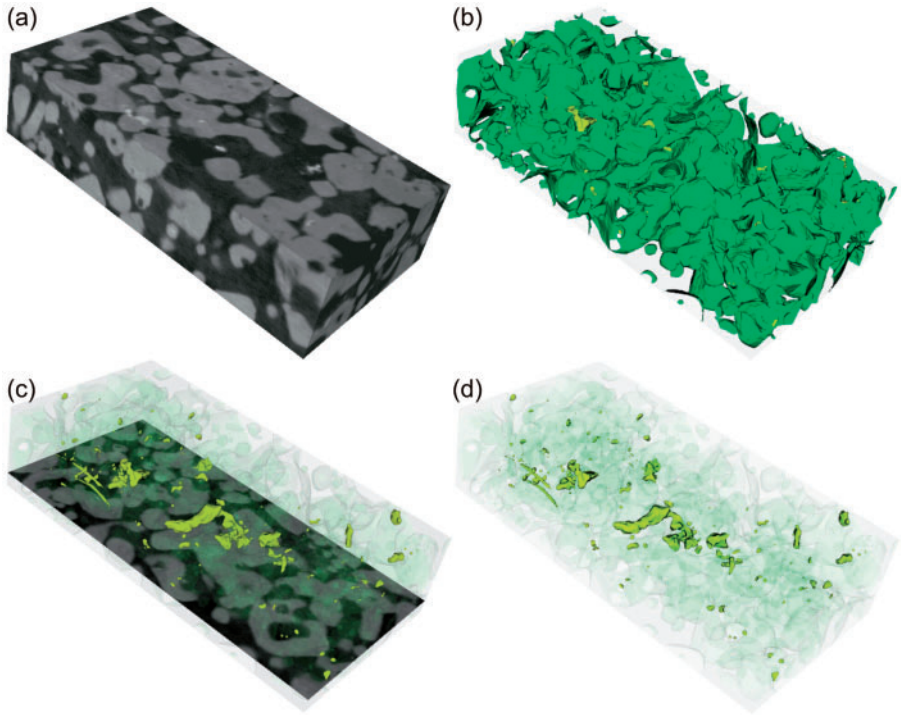

Fig. 8. X-ray 3D tomography scans through lower layer chromitite. (a) Greyscale image showing the textures of the highly corroded chromites (dark grey), sulphides (light grey) and PGM (white). (b) A 3D representation of the chromites (green) showing their highly irregular morphology. (c) Planar section displaying chromite textures together with 3D view of the sulphide and PGM distribution (yellow). (d) Distribution of the sulphides and PGM.

Although there is some evidence for PGM recrystallization where they are in contact with chromite, there is little evidence for direct nucleation and formation of PGM along the chromite margins as proposed by Finnigan *et al*. (2008) and Godel *et al*. (2010). There is a notable difference in the PGM assemblages between the two chromitite layers. The lower chromitite contains a significant proportion of Pt-sulphides (cooperite–braggite–vysotskite series) with minor Pt-sulfarsenides (platarsite) and Pt-tellurides (moncheite). In contrast, the upper chromitite contains significantly less Pt-sulphides with substantially more Pt-sulfarsenides and, crucially, sperrylite, the first appearance of which occurs exactly at the base of this layer (Fig. 10). Both chromitites contain approximately equal amounts of Ir, Ru, Rh-minerals, which typically occur as laurite, hollingworthite and irarsite, and in both layers Pd-minerals are scarce (Fig. 6; Table 1).

Layer 4: Merensky pegmatite

The silicate in contact with the upper chromitite is a 2·4–2·8 cm thick, coarse-grained, meso- to adcumulate-textured pyroxenite to melanorite containing blebby patches of intercumulus plagioclase (Fig. 4a and b). Cawthorn & Boerst (2006) defined this unit a 'pegmatitic pyroxenite . . . with a grain size of orthopyroxene greater than 2 mm (up to 5 cm)'. Although not strictly pegmatitic, this does distinguish it from the melanorite that forms the bulk of the Merensky silicate at BRPM and elsewhere.

Chromite is largely absent from the pegmatite except for occasional grains located just above the contact with the upper chromitite [as noted by Cawthorn & Boerst (2006)].

Sulphides account for *c*. 7% of the mineralogy and are relatively large (<3·00 mm) intergranular to granular, composite grains of pyrrhotite, pentlandite and chalcopyrite (Table 2). Some of the sulphides show alteration to pyrite, whereas others show pervasive disruption by talc and tremolite. Similar disruption of sulphide was described from the Platreef by Hutchinson & McDonald (2008). In other areas, alteration appears to have removed a significant component of the original sulphide, which is replaced by secondary silicates. Despite the effects of alteration, over 97% of the PGM are either directly or indirectly associated with sulphide (Table 1). The PGM assemblage is distinctly different from that of the chromitites. No Ir, Ru, Rh minerals were found and the assemblage is dominated by Pt-arsenides (sperrylite), Pt-antimonides (geversite), Pt-tellurides (moncheite) and Pt-sulfarsenides, with minor Pt-sulphides (Fig. 6; Table 1).

Layer 5: Merensky melanorite

The melanorite is broadly similar to the pegmatite except for its finer grain size and orthocumulate texture (Fig. 4a and b). Sulphides account for only 1·6% of the mineralogy and occur as disseminated, intergranular to granular composite grains of pyrrhotite, pentlandite and chalcopyrite. These are more chalcopyrite-rich,

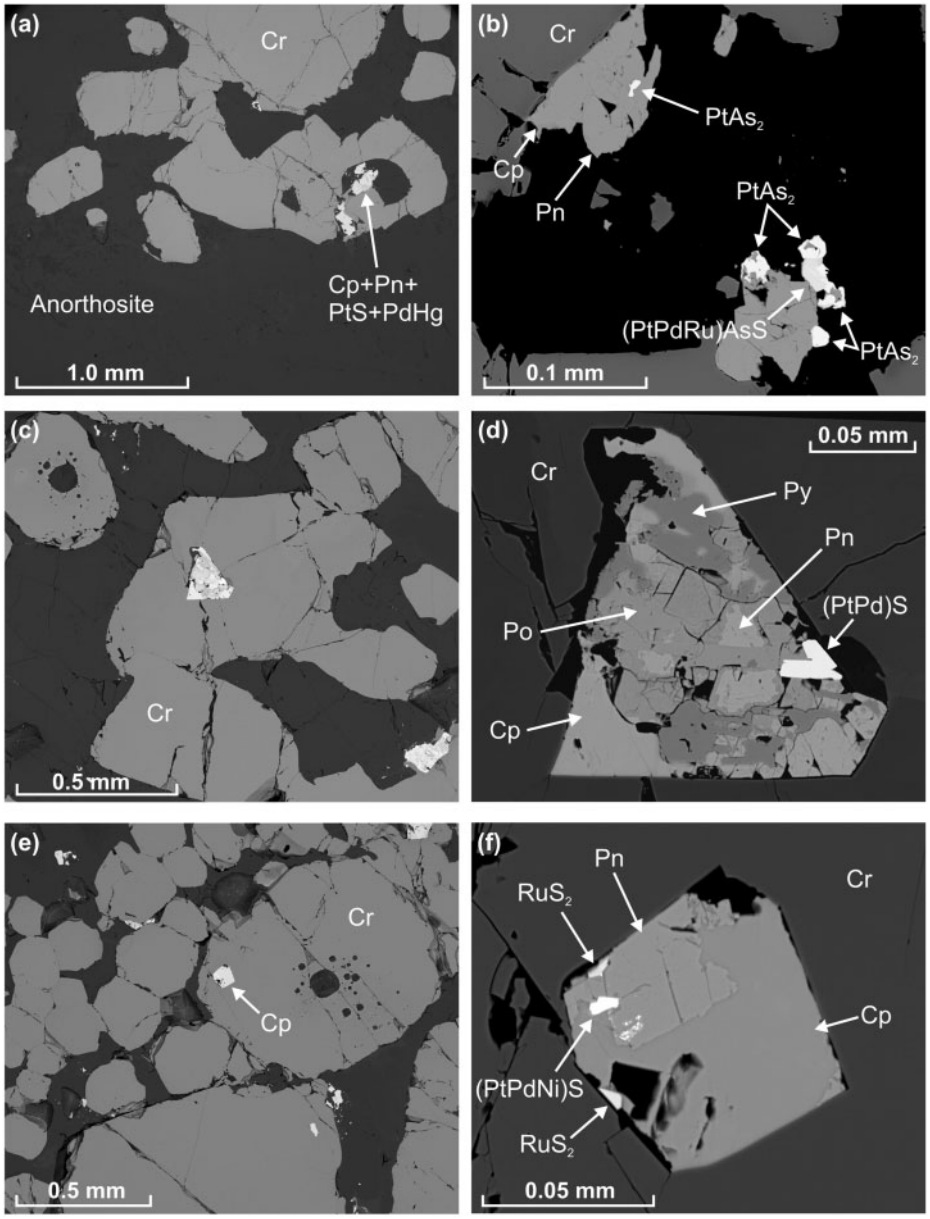

Fig. 9. Textures of the chromite, sulphide and PGM in backscatter scanning electron images. (a) Sulphide and PGM associated with a corroded lower layer chromite along the footwall contact to the anorthosite. (b) Sulphides (pentlandite and chalcopyrite) and PGM (sperrylite and platarsite) in upper layer chromitite. (c) Triangular inclusion of composite sulphide and PGM in a corroded lower layer chromite. (d) Magnified view of inclusion from (c), which shows replacement of pyrrhotite by pyrite and crystallization of cooperite–braggite [(PtPd)S] against the chromite. (e) Sulphide and silicate inclusions in lower chromitite layer. The silicate inclusion in the large chromite grain is surrounded by numerous smaller silicate inclusions. (f) Magnified view of hexagonal sulphide inclusion from (e), which shows the presence of both principal groups of PGM present in the chromitites: the Pt-group represented here by cooperite–braggite [(PtPd)S], and the IPGE group represented here by two laurites [RuS_2] that crystallized against the chromite. Cr, chromite; Cp, chalcopyrite; Pn, pentlandite; Po, pyrrhotite; Py, pyrite.

and smaller (<1·50 mm) than those in the pegmatite (Table 2).

The melanorite contains relatively large granular apatites together with other rare earth element (REE)-bearing phases including monazite and a Th-silicate. In addition, centimetre-sized clots and intercumulus regions of quartz and feldspar are common, many containing albite–anorthite–orthoclase symplectite. Although these have been described as intercumulus phases on textural grounds (e.g. Cawthorn & Boerst, 2006), in some areas they appear to have resisted the downward settling of cumulus orthopyroxene crystals. Like the pegmatite, the majority of the PGM (96%) occur directly or indirectly associated with sulphides (Table 1). These are noticeably different from the preceding layers. Compared with the pegmatite, the PGM assemblage in the melanorite contains twice the amount of Pt-tellurides (moncheite), half the amount of Pt-antimonides (geversite), but equal amounts of Pt-arsenides (sperrylite). Like the pegmatite, no Ir, Ru, Rh

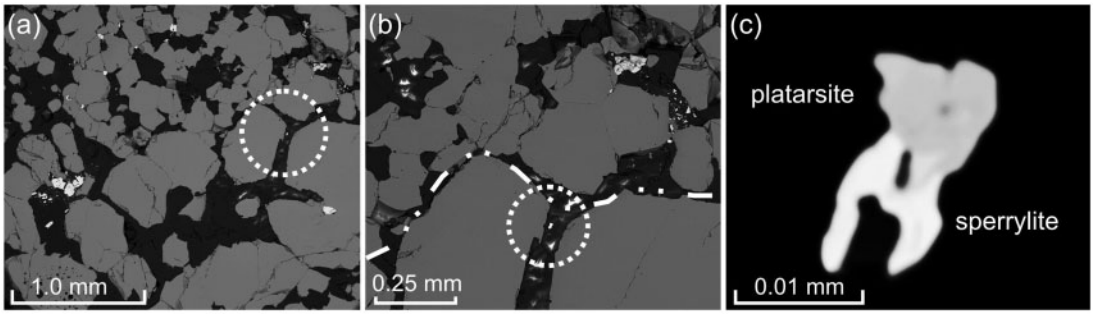

Fig. 10. First occurrence of sperrylite in the upper chromitite layer. (a) Sperrylite (circled) along the contact between the lower coarser-grained and upper finer-grained chromitite. (b) Magnified view of (a) with contact shown by a dot–dash line. (c) PGM is a composite sperrylite and platarsite hosted within silicate.

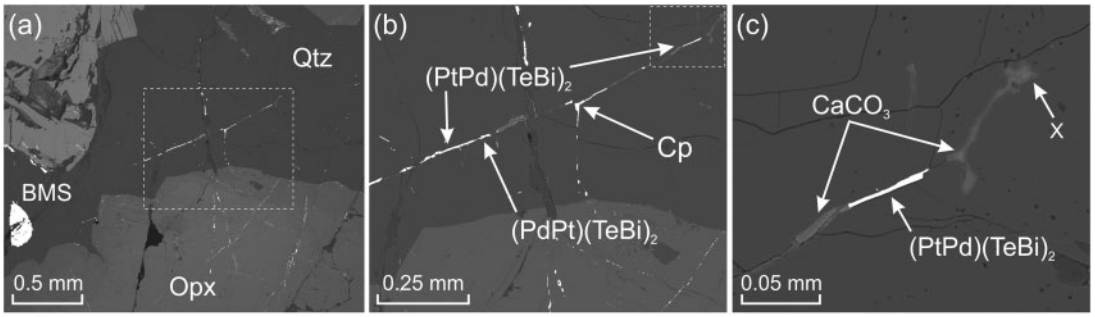

Fig. 11. Mineralized vein in quartz in the Merensky melanorite filled with carbonate, BMS and PGM. (a) Orthopyroxene (Opx) surrounded by quartz (Qtz) hosting BMS. (b) Magnified view of the boxed region from (a) showing a vein filled with chalcopyrite (Cp), carbonate and PGM of merenskyite and moncheite. (c) Magnified view of boxed region from (b) showing the termination of the PGM-bearing carbonate vein at 'x'.

minerals are present (Fig. 6; Table 1). Late-stage veins filled with carbonate, chalcopyrite and PGM of moncheite and merenskyite were observed cutting quartz and orthopyroxene (Fig. 11).

PETROGRAPHIC OBSERVATIONS: PLATREEF

The mineralogy and geochemistry of a core from Turfspruit, immediately south of Tweefontein, has been documented by Hutchinson & Kinnaird (2005) and Hutchinson & McDonald (2008). The aims of the current study on the Platreef are (1) to extend the scope of the previous work to an adjacent area located on different footwall rocks (including iron formations), and (2) to incorporate LA-ICP-MS mapping to supplement the laser spot data and SEM observations made here and reported in the literature.

The Platreef at Tweefontein can broadly be divided into three packages: (1) 'Lower Reef' composed of pervasively overprinted and recrystallized norites and feldspathic pyroxenites with numerous country-rock xenoliths, especially towards the base (Fig. 3): (2) 'Central Reef' comprising igneous peridotite, recrystallized 'vari-textured' mafic rocks and metasedimentary xenoliths (which may include metasedimentary peridotites and serpentinites); (3) 'Upper Reef' largely of plagioclase-bearing pyroxenite and norite, which grades toward norite and gabbronorite approaching the Main Zone contact. Xenoliths are rare, although a small disaggregating chromitite was observed within feldspathic pyroxenite close to the top of the reef (Fig. 3).

The igneous lithologies within the Lower and Central Reef have been geochemically overprinted and recrystallized to a range of websterites, wehrlites and peridotites, all with variable amounts of plagioclase, olivine, and pyroxene. Metamorphic inverted pigeonite is common. Pervasive infiltration of felsic melts has occurred throughout the Platreef from metre-wide granite dykes (locally known as 'QF' for quartzo-feldspathic), to mineral-scale intercumulus patches of quartz and feldspar, many of which contain symplectites composed of albite–orthoclase–plagioclase–quartz (Hutchinson & Kinnaird, 2005).

The sedimentary lithologies in the footwall belong to the lower portion of the Transvaal Supergroup. At drillhole TN207 the reef contacts the Penge (iron formations), which is overlain by the Duitschland Formation (largely shales), and underlain by the Malmani Subgroup (mostly carbonates including the Malmani Dolomite). In detail, the iron formations are intercalated with shales, calc-silicates and quartzites. These have also been texturally recrystallized, geochemically overprinted, and variably retrogressed and altered to hornfels (variably magnetite–olivine–plagioclase–clinopyroxene-bearing), meta-quartzite, websterite (variably olivine–pigeonite-bearing with pyroxene Mg#

15–17) and dunite (of almost pure fayalitic composition Mg# = 5). In some cases the textures can appear igneous owing to the coarse grain sizes and presence of pyroxene (the term 'para-pyroxenites' is commonly used for these rocks). The degree of alteration and retrograde metamorphic reaction varies throughout the drill-hole, with the development of sericite, clays, serpentine, talc and amphibole.

Many of the meta-igneous and meta-sedimentary lithologies display textures indicative of high-grade metamorphism, including the development of sub-granoblastic to consertal grain margins. A single thin-section can exhibit several domains with different mineralogy and textures. In some cases, the level of textural destruction, combined with prograde and retrograde metamorphic minerals and alteration, makes identifying the protoliths difficult. Magnetic susceptibility was found to aid in the recognition of recrystallized iron-rich sediments that may otherwise appear very similar to a coarse-grained igneous pyroxenite.

Many of the sulphides, particularly the larger grains in the metasomatized portions of the reef, are surrounded by felsic assemblages. Typically, these are poor in chalcopyrite, whereas chalcopyrite may be present in the intercumulus silicate that surrounds them [see fig. 7e of Hutchinson & Kinnaird (2005) from Turfspruit]. In some cases, large sulphides are observed with trails of chalcopyrite and pentlandite leading away from a remnant pyrrhotite-rich core. Several examples of this texture have been observed throughout the reef and they are not restricted to the highly metasomatized zone towards the base. Occasionally, PGM are attached to fragments of disrupted sulphide, whereas in other cases PGM are locked within unaltered silicates without any apparent association with sulphide.

Greater than 99% of the PGM occur as As, Sb, or Te–Bi phases that are more commonly associated with large sulphides than small ones. Samples from the very top of the reef immediately below the contact with the Main Zone do not contain PGM (Supplementary Data Electronic Appendix 2). Pd and Ir-group PGE (IPGE) minerals (hollingworthite–irarsite series) are more common in the Central and Lower Reef, with a greater percentage of PGM hosted in silicate, although they are still spatially associated with large sulphides.

A number of distinctive accessory minerals occur in the lower parts of the Platreef, including molybdenite together with a range of semi-metal and trace-metal phases such as cobaltoan gersdorffite [(NiCo)AsS], nickeline (NiAs) (possibly associated with maucherite; $Ni_{11}As_8$), altaite (PbTe) and tsumoite (BiTe). Many are spatially associated with sulphides and PGM (particularly Rh, Ru and Ir minerals).

MINERAL CHEMISTRY (MERENSKY REEF)

Chromite grains from the lower chromitite display a broad compositional range with a slight upward decrease in $Cr/(Cr + Al)$, $Cr/(Cr + Al + Fe^{3+})$ and TiO_2, with a corresponding increase in $Mg/(Mg + Fe^{2+})$ (Fig. 12). In contrast, the upper layer appears to be bimodal with two distinct geochemical populations: (1) small chromites; (2) larger single grains and grain-clusters (Figs 7 and 12). The smaller grains define intricate upward trends with restricted compositional ranges for a given height. The TiO_2 contents of these grains show a progressive up-section increase that appears to have a maximum TiO_2 for a given height (Fig. 12d). A traverse across a typical small grain from the upper layer chromitite shows a narrow compositional range that lies within the overall trend defined by the small grains (Fig. 12a–d). A traverse through one of the larger grains in the upper layer shows a compositional range more similar to that of grains from the lower layer that extends beyond the general trend defined by the smaller grains. The compositional range displayed by a cluster of large grains in the upper layer chromitite is also more similar to that of the chromites in the lower layer. Traverses across single lower layer chromite grains show a broad range in composition with no systematic zonation.

Plagioclase in the anorthosite shows a slight up-section decrease from $\sim An_{78}$ at the sample base to An_{76} at the contact with the chromitite (Fig. 13a). In the chromitites extremely broad ranges in An and Or content are present in the different textural groups from both layers (i.e. the poikilitic domains and the inclusions). Plagioclase in the pegmatite shows a progressive upward decrease in An together with upward increase in Or. The base of the melanorite marks the position of a noticeable compositional break to higher An and lower Or, respectively.

In the anorthosite, the dominant pyroxene is clinopyroxene that shows an upwards increase in $Mg/(Mg + Fe^{2+})$, $Cr/(Cr + Al)$ and En with a curving decrease in Fs (Fig. 14). No clearly defined compositional breaks are observed at the contact with the lower chromitite and no distinction exists between different textural groups in the two chromitites (i.e. the poikilitic domains and the inclusions). There is, however, a compositional break at the contact between the upper chromitite and the pegmatite, shown most clearly by Fs and $Mg/(Mg + Fe^{2+})$. There is also a notable compositional break between the pegmatite and melanorite, shown most clearly in $Cr/(Cr + Al)$. The melanorite displays saw-tooth pattern reversals in composition, most clearly shown in Fs (Fig. 14d).

WHOLE-ROCK GEOCHEMISTRY

Absolute PGE contents of the anorthosite are relatively high (1896 ppb, Pt/Pd = 1·4). However, this is eclipsed by the values reported in the chromitites (Mer-ChL = 61 630 ppb, Pt/Pd = 10·8; Mer-ChU = 44 006 ppb, Pt/Pd = 11·1). The pegmatite is also highly enriched in PGE with 34 491ppb, but its Pt/Pd ratio of 3·0 is much lower than that of the chromitites. The melanorite has a

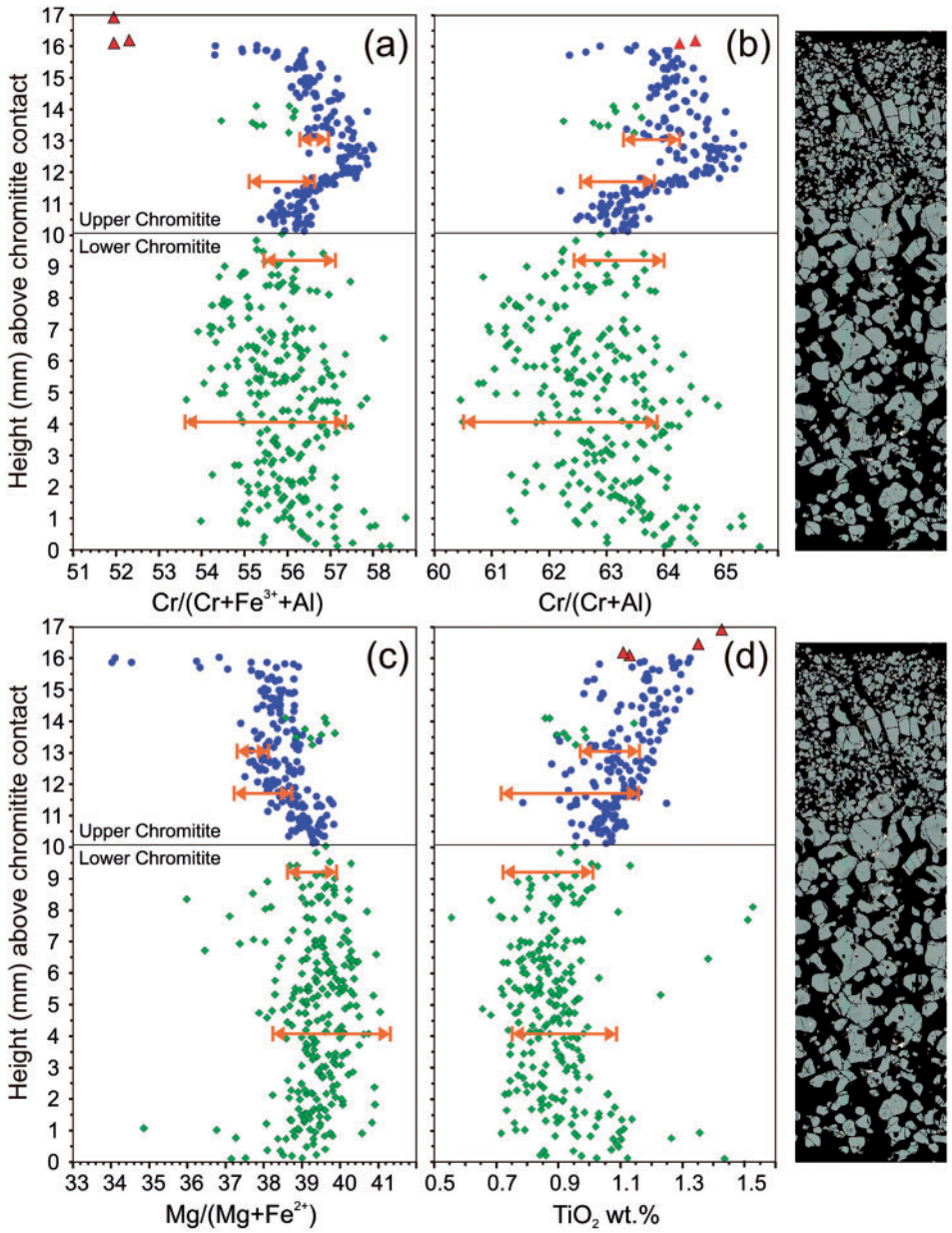

Fig. 12. Chromite compositions through the BRPM sample as a function of height above the chromitite contact (a) 100Cr/(Cr + Fe^{3+} + Al). (b) 100Cr/(Cr + Al). (c) 100 Mg/(Mg + Fe^{2+}). (d) TiO_2 wt %. Green diamonds, lower layer chromites; blue circles, upper layer chromites; red triangles, chromites in pegmatite. Orange lines indicate transects across single grains. It should be noted that for the pegmatite the Mg/(Mg + Fe^{2+}) range is from 12·6 to 25·4, which lies outside the scale shown. Reflected light image to the right shows the textural characteristics of the chromite grains analysed in the two chromitite layers. Data are from Supplementary Data Electronic Appendix 4.

similar PGE content to the anorthosite at 1949 ppb, but its Pt/Pd ratio is lower at 0·4.

The Merensky Reef and the upper portion of the Platreef share the characteristic primitive mantle normalized arched PGE profiles common in layered intrusions and PGE reefs in particular (Barnes *et al.*, 1988; Fig. 15). The PGE profiles of the Merensky melanorite and Platreef overlap and levels of Ni and Cu are similar in all samples excluding the anorthosite. Major differences are evident in the Merensky chromitites, which show highly elevated Ir, Ru, Rh and Pt but not Pd, as reflected in their distinctively high Pt/Pd (~11) and low Pd/Ir (3·5) ratios (Table 2).

By far the highest Pt and Pd tenors in the Merensky sulphides are in the chromitites, which for Pt are an order of magnitude above the silicate samples (in ppm Mer-Ano = 507, Mer-ChL = 6857, Mer-ChU = 4560, Mer-Peg = 350, Mer-Nor = 31; Table 2). Modelling the calculated Pt tenors of the lower chromitite by a process of PGE capture by sulphide liquids requires a K_d value close to 500 000, which is more than three times the 160 000 value published by Campbell *et al.* (1983),

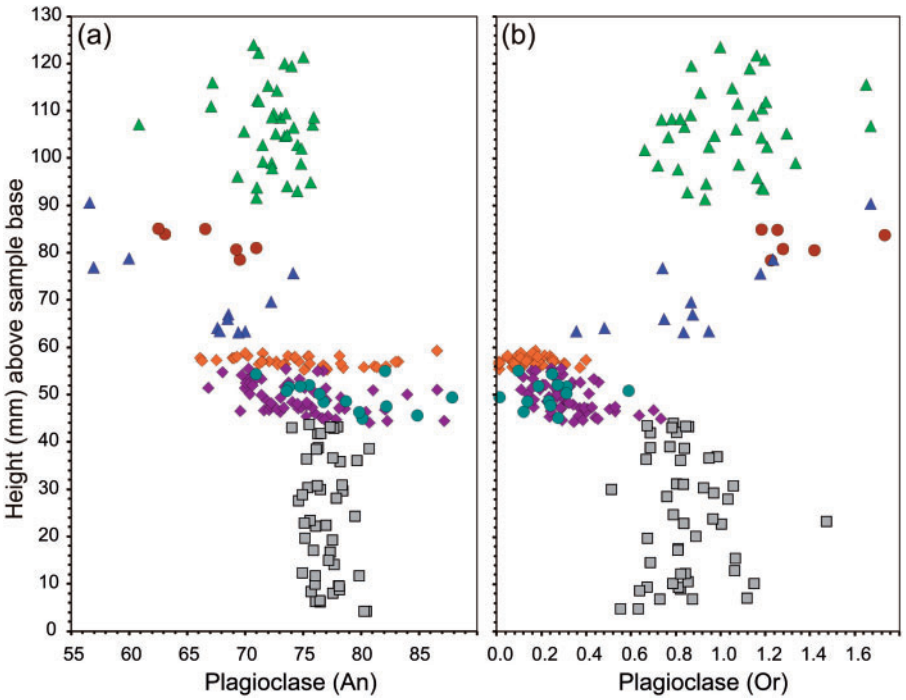

Fig. 13. Geochemical profiles for the various textural groups of plagioclase through the BRPM sample. The *y*-axis 'height' is relative to the bottom of the thin-section (blue dashed line shown in Fig. 4). (a) An%, (b) Or%. It should be noted that the Ab pattern is the mirror image of that for An. Grey squares, anorthosite; purple diamonds, poikilitic plagioclase within lower layer chromitite; blue–green circles, inclusions in lower layer chromites; orange diamonds, poikilitic plagioclase within upper layer chromitite; blue triangles, intercumulus feldspar in pegmatite; brown circles, plagioclase clots in pegmatite; green triangles, intercumulus plagioclase in melanorite. Data are given in Supplementary Data Electronic Appendix 5.

together with R factors of 5×10^6 (or N factors of $1{\cdot}3 \times 10^6$) (Fig. 16). Modelling using lower published K_d values cannot attain the calculated sulphide tenors for Pt in the lower chromitite; for example, based on $K_d = 6{\cdot}5 \times 10^3$ (Campbell *et al.*, 1983), $3{\cdot}0 \times 10^4$ [used by Barnes & Maier (2002*a*), based on work by Peach *et al.* (1990) and Fleet *et al.* (1999)] and $1{\cdot}0 \times 10^3$ [used by Naldrett *et al.* (2009)].

Whole-rock geochemistry: trace element patterns

The primitive mantle normalized trace element patterns for the Merensky pegmatite and melanorite show some striking similarities to the Platreef (Fig. 17; Table 2). All the patterns exhibit enrichments in incompatible elements, particularly from Cs to U and Pb, Mo, Sb and Li. Also enriched are As, Te, Cd and Sn (Table 2). The Lower Platreef has significantly higher levels of trace element enrichment than the Upper Reef, although the patterns are otherwise similar (Fig. 17).

LA-ICP-MS (mapping supported by spot analyses)

Merensky Reef sulphide

Except for Pd and Rh, which are always present in pentlandite, the Merensky sulphides generally contain very low abundances of Pt, Ru, Os, and Ir (Table 3; Supplementary Data Electronic Appendix 9). Low-level Pt is present in some of the pentlandite and pyrrhotite (e.g. Fig. 18c; Table 3). One exception includes a sulphide from the lower chromitite that contains extremely high Rh and Ir together with minor Ru and Pt in pentlandite, whereas the pyrrhotite has the highest recorded Pt (116 ppm) associated with high Rh and Ir, and minor Ru and Pd (Fig. 18a; Table 3). Both these pentlandites and pyrrhotites contain extremely high Co (4268–5115 ppm), whereas Bi appears to be present only in the pyrrhotite. Examination of the 'time-resolved' data showed that the PGE are distributed homogeneously in these sulphides (Fig. 19). Other examples of high Co associated with increased PGE in pentlandite include Merensky-4 Laser-12', where Bi, Pt, Ir, Os and Ru are more enriched in Co-rich pentlandite (cobaltian pentlandite), whereas Rh prefers the low-Co pentlandite (Fig. 18b; Table 3). Several other sulphides show a correlation between high Co and high Pt (>1 ppm), with or without other PGE (e.g. Merensky-2 Laser-2; Table 3). It is not clear whether the controlling factor in these situations is growth zoning or if it is an inherent feature caused by the presence of high Co. Evidence for growth zoning is observed, including a small composite sulphide containing two different pyrrhotite domains ringed by Ir–Ru–Pt micro-inclusions (Fig. 18c). These are similar to the sub-micron-sized PGM around the margins of some sulphides (e.g. Supplementary Data Electronic Appendix 11c).

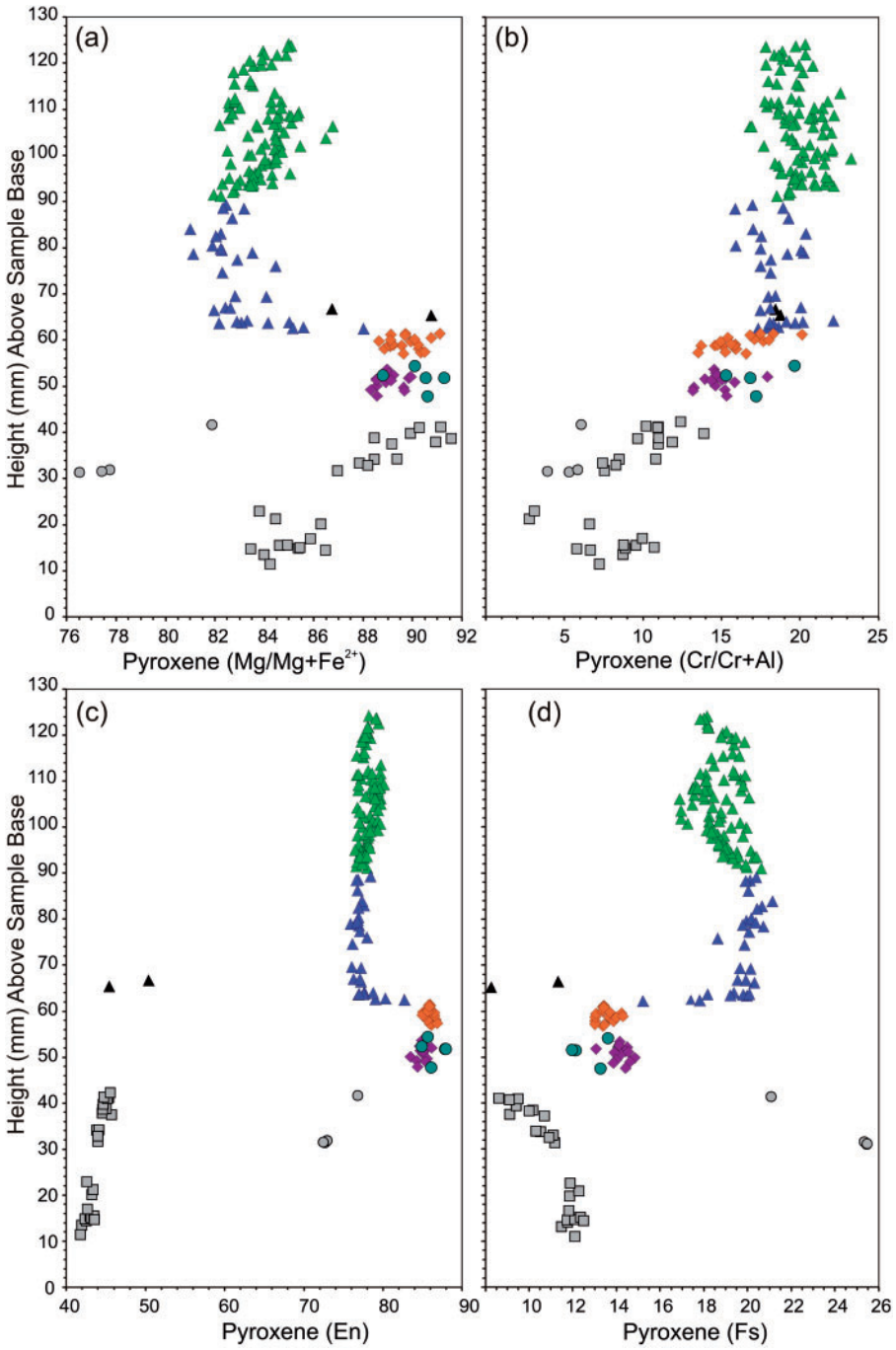

Fig. 14. Geochemical profiles for the various textural groups of pyroxene through the BRPM sample. The *y*-axis 'height' is relative to the bottom of the thin-section (blue dashed line shown in Fig. 4). (a) 100 Mg/(Mg + Fe^{2+}). (b) 100Cr/(Cr + Al). (c) En%. (d) Fs%. It should be noted that the Fs pattern is the mirror image of that for En. Grey squares, cpx in anorthosite; grey circles, opx in anorthosite; purple diamonds, poikilitic opx within lower layer chromitite; blue-green circles, opx inclusions in lower layer chromites; orange diamonds, poikilitic opx within upper layer chromitite; black triangles, cpx in pegmatite; blue triangles, opx in pegmatite; green triangles, opx in melanorite. Data are given in Supplementary Data Electronic Appendix 6.

Platreef sulphide

Platreef sulphides, like those in the Merensky Reef, show strong partitioning of Pd and Rh into pentlandite (e.g. Fig. 18d and e). Apart from the Upper Reef, where Pt can occur in very low levels in pyrrhotite and pentlandite, Pt is largely absent in the sulphides. Ir, Ru and Os preferentially reside within the pyrrhotite, although only marginally more so than pentlandite (e.g. Fig. 18d). Bi is generally low, although Pt–Bi micro-particles occur around some of the sulphide margins, especially those from the top of the reef (e.g. Fig. 18e). There is a noticeable decrease in Pt, Rh, Ru, Os and Ir but not Pd down the drill-core (Table 3; Fig. 18e–g; Supplementary Data Electronic Appendices 9 and 11f).

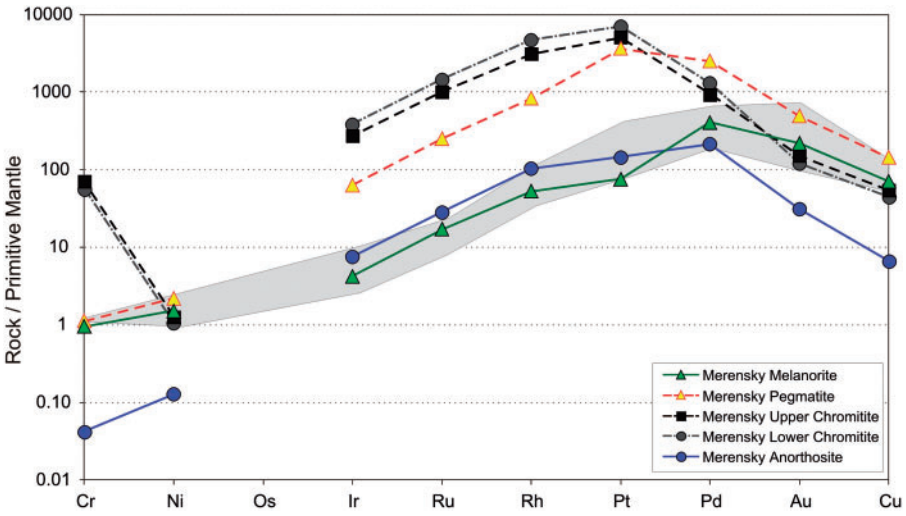

Fig. 15. Primitive mantle normalized PGE diagram for the Merensky samples and upper portion of the Platreef from Tweefontein (shaded field). Data are normalized to primitive mantle values from Palme & O'Neill (2004).

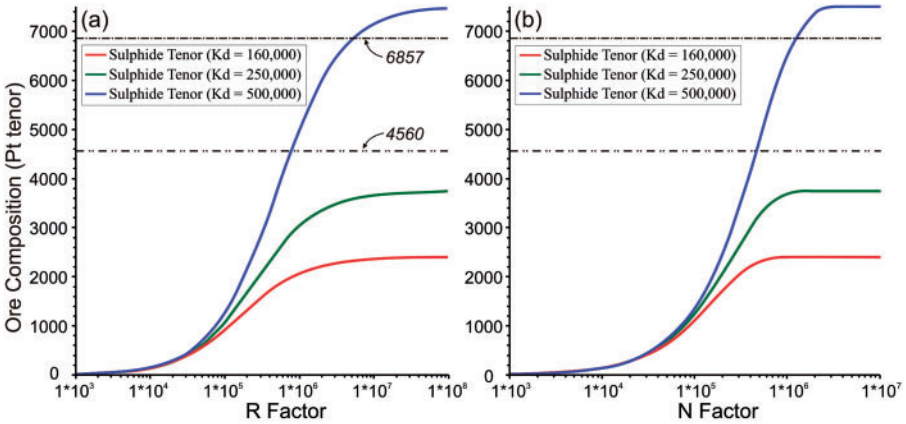

Fig. 16. Results of 'R' and 'N' factor modelling for Pt in the lower Merensky chromitite using $D^{Sul/Sil}$ values of 160 000, 250 000 and 500 000. Starting melt composition 15 ppb. Dot–dash lines show the position of the Pt tenors calculated from the whole–rock data for the lower chromitite (6857 ppm) and upper chromitite (4560 ppm) layers in the BRPM sample. 'R' factor is mass ratio of silicate magma (bulk) to sulphide liquid under equilibrium conditions (Campbell & Naldrett, 1979); 'N' factor is mass ratio of sulphide liquid to the total mass of silicate magma involved in the equilibration (see Naldrett, 2004, and references therein).

Merensky Reef chromites

Chromite is commonly regarded as a potential host for PGE (especially the IPGE; e.g. Hiemstra, 1979; Talkington & Watkinson, 1986). A vertical traverse through both chromitite layers and into the base of the pegmatite was conducted to investigate whether the chromites at BRPM contain PGE. Of the 18 grains investigated, six analyses contain barely detectable concentrations of Ru (maximum 0·01 ppm), one has Os (0·01 ppm), one has Ir (0·02 ppm), and two have Pt and Au (0·01 ppm; Supplementary Data Electronic Appendix 8).

DISCUSSION

Merensky Reef: broad observations

Many of the chromitites in the Bushveld, including those in the Merensky Reef, occur as laterally continuous horizons that can be traced along strike for hundreds of kilometres (e.g. Wagner, 1929; Cousins & Feringa, 1964; Vermaak, 1976; McLaren & De Villiers, 1982; Campbell *et al.*, 1983; Lee, 1996; Kruger & Schoenberg, 1998; Cawthorn & Webb, 2001; Barnes & Maier, 2002*a*; Cawthorn *et al.*, 2002). Even so, rather than representing single layers many of these, including UG-2, can better be regarded as packages formed of a number of superimposed layers (e.g. Hiemstra, 1985, 1986; Scoon & Teigler, 1994; Lee, 1996; Kinnaird *et al.*, 2002; Cawthorn, 2004; Cawthorn, 2010).

In some areas the Merensky Reef noticeably cuts through layering in the footwall (Fig. 5). This has led to the recognition that the contact represents an erosional surface with the lowermost unit above the unconformity comprising chromitite (most common), pegmatitic pyroxenite or melanorite (e.g. Feringa, 1959; Viljoen *et al.*, 1986*a*, 1986*b*; Eales *et al.*, 1988; Mathez *et al.*, 1997; Kruger, 2005b; Naldrett *et al.*, 2009). At BRPM, the Merensky contact cuts several metres down into the anorthosite, as shown by the truncation of both pyroxene

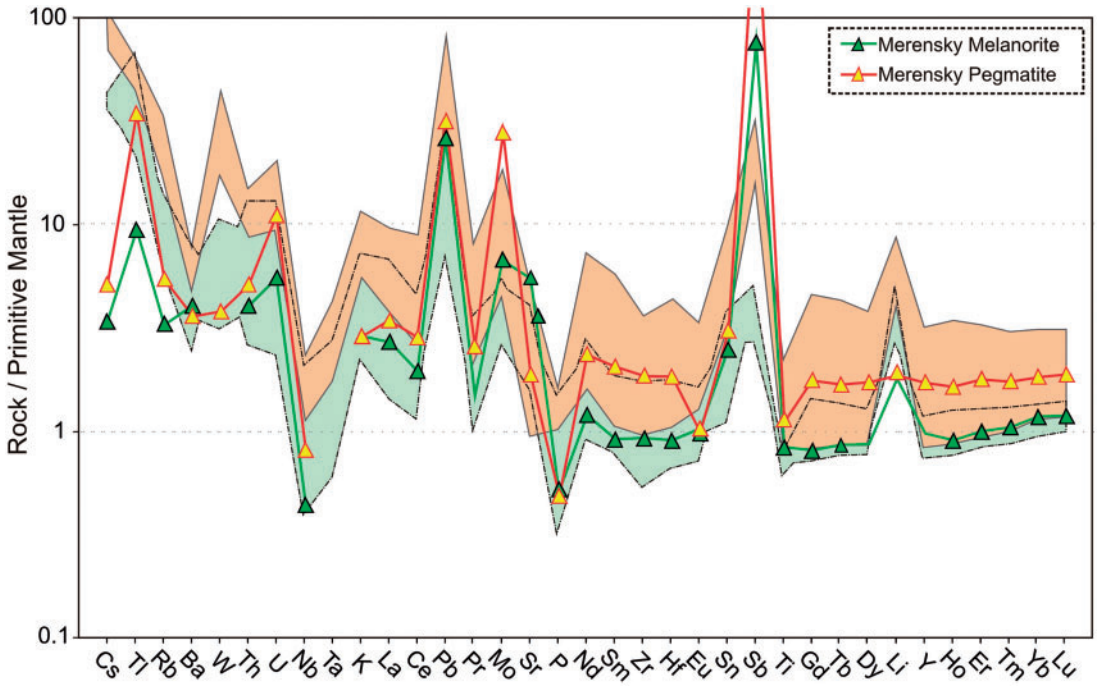

Fig. 17. Primitive mantle normalized trace element patterns for the Merensky pegmatite and melanorite together with fields for the upper (green) and lower (orange) portions of the Platreef. Data are normalized to primitive mantle values from Palme & O'Neill (2004).

layering and single pyroxene oikocrysts (mottles) (Figs 4a and 5). The same feature is also shown by our Impala sample (Fig. 4c).

The stratigraphy of the Merensky Reef varies around the complex. For example, up to four chromitites have been recorded in some areas (e.g. Lee, 1996), including at Western Platinum Mine (Cawthorn & Boerst, 2006). In some parts of the reef a pegmatite, or coarse-grained melanorite, occurs between the two lower chromitites, as, for example, in some areas of BRPM (Moodley, 2008), Impala (Barnes & Maier, 2002*a*; Cawthorn & Boerst, 2006; Godel *et al.*, 2007) and Rustenburg Platinum Mines (RPM) (Ballhaus & Stumpfl, 1986; Nicholson & Mathez, 1991; Prichard *et al.*, 2004*a*; see also Wagner, 1929). In other parts of the reef this silicate layer is absent, which includes both our samples from BRPM and Impala (Fig. 4). In the RPM sample studied by Vukmanovic *et al.* (2013) this silicate layer is only millimetres thick. Both our samples do, however, include a pegmatite above the upper chromitite, although it is notably thinner in the Impala sample and in places is only a few grains deep (Fig. 4). Naldrett *et al.* (2009) also noted that the basal chromitite, particularly in the SW of complex, may comprise only one layer. These relationships seem perplexing, but the explanation proposed by Naldrett *et al.* (2009) is that emplacement of the Merensky magmas led to substantial erosion of the magma chamber floor, which in the NW of the complex may be up to 16 m. The presence or absence, and apparent thinning, of single units can, therefore, be attributed to various degrees of erosion (or non-deposition) of pre-existing layers together with deposition of new ones [broadly as suggested by Eales *et al.* (1990), Cawthorn & Walraven (1998), Cawthorn & Boerst (2006), Naldrett *et al.* (2009) and Cawthorn (2010)]. It was further noted by Eales & Cawthorn (1996) that 'small influxes [of magmas] yielded localized partial cyclic units <1 m thick' (i.e. magmatic events can produce thin layering). These ideas are consistent with other research on the Bushveld that invokes thermo-mechanical erosion of existing layering to explain the origin of potholes and dimpling (e.g. Schmidt, 1952; Ferguson & Botha, 1963; Irvine *et al.*, 1983; Campbell, 1986; Eales *et al.*, 1988; Viljoen, 1999; Kruger, 2005*b*; Roberts *et al.*, 2007; Naldrett *et al.*, 2009).

Chromitites at BRPM

The presence of two chromitite layers in our BRPM sample can be distinguished on textural, geochemical and mineralogical grounds (Figs 7 and 12; Tables 1 and 2). The sizes of the chromite grains have attracted a lot of interest. Hulbert & Von Gruenewaldt (1985) proposed that 'sintering' of smaller grains, such as those found in our upper chromitite, could produce larger grains. Their sintering model explains the floating 'island-like' textures similar to those in our lower chromitite and the silicate inclusions that are in optical continuity with the adjacent silicates. Eales (2000) also considered that larger chromites formed in response to annealing, whereas Li *et al.* (2005) believed that chromites at Impala represent single crystals. A recent study by Vukmanovic *et al.* (2013) of similarly textured grains to our lower chromitite, taken from nearby RPM, suggests that the larger chromites are single grains. Additional evidence to support a single

Table 3. Summary of PGE, Bi and Co concentrations (ppm) in sulphides from the Merensky and Platreef samples shown in Fig. 19a–g

Sample	Lithology	Depth*	Phase	Os	Ir	Ru	Pt	Pd	Rh	Bi	Co
Merensky-4 Laser-4	Chromitite (Mer-ChL)	0–1·1 cm	Cp	<0·110	0·21	0·30	0·05	0·42	10·29	<0·027	9·0
			Pn	0·15	90·71	6·07	4·59	98·55	3401·3	<0·016	4267·7
			Po	<0·045	40·06	3·90	116·31	5·14	338·00	18·18	5114·7
Merensky-4 Laser-12	Pegmatite (Mer-Peg)	1·6–1·9 cm	Cp-2	<0·059	<0·006	0·24	0·04	0·08	0·42	0·03	0·1
			Cp-3	<0·006	<0·002	0·27	0·04	0·06	0·23	0·04	0·3
			Pn-5	1·72	2·21	5·39	4·56	83·31	22·50	<0·018	5458·5
			Pn-6	6·91	0·91	29·96	5·56	87·38	18·53	0·02	5450·0
			Pn-7	1·30	2·14	1·60	4·86	84·38	15·85	<0·016	5371·8
			Po-3† (low-Co)	<0·238	<0·044	<0·205	0·43	<0·096	<0·023	0·60	22·5
			Po-3† (high-Co)	<0·522	1·41	2·16	8·19	<0·228	1·53	2·40	622·9
Merensky-2 Laser-2	Melanorite (Mer-Nor)	4·2–6·9 cm	Cp-1	<0·060	<0·017	<0·119	<0·004	<0·053	<0·102	0·43	<0·163
			Cp-2	<0·063	<0·018	<0·124	<0·008	<0·055	<0·073	0·25	<0·157
			Pn-1	2·76	0·79	28·37	0·66	171·47	43·53	0·75	6839·5
			Pn-2	1·61	0·57	13·73	0·73	153·34	32·98	3·99	6771·3
			Po-1	2·04	3·57	18·61	1·02	1·95	1·94	1·23	107·0
			Po-2	1·16	1·66	6·86	0·06	<0·071	0·12	0·24	31·6
Platreef-9i Laser-1	Feldspathic pyroxenite	254·06–254·14 m	Cp-1	<0·012	<0·003	<0·023	<0·024	<0·012	<0·07	0·31	0·1
			Cp-2	<0·692	<0·190	<1·349	0·33	<0·696	<0·724	<0·787	<1·622
			Pn-1	1·38	1·10	6·22	0·05	88·34	6·40	0·33	6593·7
			Pn-2	0·30	1·21	0·94	0·02	92·07	4·84	0·04	6519·1
			Po-1	1·06	1·33	3·81	0·45	<0·010	0·02	0·33	85·9
			Po-2	1·25	1·44	5·21	0·13	0·05	0·03	0·14	93·7
Platreef-23i Laser-3	Vari-textured feldspathic pyroxenite	293·02–293·31 m	Cp-1	<0·011	<0·003	<0·021	0·01	<0·010	0·05	0·64	0·4
			Cp-2	<0·524	<0·142	<1·010	<0·080	<0·564	<0·648	<0·441	<0·294
			Pn-1	0·38	0·36	1·28	0·03	73·05	4·02	0·10	9117·9
			Pn-2	0·25	0·56	1·91	0·07	64·42	5·78	<0·158	8839·0
			Po-1	0·39	0·60	2·24	0·20	<0·008	0·03	0·40	106·7
			Po-2	0·45	0·60	1·79	0·09	<0·024	0·05	0·22	100·3
			Po-3	0·40	0·59	2·46	0·02	<0·006	0·02	0·32	98·2
Platreef 24ii Laser-2	Vari-textured feldspathic pyroxenite	295·22–295·39 m	Cp-1	<0·561	<0·154	<1·101	<0·087	<0·526	0·83	<0·458	<1·286
			Pn-1	0·20	<0·032	3·82	<0·024	109·47	<0·145	<0·080	8609·6
			Po-1	0·48	<0·002	3·89	<0·001	<0·006	<0·009	0·03	38·8
Platreef 31i Laser-1	Vari-textured feldspathic pyroxenite	310·86–310·96 m	Cp-1	<1·833	<0·515	<3·556	<0·214	<1·756	<2·357	<1·593	<2·045
			Cp-2	<0·053	<0·015	<0·102	<0·007	0·09	<0·060	0·03	1·3
			Pn-1	0·30	0·11	1·12	0·01	141·02	2·71	0·07	8087·8
			Pn-2	0·43	0·09	2·29	<0·005	140·70	1·65	0·03	8009·2
			Po-1	0·42	0·47	2·05	0·02	0·07	0·07	0·09	46·6
			Po-2	0·40	0·51	2·12	0·02	0·02	0·20	0·04	42·7

*Depth for the Merensky samples denotes height relative to the anorthosite-chromitite contact.
†Po-3 (low-Co) and Po-3 (high-Co) zones of low and high Co in the same pyrrhotite.
<*x*, concentration below detection. Po, pyrrhotite; Pn, pentlandite; Cp, chalcopyrite. Additional data are given in Supplementary Data Electronic Appendix 9.

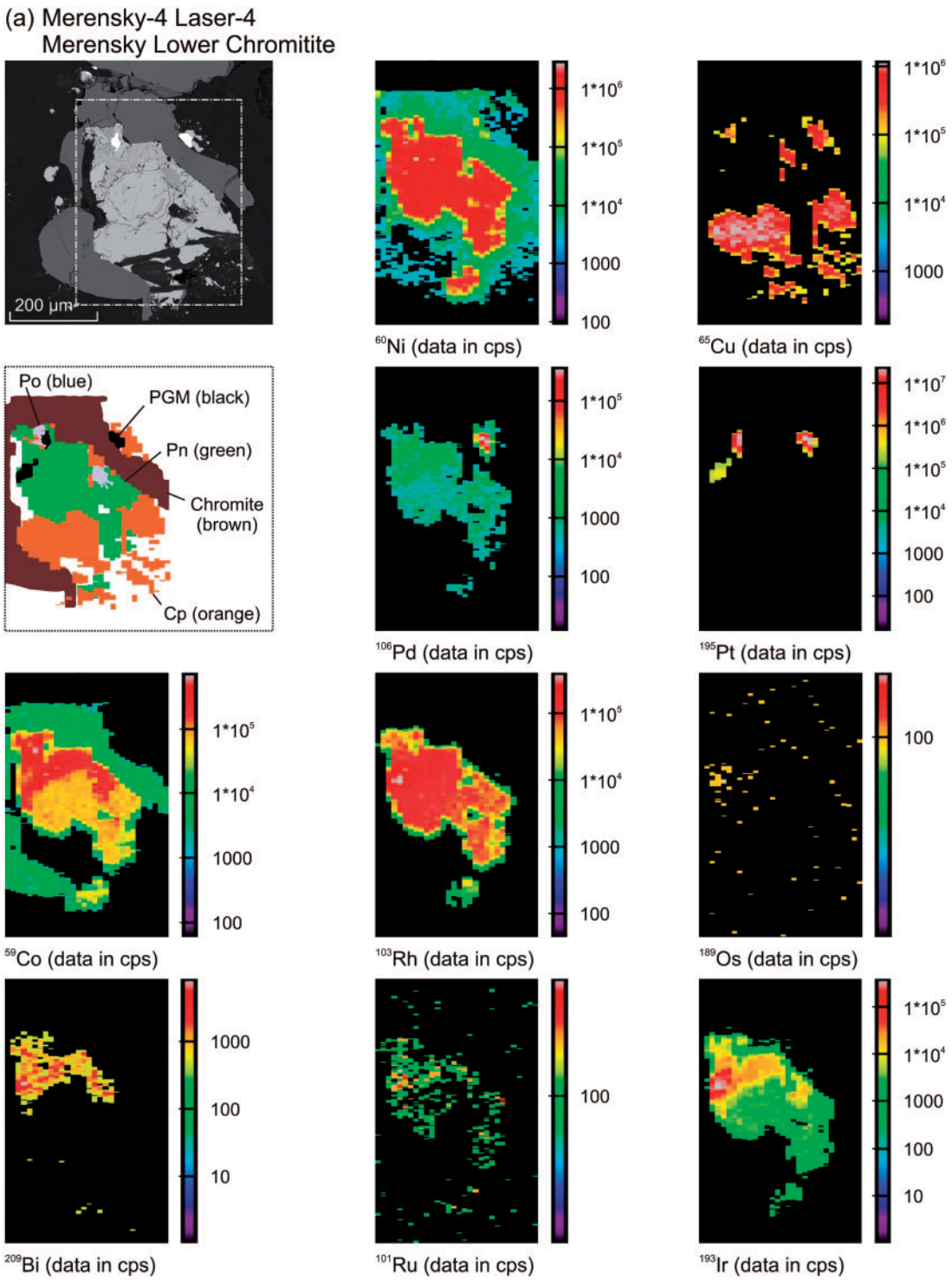

Fig. 18. Selected LA-ICP-MS trace element maps for Merensky and Platreef sulphides. Top left, backscattered electron image. Below, a colour coded map for the sulphides. Counting times for all elements were 20 ms, except for Pt (200 ms). (a) Merensky lower chromitite (Mer-ChL), (b) Merensky pegmatite (Mer-Peg) and (c) Merensky melanorite (Mer-Nor). (d–g) Sulphides from the upper (moderately contaminated), and central to lower (highly contaminated) Platreef from drill-hole TN207. Quantified spot analysis concentrations are given in Table 3 and Supplementary Data Electronic Appendix 9. The presence of large Pt-PGM has masked the presence of Pt in the sulphide shown in (a) (Merensky-4 Laser-4). Spot data for this sulphide are given in Fig. 19 and Table 3. cps, counts per second.

(continued)

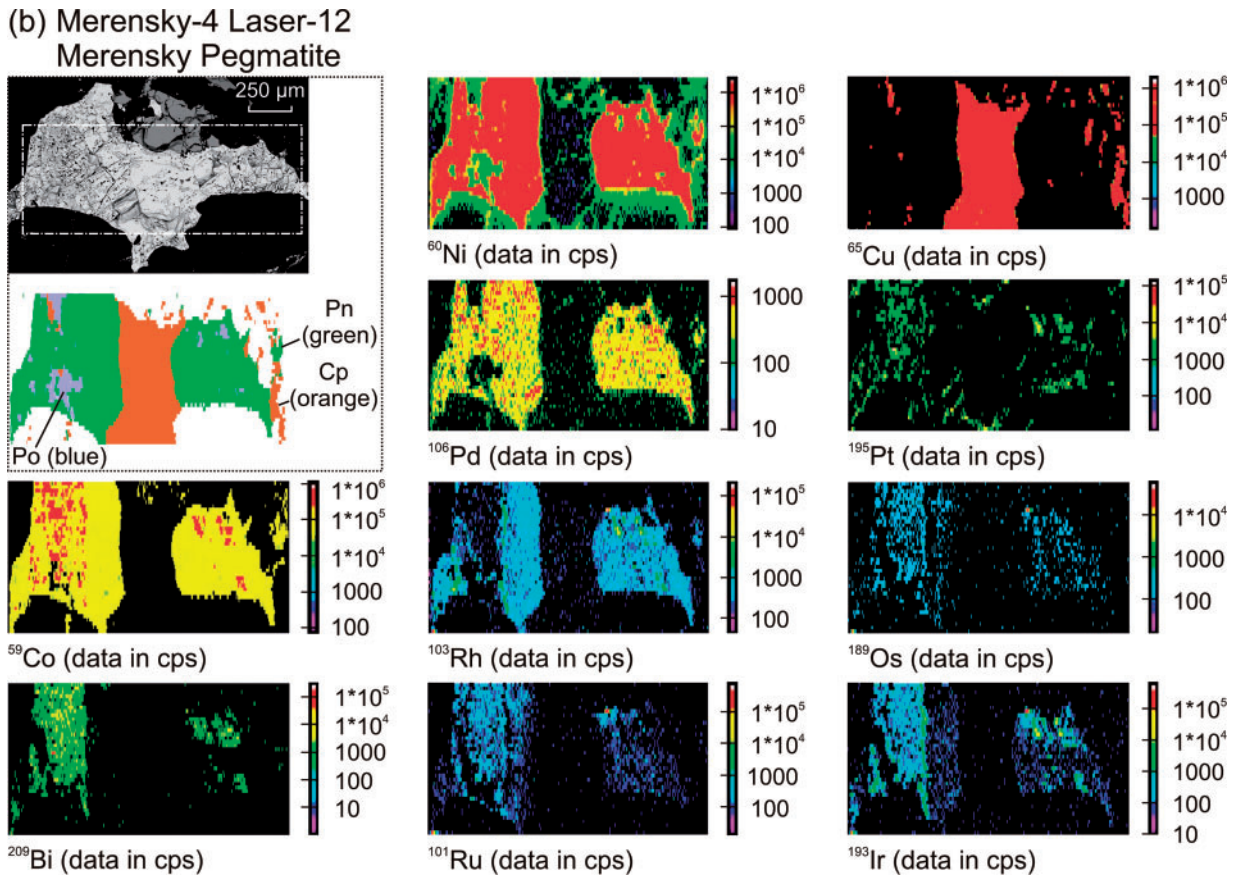

Fig. 18. (continued)

grain origin from this study comes from: (1) The non-annealed nature of the smaller, and more closely packed chromite grains in the upper layer (Fig. 7); this is significant given that the chromites in the upper layer are similarly enclosed within plagioclase and orthopyroxene oikocrysts that might otherwise suggest that conditions were conducive for their recrystallization into larger grains, (2) The presence of larger chromite grains and clusters within the finer grained upper layer that have comparable compositions to those of the lower layer (Fig. 12), and (3) The observation that the larger upper layer grains are texturally similar to some of the subhedral textured grains in the lower layer. The latter two points suggest that the size of the larger grains is an original crystallization feature and that their presence in the upper layer is due to inheritance (i.e. they did not form in-situ but were transported into their current position). Together with the textural evidence for the subhedral morphology exhibited by some grains in the lower layer (Fig. 7), it is suggested that the chromites originally had euhedral to subhedral textures and that their current irregular shapes are the result of post-magma emplacement processes.

Competing models for chromitite formation

A number of mechanisms have been proposed for the origin of chromitites in the Bushveld and elsewhere. These include the following: (1) magmatic differentiation, which typically requires olivine on the liquidus (Wager & Brown, 1968); (2) an increase in silica (Irvine, 1975); (3) mixing of a primitive mafic magma with a more evolved magma (Irvine, 1977*a*, 1977*b*); (4) increasing temperature (Sampson, 1932); (5) changes in fO_2 (Cameron & Desborough, 1969; Ulmer, 1969); (6) increasing pressure (Cameron, 1977; Lipin, 1993); (7) breakdown of pyroxene in the presence of volatile-rich fluids (e.g. Nicholson & Mathez, 1991; Mathez, 1995).

The argument proposed by Cawthorn (2005), based on the ideas of Cameron (1977) and Lipin (1993), for chromite crystallization within a magma owing to instantaneous pressure increase is appealing. However, it has been shown experimentally that Cr solubility in a mafic melt may actually increase with increasing pressure (Roeder & Reynolds, 1991). It is also hard to reconcile this model given the limitation that, at any given time, the roof of the complex was most probably 'floating' on the mafic magmas (Kinnaird *et al.*, 2002; Kruger, 2005b; Cawthorn, 2013). It was also noted by Hatton & Von Gruenewaldt (1989) that pressure increases >1 kbar would be required to initiate chromite formation, although this is not reflected in the mineralogy (Hatton, 1984). Furthermore, the chromites in our lower layer are relatively coarse grained, which would have required elevated and sustained pressures over an extended length

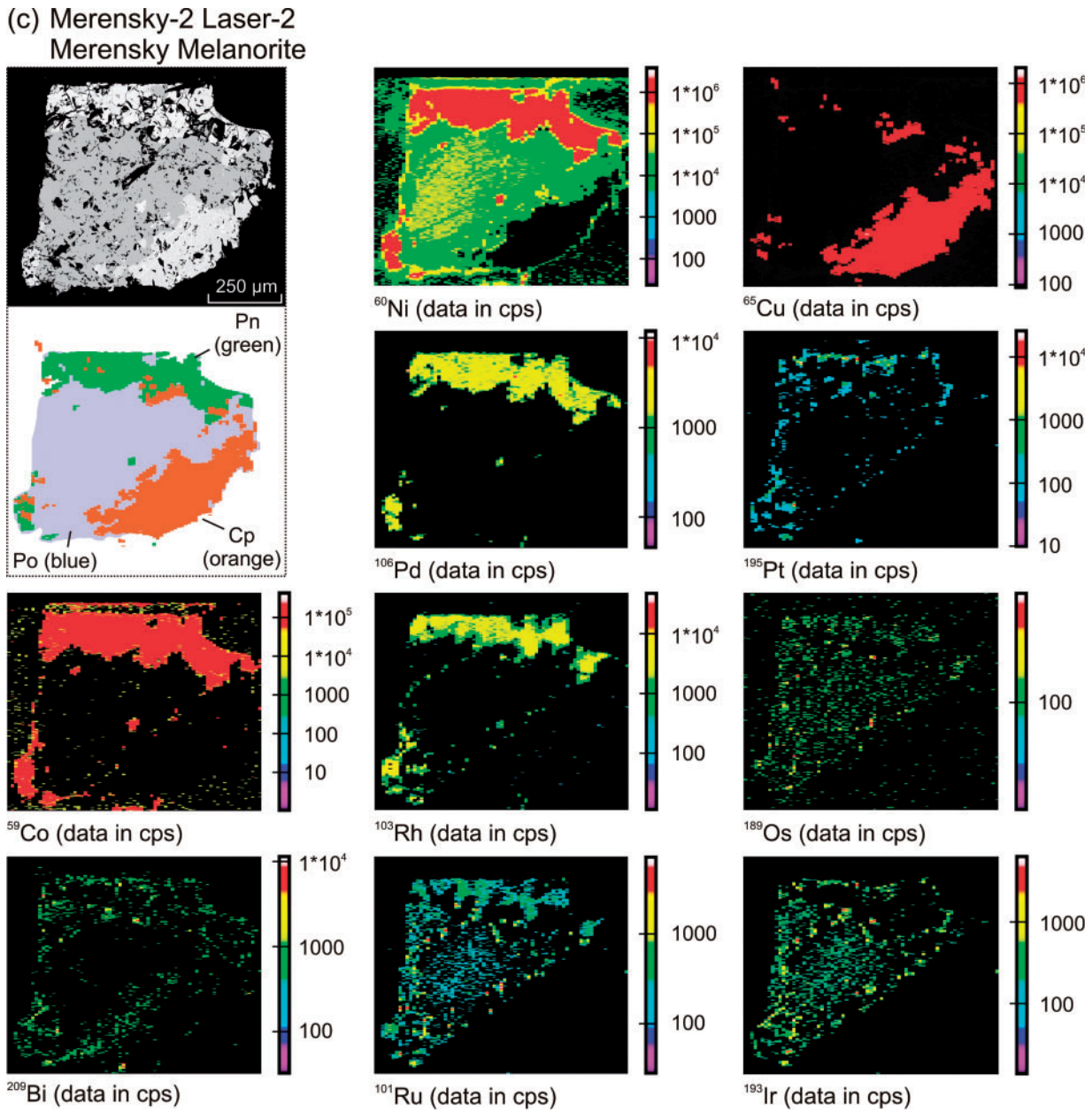

Fig. 18. (continued)

of time; this seems unlikely given the arguments above. Lastly, models involving pressure increase leading to chromitite formation cannot easily explain the observed variability in the number, thickness and relative positions of the chromitites within the Merensky Reef.

Models involving the addition of silica to form the Merensky chromitites through the digestion of the magma chamber roof have been favoured by many researchers (e.g. Scoon & Teigler, 1994; Kruger & Schoenberg, 1998; Schoenberg *et al.*, 1999). This is supported by evidence that the magmas in the Upper Critical Zone have assimilated Si from the digestion of crustal rocks (e.g. Arndt *et al.*, 2005). However, models of Si addition alone that lead to chromite precipitation were later refuted by Irvine (1977*a*) on the grounds that they would require implausible amounts of siliceous rock assimilation [see also discussion by Mondal & Mathez (2007)].

Models for the origin of the chromites involving magma mixing remain popular (e.g. Eales *et al.*, 1990; Schoenberg *et al.*, 1999; Li *et al.*, 2005; Voordouw *et al.*, 2009). However, this was rejected for the origin of the UG-2 chromites by Mondal & Mathez (2007), although some of their arguments against it may in fact be valid for the Merensky Reef. For example, they pointed out that there is no compositional change in the silicates from the footwall to the hanging wall and no olivine is present as predicted from this process. However, olivine is present in the Merensky Reef silicates in the NW Bushveld and its footwall is demonstrably erosional

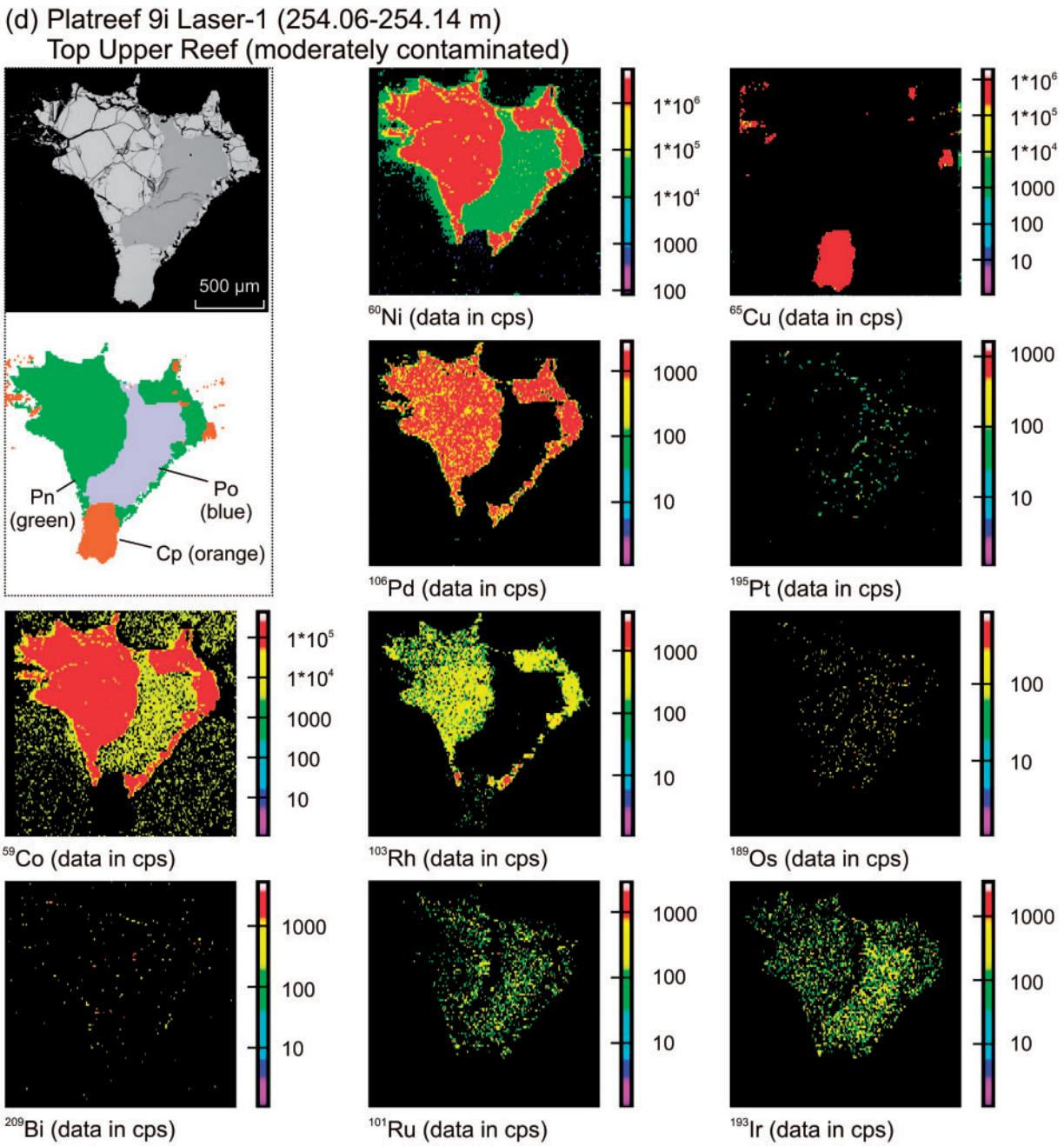

Fig. 18. (continued)

(Naldrett *et al.*, 2009), which raises uncertainty about the composition of the footwall silicates at the time of magma emplacement.

A number of researchers have concluded instead that a combination of processes lead to the formation of chromite; for example, Si addition combined with magma mixing (e.g. Scoon & Teigler, 1994; Kinnaird *et al.*, 2002; Kruger, 2005b). One of the fundamental problems faced by models that attempt to explain the formation of chromitites is the so-called 'Cr-paradox'. This recognizes that the combined amount of Cr contained within chromite and silicate phases cannot be accounted for by the volume of magma from which they were derived (Eales & Cawthorn, 1996; Cawthorn & Walraven, 1998; Eales, 2000; Eales & Costin, 2012). As discussed by Eales (2000), this paradox can be resolved if the chromites themselves were emplaced as 'phenocrysts'.

The model preferred by Mondal & Mathez (2007) for UG-2 is elegantly simple and hinges largely on the principle that chromite and opx are both liquidus phases based on their modelling using MELTS. They proposed that a 67 cm thick chromitite can be produced from a magma column 56 m high, with a volume of $2{\cdot}5 \times 10^3$ km^3, containing 1·2% (mode) of chromite. Based on calculations by Rice & Eales (1995) for the

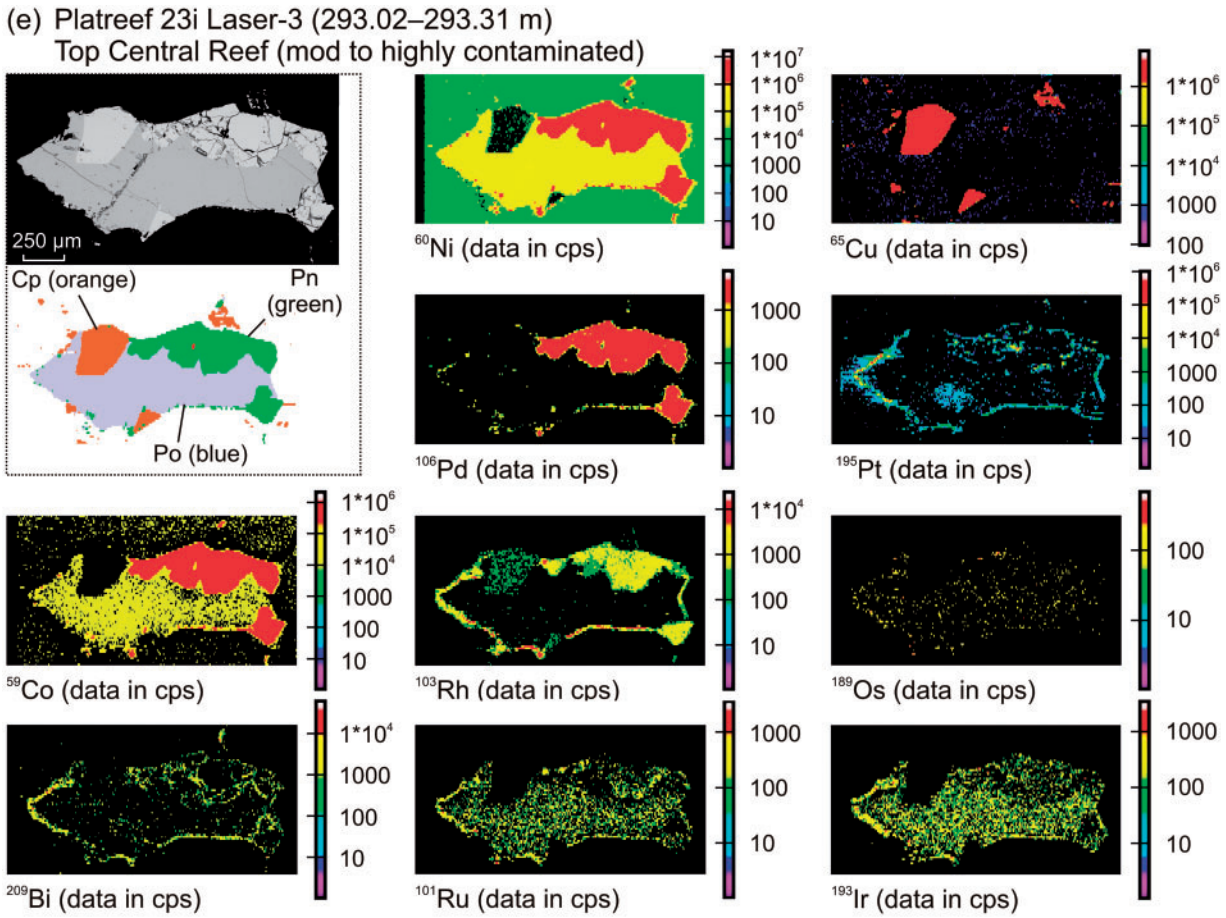

Fig. 18. (continued)

magma transporting capacity for olivine and pyroxene (~1 mm in size), the magmas were more than capable of transporting the larger Merensky chromites (~4·6 g cm^{-3} and ~2 mm). However, to produce a chromitite layer grains of chromite must be separated from the magma column, which Mondal & Mathez (2007) postulated may be a mechanism known as 'kinetic sieving', after Marsh (2004) and Gray *et al.* (2006). The limitations with the Mondal & Mathez (2007) model are (1) the regional-scale emplacement of opx-rich magma (i.e. crystal mush) and (2) the high degree of efficiency required to separate all the chromite from an orthopyroxene-phyric magma (the silicates overlying the chromitites contain very little chromite). These problems largely disappear if some mechanism allowed chromite saturation to occur before opx.

Different lines of reasoning have led to the development of two alternative mechanisms for the origin of chromitite layering. The common theme of these models is that chromite grains form *in situ*, either by direct crystallization from a magma (e.g. Latypov *et al.*, 2013; Vukmanovic *et al.*, 2013), or through replacement of pre-existing silicate rocks (e.g. Nicholson & Mathez, 1991; Mathez, 1995). The observation of biotite in inclusions within the chromite (e.g. Li *et al.*, 2005) adds weight to the argument that the chromites formed as a consequence of hydromagmatic processes (e.g. Nicholson & Mathez, 1991; Mathez, 1995). Supporting evidence from the study by Nicholson & Mathez (1991) includes the presence of 'inclusions of pyroxenite identical to the hanging-wall and of leuconorite identical to the footwall' in the pegmatite. Similar observations have been reported elsewhere (e.g. Viljoen & Hieber, 1986; Naldrett *et al.*, 2009). The explanation by Naldrett *et al.* (2009) was for 'the incorporation of blocks of footwall cumulates into the Merensky pyroxenite' (i.e. mechanical processes). Mondal & Mathez (2007) later rejected models involving 'replacement' for the origin of the UG-2 chromitite, owing in part to the enormous volume of silicate rock that would be required to 'dissolve'. Although the volume of silicate rock required to form our lower ~9 mm layer chromitite is less than UG-2 [67 cm as used in the Mondal & Mathez (2007) model], the same principle applies. Additional evidence for hydrothermal–hydromagmatic processes comes from the presence of volatile-rich saline fluids in quartz found in parts of the reef [e.g. Ballhaus & Stumpfl, 1986; see also discussion by Mathez (1995) and Mondal & Mathez (2007)]. Even so, hydromagmatic–hydrothermal models for the origin of the Merensky Reef chromitites cannot account for the presence of two texturally, mineralogically and geochemically different chromitites

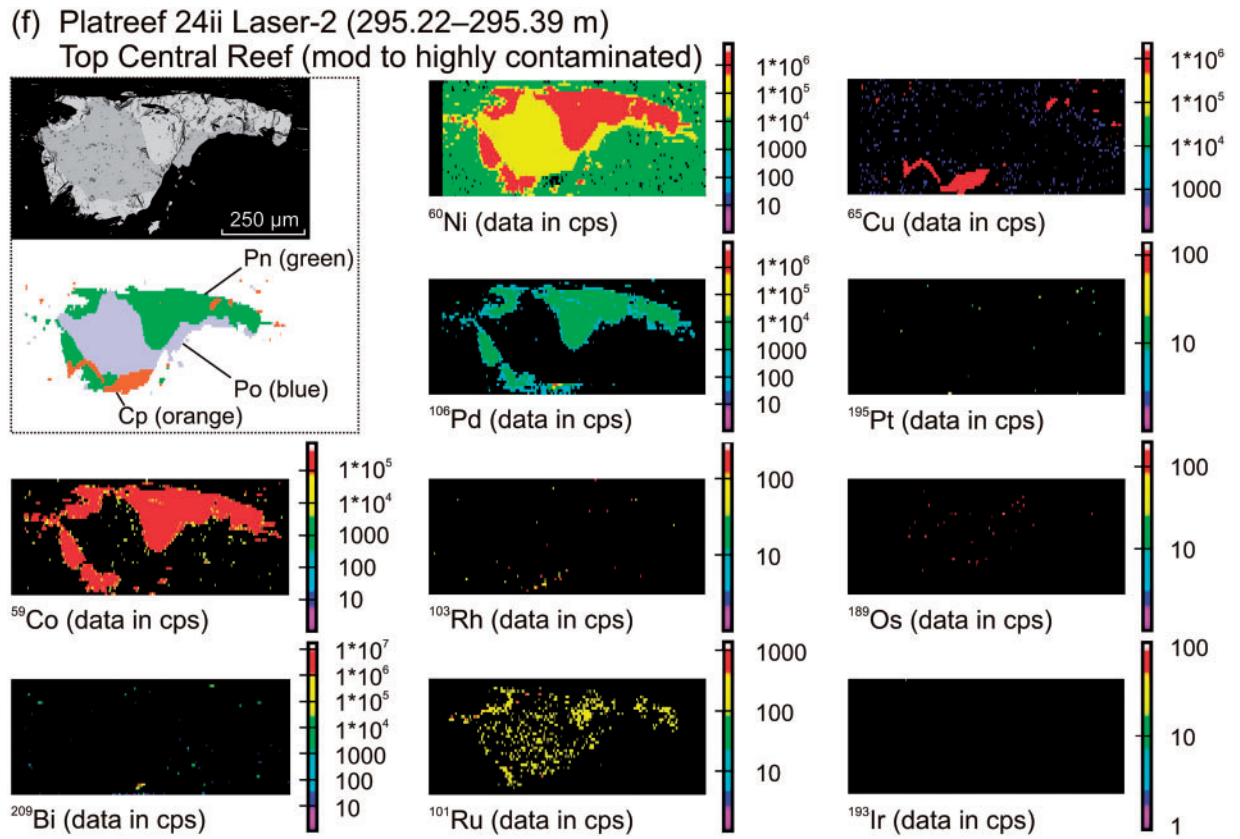

Fig. 18. (continued)

superimposed on one another (Figs 4, 7 and 12). We have also observed subvertical fractures in the lower chromitite filled with chromite from the upper layer (Fig. 7). This is hard to explain though hydrothermal processes; however, it is consistent with a magmatic origin, as it shows that the lower chromitite was near fully crystallized with open-spaced brittle fractures within which the smaller grains from the upper layer chromitite were trapped.

Recent publications have instead proposed that the chromites crystallized *in situ* from magma within the chamber (e.g. Latypov *et al.*, 2013; Vukmanovic *et al.*, 2013). Latypov *et al.* (2013) argued that the chromitites follow the undulations in the footwall topography with constant thicknesses, based on cross-sections published by Viljoen (1999) and redrawn by Naldrett *et al.* (2009). Models involving *in situ* crystallization of chromite would be expected to produce near-constant layer thicknesses, with grains either in contact with one another if chromite-only crystallization occurred, or grains dispersed within silicates as the magma–silicate interface grew. However, Naldrett *et al.* (2009, fig. 4c) drew attention to the fact that the published cross-sections are sketches and that field observations from the underground section at RPM 'Townlands Shaft' show that 'the thickness of the chromite is controlled by undulations in the contact'. They ascribed this to 'chromite carried as a bottom load that became concentrated in hydraulic traps'. This observation is pivotal, and is supported by our observations from BRPM that show chromite filling an erosional scour channel cut into the footwall anorthosite (Fig. 5c). Elsewhere, features including xenoliths of silicate rocks (anorthosite and melanorite) have been observed within the UG-1 and UG-2 chromitites (Voordouw *et al.*, 2009, table 7). Such features are not easily explained by *in situ* crystallization of chromitite or by hydrothermal–hydromagmatic processes. They are, however, consistent with physical processes including transport and deposition of grains and rafts by magmas that were eroding their floor; and with our observation of subvertical fractures in the lower chromitite filled with chromite from the upper layer, as discussed above. None of these arguments tell us where the chromites formed, only that they were transported and deposited by high-energy magmas. This could have arisen in response to (1) remobilization of pre-existing layering within the chamber [i.e. the subsidence-induced slumping model of Maier *et al.* (2013)], (2) crystallization with transport and deposition of chromite inside the chamber, possibly near a feeder (e.g. Scoon & Teigler, 1994; Kruger & Schoenberg, 1998; Schoenberg *et al.*, 1999; Naldrett *et al.*, 2009), or (3) chromite formation in a staging chamber (e.g. Eales, 2000; Arndt *et al.*, 2005; Mondal & Mathez, 2007; Eales & Costin, 2012) or conduit (e.g. Maier & Barnes, 2008; Voordouw *et al.*, 2009).

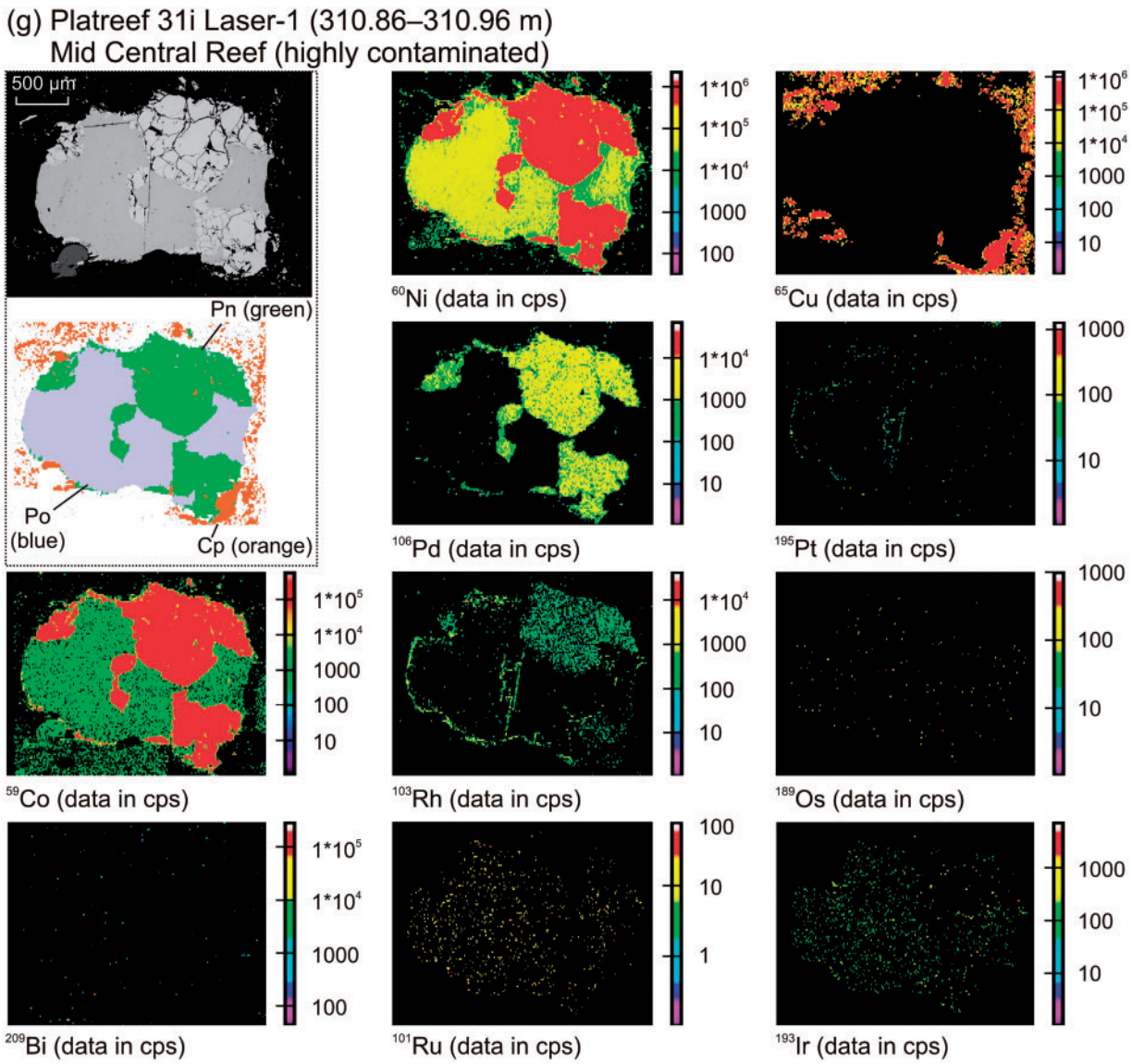

Fig. 18. (continued)

Origin of the poikilitic silicate textures

It was noted that the plagioclase in the footwall anorthosite has a restricted range in An content (74–81; Fig. 13). This is similar to plagioclase compositions reported elsewhere that range from An_{78} to An_{80} (e.g. Vermaak, 1976; Kruger & Marsh, 1985; Naldrett *et al.*, 1986). Conversely, the poikilitic plagioclase in the chromitite layers above the anorthosite has a significantly broader range of An (66–89; Fig. 13). A key observation is the recognition of ghost outlines of plagioclase crystals within the large feldspar oikocrysts in the lower chromitite. These are of a similar size and shape to the plagioclase crystals in the anorthosite immediately below the chromitite. Together with the compositional evidence, the origin of the plagioclase in the lower chromitite can best be explained as the product of partial melting and recrystallization of pre-existing cumulus crystals derived from the footwall. Eales *et al.* (1988, 1990) recognized that erosion of anorthosite in the footwall would release significant amounts of plagioclase into an intruding magma. They argued that a portion of this plagioclase would be resorbed, whereas some would become trapped as inclusions within crystallizing silicates (e.g. orthopyroxene). Those plagioclase grains that survived would be expected to exhibit textures indicative of disequilibrium, as observed in Merensky norites by Eales *et al.* (1990). Similar arguments can be applied to the pyroxene. Broadly speaking, two groups of orthopyroxene are recognized from the major and trace element geochemistry (Figs 14 and 20): (1) those in the anorthosite and both the chromitites; (2) those in the pegmatite and melanorite. The orthopyroxene in the chromitites and anorthosite could, therefore, be genetically related, as could the cumulus pyroxenes in the pegmatite and melanorite; however, the differences between these two groups suggests that they are not related to the same parent melt [as similarly concluded by Mathez (1995)]. The poikilitic pyroxene in the

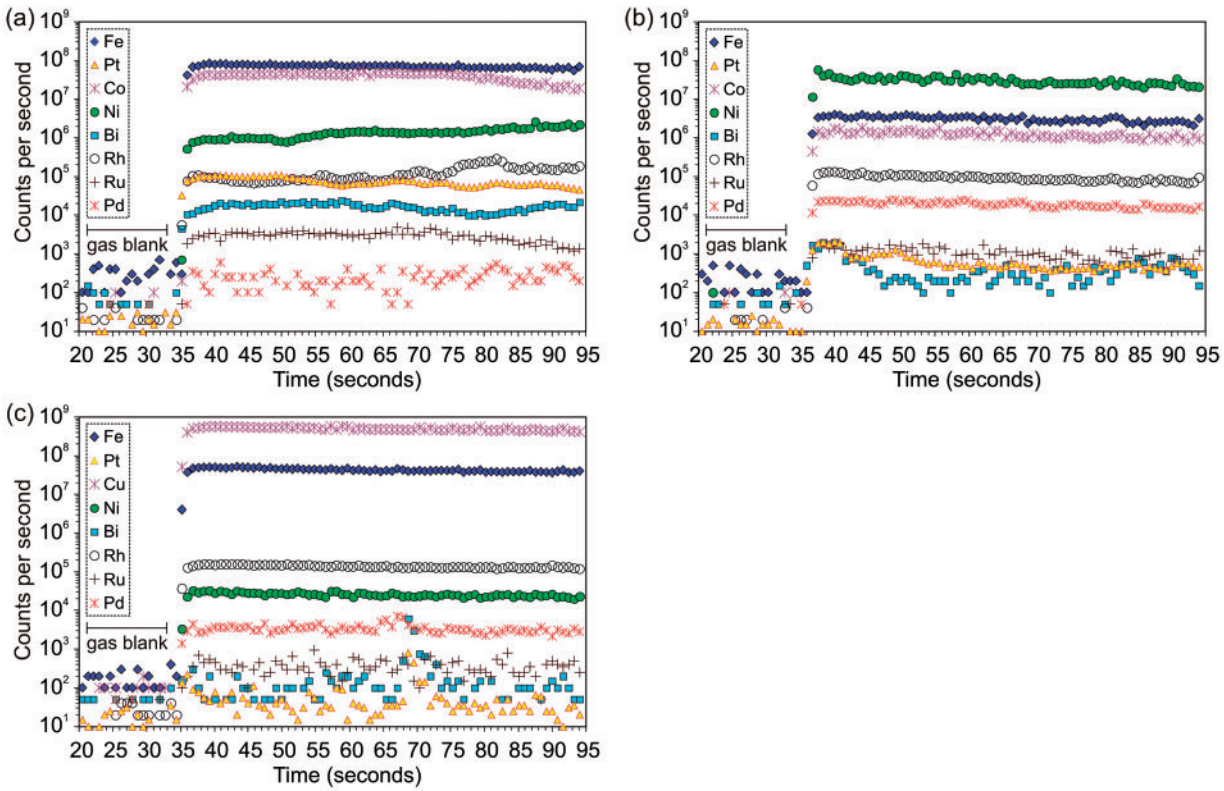

Fig. 19. Time-resolved analysis (TRA) diagram for sample Merensky-4 Laser-4. (a) Pyrrhotite. (b) Pentlandite. (c) Chalcopyrite. All analyses include a 35 s gas blank followed by 60 s of analysis.

chromitites, like the plagioclase, may therefore be the recrystallized product of material reworked from the footwall. Additional evidence to support this comes from the presence of small zircon and rutile crystals within the chromitites that are relatively common accessory minerals in the anorthosite, but are less common in the Merensky silicates. The presence of material reworked from the footwall may explain the 'island-like' floating textures of the chromite in the lower chromitite, as it would have restricted any downward settling of crystals. This did not occur in the upper chromitite and, consequently, these chromite grains are closely packed.

The origin of the chromite textures at BRPM

The highly irregular textures of the lower layer chromites are suggested to have originated by reaction with partial melts that formed the poikilitic plagioclase. Supporting evidence comes from the broad spread of Cr/(Cr + Al) in the chromites in this layer (e.g. Roeder & Reynolds, 1991). Evidence of their pre-corrosion textures is found in the upper chromitite layer, which contains large inclusion-free singular grains and grain-clusters with subhedral textures that geochemically are similar to the large grains in the lower layer. For the most part, the apparent silicate inclusions in the lower layer chromites are artefacts caused by 2D sections cut through highly irregular 3D grains (Fig. 8). In the rare cases where silicates are fully enclosed by chromite, these most probably formed through the mechanism outlined by Cawthorn & Boerst (2006) for the pegmatites: 'The reconstitution process envisaged here involved both recrystallisation and remelting; both occurred concurrently. An analogy may be noted in which packed ice cubes in a glass of water may both melt and combine into a single, solid mass.' The presence of micron-sized inclusions that often form rings around the larger inclusions provides additional evidence to support a chemical corrosion model (Fig. 9c and e). Rather than a mineral growth phenomenon, these formed as a consequence of corrosive fluids channelled along preferred crystallographic orientations.

Competing models for sulphide and PGE mineralization

Models developed to explain the petrogenesis of our sample need to account for several coexisting features: (1) similarity in the PGE contents in the two chromitite layers, but with distinct differences to three silicate layers (Table 2); (2) extremely high Pt/Pd ratios in the chromitites (~11), with lower Pt/Pd in the pegmatite (3·0) and melanorite (0·4) (Table 2); (3) selective PGE enrichments in the chromitites, specifically for Pt, Ru, Ir and Rh (Fig. 15; Table 2); (4) the presence of unique PGM assemblages in each of the five main petrological and mineralogical layers (Fig. 6; Table 1), including the

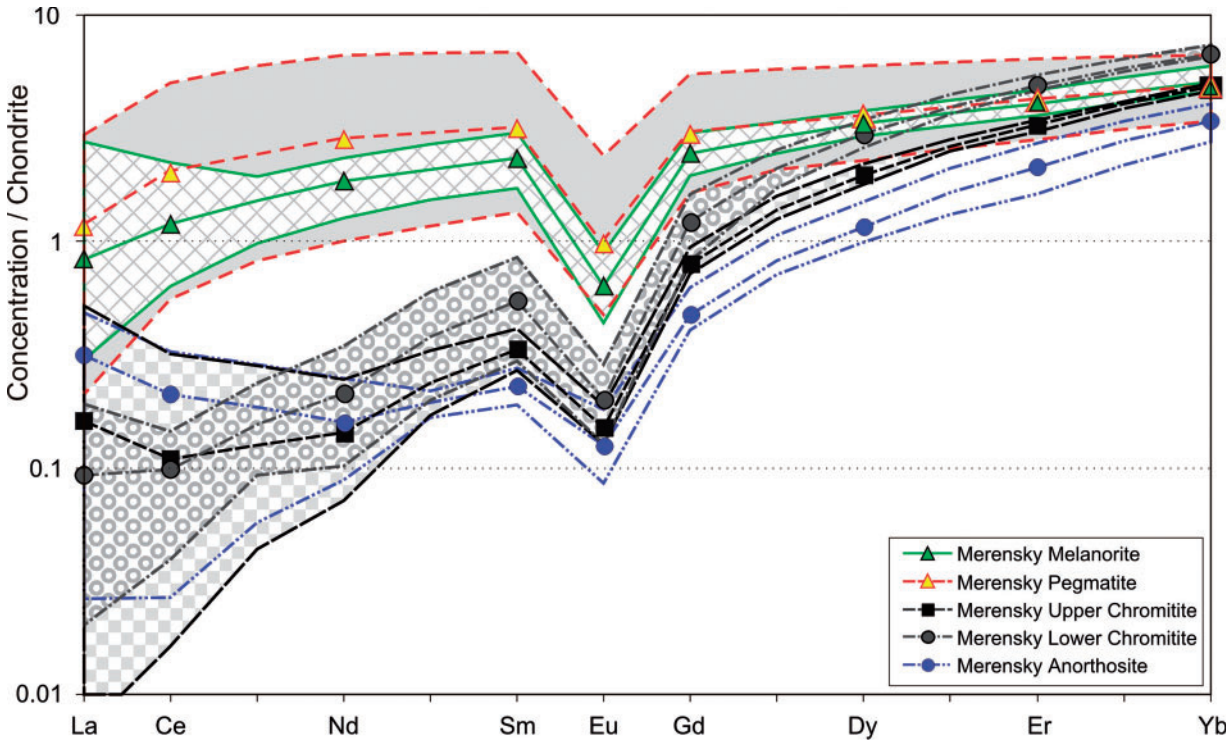

Fig. 20. Chondrite-normalized REE patterns for orthopyroxene. Concentration ranges are shown as shaded fields with averaged data as lines with symbols. Normalized to chondrite values from McDonough & Sun (1995).

occurrence of IPGE minerals only in the chromitites (10·6 and 13·3% mode in lower and upper chromitite respectively) and the presence of Pt-arsenides only in the upper chromitite; (5) the low abundance of sulphide in the chromitites (~0·7%) together with their Fe-poor and Ni–Cu-rich compositions (Table 2); (6) the low Pt, Ru, and Ir contents in the sulphides, with the exception of Pd and Rh that occur in pentlandite (Table 3; Supplementary Data Electronic Appendix 9); (7) calculated tenors, particularly for Pt in the chromitites, that are too large to be modelled by mechanisms of PGE capture from sulphide liquids (Fig. 16; Maier & Barnes, 1999; Ballhaus & Sylvester, 2000; Barnes & Maier, 2002*a*; Godel *et al.*, 2007; Naldrett *et al.*, 2009); (8) the observed variability in the number and relative positions of the chromitite and silicate layers in different parts of the complex.

Similar to the chromite, sulphide liquids can form in response to mixing of an evolved melt with a more primitive melt (Campbell *et al.*, 1983; Naldrett *et al.*, 1990), or a decrease in Fe content through the formation of oxide or silicate minerals (e.g. Haughton *et al.*, 1974; Mathez, 1976). Consequently, assimilation of siliceous wall-rocks combined with magma mixing can promote the formation of both chromite and sulphide liquids. Arndt *et al.* (2005) proposed that the siliceous character of the Merensky magmas was a result of interaction between the magmas and sedimentary wall-rocks, and that sulphide saturation was due to contamination and mixing within a sub-Bushveld staging chamber. This is similar to the ideas of Schoenberg *et al.* (1999), who believed that precipitation of sulphide liquids occurred concurrently with chromite. This, they suggested, was in response to the mixing of primitive and Si-contaminated magmas in the Bushveld magma chamber. A number of researchers have attributed sulphide formation in the Bushveld to magma mixing only (e.g. Eales *et al.*, 1990; Scoon & Teigler, 1994; Schoenberg *et al.*, 1999; Kinnaird *et al.*, 2002; Li *et al.*, 2005; Voordouw *et al.*, 2009). Alternatively, other researchers have argued that the trigger for sulphide saturation is chromite precipitation (e.g. Buchanan, 1976; Teigler & Eales, 1993), as have a number of researchers for other locations (e.g. Page, 1971; Talkington *et al.*, 1983; Prichard & Brough, 2009). Evidence for coeval formation of chromite and magmatic PGE-enriched sulphide liquids in our lower chromitite comes from the presence of PGM-bearing sulphide inclusions with negative shapes in some of the chromite grains (Fig. 9c–f). Similar features have been documented from the Platreef by Holwell *et al.* (2011), which were believed to represent trapped PGE-enriched sulphide liquids. The presence of pyrite in these inclusions can most probably be linked to excess S released by reaction of FeS with chromite (Von Gruenewaldt *et al.*, 1986; Naldrett & Lehmann, 1988; Naldrett *et al.*, 1987). In a closed system this S will react with pyrrhotite to form pyrite (e.g. Holwell *et al.*, 2011).

Three mechanisms can explain the observed Fe-poor (Ni- and Cu-rich) character of the sulphides in the Merensky chromitites as noted here and elsewhere (e.g. Naldrett & Lehmann, 1988; Von Gruenewaldt *et al.*,

1989), as follows: (1) resorption of the FeS from the Ni–Cu–Fe-sulphide; (2) post-crystallization hydromagmatic (particularly chromatographic) processes; (3) decoupling of fractionated sulphides (i.e. Fe-rich monosulphide solid solution 'MSS' from evolved Ni–Cu-rich intermediate solid solution 'ISS' liquids). These are discussed in detail below.

Role of sulphide loss to explain the observed Ni–Cu–PGE mineralization in the Meensky Reef

It has been suggested that sulphide resorption explains the observed low sulphide abundance with high PGE concentrations in the Merensky Reef (Gain, 1985; Naldrett *et al.*, 1987; Naldrett & Lehmann, 1988; Von Gruenewaldt *et al.*, 1989; Mathez, 1999; Barnes & Maier, 2002*a*; Kerr & Leitch, 2005; Naldrett *et al.*, 2009). These models are based on concepts of partial resorption of PGE-bearing sulphides, either owing to interaction with sulphide undersaturated magmas that preferentially remove FeS (i.e. Kerr & Leitch, 2005; Naldrett *et al.*, 2009), or through reaction of FeS with chromite that consumes it (Von Gruenewaldt *et al.*, 1986; Naldrett *et al.*, 1987; Naldrett & Lehmann, 1988; Mathez, 1999; Barnes & Maier, 2002*a*). Some have argued that this occurred *in situ* within the Merensky magma chamber (e.g. Naldrett *et al.*, 1987; Naldrett & Lehmann, 1988; Mathez, 1999; Barnes & Maier, 2002*a*; Kerr & Leitch, 2005), whereas others considered that this occurred in a staging chamber (e.g. Naldrett *et al.*, 2009).

In our chromitites [as with the Impala sample investigated by Barnes & Maier (2002*a*) and Godel *et al.* (2007)], the amount of sulphide in the chromitites is too low for the level of PGE enrichment. This leads to calculated tenors, particularly for Pt, that are too large to be modelled by mechanisms of PGE capture from sulphide liquids (Fig. 16; as also noted by Maier & Barnes, 1999; Ballhaus & Sylvester, 2000; Barnes & Maier, 2002*a*; Godel *et al.*, 2007). Models based on 'in-chamber' processes to explain the observed PGE enrichments in the Merensky chromitites, combined with extremely low amounts of sulphide, involve increasingly complex mechanisms (see review by Barnes & Maier, 2002*a*). Many of these rely on crystallization of PGM as alloys directly from a silicate magma with various mechanisms that lead to their collection and concentration (e.g. Hiemstra, 1979; Keays & Campbell, 1981; Tredoux *et al.*, 1995; Cawthorn, 1999*c*; Ballhaus & Sylvester, 2000; Godel *et al.*, 2007; see review by Barnes & Maier, 2002*a*). One such collector proposed for PGE alloys is chromite (e.g. Hiemstra, 1979; Talkington & Watkinson, 1986; see also Barnes & Maier, 2002*a*). Our analyses of 18 chromites by LA-ICP-MS revealed barely detectable levels of Ru in six analyses, Os and Ir in one, and Pt and Au in two (Supplementary Data Electronic Appendix 8). Furthermore, only one PGE alloy was found in our study out of several hundred PGM (Table 1).

It has been suggested that geologically plausible 'R' and 'N' factors can be achieved by increasing the starting concentrations of Pt (e.g. Naldrett *et al.*, 2009). This model relies on 'up-scaling' of PGE concentrations through the resorption of pre-existing sulphide in a staging chamber. This is comparable with the ideas of other researchers who have suggested the existence of a staging chamber in the Bushveld where sulphide liquids had both formed and captured PGE (e.g. Barton *et al.*, 1986; Lee, 1996; Harris & Chaumba, 2001; Arndt *et al.*, 2005; Hutchinson & Kinnaird, 2005; Holwell & Jordaan, 2006; Holwell & McDonald, 2007; McDonald & Holwell, 2007; Holwell *et al.*, 2007; Mondal & Mathez, 2007; Hutchinson & McDonald, 2008). Nevertheless, the data used for modelling by Naldrett *et al.* (2009) represent bulk averages taken across layering over intervals of 10 or 20 cm (see their table 1). Within an interval of 5 cm in our sample from BRPM we recognize four discrete layers that form part of the Merensky Reef stratigraphy, many of which have widely different PGE contents and Pt/Pd ratios (Fig. 4a; Table 2). The tenors calculated from our two chromitites, together with those reported by Barnes & Maier (2002*a*) from Impala, are substantially higher than those of Naldrett *et al.* (2009). Even considering the potential loss of FeS by the mechanisms outlined above, a five-fold increase in the current volume of pyrrhotite leads to only a 50% reduction in the calculated Pt tenors. This still leads to calculated tenors that are too high to be explained by mechanisms of PGE capture by sulphide liquids. Furthermore, the potential loss of sulphide does not explain the high Pt/Pd ratios (~11) and low Pd/Ir ratios (3·5) in the chromitites (Table 2). Consequently, none of the above arguments can adequately explain the combined characteristics of the Ni–Cu–PGE mineralization in the Merensky Reef outlined in points (1)–(8) in the section 'Competing models for sulphide and PGE mineralization'.

The role of volatiles to explain the observed Ni–Cu–PGE mineralization in the Merensky Reef

Very different lines of reasoning have led to models involving late-stage, volatile-rich fluids to account for the PGE mineralization in the Merensky Reef (e.g. Lauder, 1970; Vermaak, 1976; Kinloch, 1982; Boudreau, 1986, 1988, 2008; Boudreau *et al.*, 1986; Nicholson & Mathez, 1991; Mathez, 1995; Boudreau & Meurer, 1999; Cawthorn *et al.*, 2002). These fall into the category of hydrothermal–hydromagmatic–chemical diffusion models (i.e. the so-called 'uppers' of Naldrett *et al.*, 2009). Many of these require PGE to be sourced from the footwall lithologies and redeposited, either owing to a change in host-rock chemistry (i.e. redox boundaries) or along a reaction front (chromatographic model). It might, therefore, be expected that the footwall would be depleted in PGE, especially Pd with its higher mobility, and that the basal chromitite should be enriched in Pd. This is not the case. The footwall at BRPM, and also in other regions of the reef (e.g. Impala; Barnes & Maier, 2002*a*), shows no preferential depletion in Pd, nor any other PGE (e.g. Fig. 15; Table 2). Rather, the sulphide and PGM assemblage present in the mottled

anorthosite reflects its formation from a highly evolved magma that generated small, highly disseminated, Cu-rich, Fe–Ni-poor sulphides. Hence, the argument proposed by Willmore *et al*. (2000) that the PGE in the Merensky Reef were derived from the footwall is not supported by our data (although this does not preclude it from occurring elsewhere (e.g. Wagner, 1929; Cawthorn, 1999*b*, 2010).

A thorough review of the hydrothermal–hydromagmatic models to explain the origin of the PGE mineralization in the Merensky Reef and UG-2 was presented by Cawthorn (2010). Several key points were raised, including the observation that PGE grades in the Merensky Reef and UG-2 are unaffected by the thickness of the footwall succession, on which he wrote 'such a relationship argues against the hypotheses that envisage scavenging of footwall cumulates of their PGE and redeposition at appropriate layers in the sequence'. A further line of reasoning relates to Os isotope evidence: 'the initial $^{187}Os/^{188}Os$ values for laurite grains from the Merensky Reef differ from values in the entire footwall succession, a distinction not expected if the Os, and by inference the other PGE, were largely extracted from the footwall rocks'. Maier & Barnes (1999) also pointed out that there is no obvious reason why hydromagmatic processes would lead to preferential S loss in the chromitites compared with the silicate rocks that immediately overlie them. Two additional lines of reasoning against such models are presented here. The first relates to the Impala sample investigated by Barnes & Maier (2002*a*). They observed two chromitite layers that are separated by several centimetres of a coarse-grained melanorite. Both chromitites have similar levels of Pt enrichment, with similar high Pt/Pd ratios (8·9 and 11·1 lower and upper, respectively), whereas the intervening silicate layer has a significantly lower Pt enrichment and a lower Pt/Pd ratio (4·8). The data for their two chromitites are similar to ours (Table 2). Models that lead to PGE precipitation at a redox boundary, although plausible for a single layer, would not be able to duplicate the extreme PGE concentrations and high Pt/Pd ratios within centimetres of each other. Such models also cannot account for the sudden change from a Pt-sulphide dominated assemblage in our lower chromitite to a Pt-arsenide and -sulfarsenide dominated assemblage in the upper chromitite (Table 1; Fig. 6). This takes place exactly at the contact between the two chromitites where there is no redox boundary (Fig. 7). It could be argued that the chromitites are not temporally related, along the lines of the argument of Naldrett *et al*. (2009). In this case an explanation is needed for (1) the source of the PGE, (2) the presence of distinctly different PGM assemblages in each of our layers, (3) the high Pt/Pd but low Pd/Ir ratios in the chromitites, and (4) PGM associations with extremely small amounts of Ni–Cu-rich (Fe-poor) sulphides.

An additional problem for the hydrothermal–hydromagmatic models relates to the degree of permeability of the footwall necessary to allow the upward transport of PGE. Some evidence for downward transport of fluids was presented by Roberts *et al*. (2007), who ascribed the origin of the olivine in the troctolites to the downward migration of magmatic fluids into the anorthosite. Cawthorn (2010) also argued that the PGE-bearing sulphide liquids formed after the chromitites and silicates subsequently 'trickled down through about 1 m of permeable crystal pile', which seems to support the observations of Wagner (1929), Cawthorn (1999*b*) and Godel *et al*. (2007). However, Godel *et al*. (2006) concluded that the chromitites at RPM prevented the downward movement of sulphide liquids. At BRPM, the amount of sulphides within the chromitites is extremely small, even considering the amount of sulphide that may have been lost (i.e. at present they account for *c*. 0·7%; Table 2). The sulphides do not appear to have amalgamated into larger droplets, or to have formed large interconnected networks, and instead are closely associated with chromite (Table 1). Furthermore, the footwall at BRPM and Impala must have been near fully crystallized at the time of Merensky Reef emplacement, as shown by the angular contact relationship of the anorthosite layering with the chromitite (Fig. 5) and the beheading of singlel pyroxene oikocrysts that crystallized from interstitial liquids (Fig. 4). Consequently, the anorthosite is unlikely to have been particularly permeable, which agrees with the conclusion of Mathez *et al*. (1997), who argued that the anorthosites present 'permeability barriers'. Together these observations could explain why we do not observe any downward, density driven, percolation of PGE–PGM-enriched sulphides into the footwall at BRPM. As discussed above, the Impala sample investigated by Barnes & Maier (2000*a*) shows that PGE movement did not occur between different layers, even over centimetre scales. Likewise, our observations show that the sulphides and PGM have not moved far from their original depositional positions. Consequently, the PGE signatures together with the PGM and sulphide assemblages have been preserved in each of the layers in our sample (Table 1; Figs 6 and 15).

Similar to the arguments against sulphide loss, models involving hydrothermal–hydromagmatic–chemical diffusion cannot be the primary mechanism to explain the Ni–Cu–PGE mineralization in the Merensky Reef.

The role of sulphide fractionation and decoupling of MSS from evolved sulphide liquids

Experimental work has shown that sulphide liquid fractionation will produce an early 'cumulus' Fe-rich MSS phase and a residual Cu-rich ISS liquid (Dutrizac, 1976; Barnes *et al*., 1997). The liquidus temperature of MSS formation depends on the sulphide liquid composition, but probably lies between 900 and 1170°C (Dutrizac, 1976). Consequently, MSS can coexist with ISS liquids at typical magmatic temperatures (Fleet *et al*., 1993; Barnes *et al*., 1997). The IPGE (Ir, Os and Ru) are expected to partition into the MSS, whereas the PPGE (Pt, Pd, Rh) partition into the evolved Cu-rich ISS liquids.

This mechanism has been proposed to explain the origins of the Ni–Cu–PGE mineralization in a number of orebodies [e.g. Sudbury (Naldrett *et al.*, 1982); Noril'sk (Distler *et al.*, 1977; Czamanske *et al.*, 1992); Kambalda (Keays *et al.*, 1981); Bushveld (Maier & Barnes, 1999); and in the petrogenesis of oxide–sulphide droplets from Uruguay (Prichard *et al.*, 2004*b*)]. However, fractionation of sulphide liquids alone cannot explain the observed excess of Ir, Ru, Rh and Pt that generates the high Pt/Pd but low Pd/Ir ratios in the chromitites (Fig. 15; Table 2). The same fractionation signatures are present in the Impala sample documented by Barnes & Maier (2002*a*). Together with the observations made in points (1)–(8) in the section 'Competing models for sulphide and PGE mineralization', these fractionation effects could arise only if the chromitites contain a large addition of Pt, Ru, Rh and Ir. As noted from the petrographic observations, the two chromitites contain abundant Pt- and Ru-PGM that contain appreciable Rh and Ir (Table 1). We suggest that these were added to the Merensky magmas before they were emplaced and that the currently observed assemblage of sulphides and PGM in the chromitites does not represent a complete system of PGE-enriched base-metal sulphides (BMS).

Proposed origin of the Ni–Cu–PGE mineralization in the Merensky Reef

For the chromitites, we suggest that discrete PGM of Ir, Ru, Pt and Rh, together with minor amounts of sulphide, were carried into the Merensky magma chamber. In contrast, the Ni–Cu–PGE mineralization in the melanorite can best be explained through processes of in-chamber magma fractionation. This is supported by Cawthorn (2005), who concluded that saturation of sulphide liquids should have occurred throughout the Critical Zone. Maier & Barnes (1999) also stated that sulphide liquid fractionation is necessary to explain the PGE signatures in the silicate rocks of the Lower, Critical and Main Zones of the Bushveld.

The origin of the sulphide and associated PGE in the pegmatite is less clear, but the evidence seems to favour a combination of a component that formed through in-chamber processes with a component of sulphide and PGM that formed outside the Merensky magma chamber.

PGE distribution in sulphides using laser ablation

The application of LA-ICP-MS mapping has opened up a new window into understanding the processes influencing PGE behaviour. There is a growing amount of data on the distribution of PGE in sulphides from laser ablation studies. These include samples of Merensky Reef (e.g. Ballhaus & Sylvester, 2000; Godel *et al.*, 2007; Osbahr *et al.*, 2013) and Platreef (e.g. Holwell & McDonald, 2007; Hutchinson & McDonald, 2008). PGE contents in Merensky sulphides reported by Ballhaus & Sylvester (2000) and Osbahr *et al.* (2013) are similar to ours, whereas those reported by Godel *et al.* (2007) from Impala are generally higher.

Many of the sulphides are associated with both large and small PGM, including some with rims of sub-micron-sized particles that were too small to be resolved under the SEM but were detected using the laser (Fig. 18c; Supplementary Data Electronic Appendix 11a–c). We also note the presence of heterogeneous Pt, Rh, Ru, Os and Ir distribution in different parts of the same sulphide within single grains (e.g. Fig. 18b and c). This would not be expected if the sulphides crystallized from a single parent liquid. The presence of Pt in the pyrrhotite is also puzzling, especially where concentrations of Pt in the associated pentlandite and chalcopyrite are lower (Table 3). In some cases, higher Pt in pyrrhotite than in coexisting pentlandite or chalcopyrite is accompanied by high Co (maximum 8224 ppm; typical range 20–31 ppm). Zones of Co-rich pyrrhotite may also host higher Bi, Ir, Os and Ru than coexisting Co-poor pyrrhotite in the same sulphide (Fig. 18b; Table 3). As noted for the heterogeneous distribution of PGE, these observations are not easily explained by existing models of PGE partitioning in fractionating sulphide liquids (e.g. Hamlyn & Keays, 1986; Makovicky *et al.*, 1986; Barnes *et al.*, 1997). Apparent Pt zoning may correspond to complex growth histories (Fig. 18c). This situation could arise when some of the Pt in a sulphide liquid partitioned into MSS that crystallized to pyrrhotite. Alternatively, it could be argued that high PGE abundances associated with elevated Co indicate that Co influences the compatibility of Pt, Ir, Os, Ru and Bi in pyrrhotite, and to a lesser extent pentlandite (e.g. Fig. 18a; Table 3; Merensky-4 Laser-4). To explain the low Pt contents in coexisting pentlandite and chalcopyrite requires the removal of Pt from evolved sulphide liquids (i.e. ISS). Models to explain this were proposed by Holwell & McDonald (2007), Hutchinson & McDonald (2008), Dare *et al.* (2010) and Holwell *et al.* (2011). The common link is that introduction of As, Sb, Te and Bi into a magma promotes the formation of PGM from a sulphide liquid, particularly for Pt, Ru, Rh and Ir. These range from high-temperature magmatic phases, including sperrylite, through to lower-temperature subsolidus exsolution of PGM from sulphide minerals. Formation of PGM under magmatic conditions was shown by Glotov *et al.* (2001) and Huminicki *et al.* (2004), which for sperrylite can involve temperatures between 900 and 1000°C. This observation was used to explain the textural characteristics of sperrylite in some parts of the Platreef (e.g. at Turfspruit; Hutchinson & McDonald, 2008).

Similar features to the Merensky Reef are apparent in the laser maps from the Platreef, although the degree of PGE removal was substantially higher in samples taken from the central and lower parts of the reef (Table 3; Fig. 18d–g; Supplementary Data Electronic Appendices 9 and 11d–f). Increased levels of PGE extraction from the sulphides coincide with the following features: (1) changes in the number, type and size of the

PGM (Supplementary Data Electronic Appendix 2); (2) increased metasomatism of the original igneous lithologies; (3) presence of extremely high levels of contamination, particularly of As, Sb, Te and Bi, but also of Mo, Cd, Sn, W, Pb and Li in the lower parts of the drill-core (Fig. 17); (4) increased abundance of trace-metal-bearing mineral phases approaching the footwall contact, including cobaltoan gersdorffite [(NiCo)AsS], nickeline (NiAs) (possibly associated with maucherite; $Ni_{11}As_8$), altaite (PbTe), tsumoite (BiTe) and molybdenite; (5) the presence of Rh- and Ir-PGM (hollingworthite–irarsite) only in highly contaminated reef. These observations are consistent with those of Kinloch (1982) and Kinloch & Peyerl (1990), who recognized a regional control on the PGM assemblages linked to the footwall lithologies; PGM are dominated by semi-metal phases where the contact rocks are sediments and by Pt–Fe alloys with minor semi-metal phases where they comprise basement granite gneiss.

Sources of magma contamination

It has been suggested that the Bushveld magmas were derived from melting of previously metasomatized subcontinental lithospheric mantle (SCLM) (e.g. Lassiter & DePaolo, 1997; Richardson & Shirey, 2008). Although mantle-derived contamination merits consideration there is strong evidence that the contamination is largely from the mid- to upper crust, as follows: (1) radiogenic isotopes (Hamilton, 1977; Kruger & Marsh, 1982; Sharpe, 1985; Sharpe *et al.*, 1986; Lee & Butcher, 1990; Kruger, 1994; Harmer *et al.*, 1995; McCandless *et al.*, 1999; Schoenberg *et al.*, 1999; Maier *et al.*, 2000; Mathez & Waight, 2003; Buchanan *et al.*, 2004; Harris *et al.*, 2005; Mathez & Kent, 2005; Prevec *et al.*, 2005); (2) stable isotopes, which in some cases specifically implicates contamination by Transvaal sediments (e.g. Schiffries & Rye, 1989; Harris & Chaumba, 2001; Harris *et al.*, 2005); (3) major and trace element studies (e.g. Hatton & Schweitzer, 1995; Arndt *et al.*, 2005; Wilson & Chunnet, 2006; Eales & Costin, 2012); (4) the extremely close correspondence between the trace element signatures of the Platreef and the Merensky Reef silicates (Fig. 17). Because the contamination signature in the Platreef can be attributed to the Transvaal sediments, by implication the Merensky Reef magmas were most probably contaminated by the same rock types.

Summary of the sulphide- and associated PGM-forming processes

The PGE mineralization in the Merensky Reef lower chromitite can best be explained in terms of a combination of mechanically mixed chromite grains, Pt- and Ru-PGM and a small amount of sulphide (e.g. Hutchinson & Foster, 2009, 2010*a*, 2010*b*, 2012). This is similar in our upper chromitite, except that to explain the close-packing arrangement and complex geochemical trends of the small chromites suggests that they most likely crystallized within the Merensky magma chamber. These ideas have much in common with previous literature on the petrogenesis of the complex, including the argument for capture and concentration of PGE by sulphide droplets within one or more staging chamber(s) or conduits prior to magma emplacement (Barton *et al.*, 1986; Lee, 1996; Schoenberg *et al.*, 1999; Harris & Chaumba, 2001; Arndt *et al.*, 2005; Hutchinson & Kinnaird, 2005; Holwell & Jordaan, 2006; Holwell & McDonald, 2007; Holwell *et al.*, 2007; McDonald & Holwell, 2007; Mondal & Mathez, 2007; Hutchinson & McDonald, 2008; Naldrett *et al.*, 2009; Voordouw *et al.*, 2009).

Consequently, two stages of formation are required to account for the Ni–Cu–PGE–Cr mineralization in our lower chromitite.

Stage 1. (a) Emplacement of magmas into a staging chamber that leads to assimilation of Transvaal wall-rocks (Fig. 21a); (b) chromite crystallization in response to a combination of increased silica activity and/or mixing with evolved resident magma (Fig. 21b and c); (c) formation of immiscible sulphide liquids owing to either chromite crystallization leading to decreased Fe and changes in fO_2, or increased silica from assimilation of wall-rocks, or magma mixing, or a combination of these processes (Fig. 21b and c); (d) PGE collection by sulphide liquids; (e) formation of Pt- and Ru-minerals from the sulphide liquids, controlled by the availability of As, Te, Bi, Sb ± S from assimilated Transvaal sediments.

Stage 2. (a) Upward displacement of magma from the staging chamber, carrying a load of crystallized chromite, sulphide and Pt- and Ru-PGM (± opx from the resident magma in the staging chamber; Fig. 21d); (b) emplacement of magma into the Merensky magma chamber leading to thermo-mechanical erosion of the floor (Fig. 22a and b); (c) deposition of the basal chromitite containing sulphide and PGM together with material eroded from the footwall (Fig. 22b and c).

Stages 1 and 2 are similar to those of Naldrett *et al.* (2009), although those researchers considered that the chromite and sulphide formed within the Merensky magma chamber. Stage 2 is broadly consistent with Scoon & Teigler (1994) and Arndt *et al.* (2005) and is similar to the ideas of other researchers including (1) the origin of the chromitite layers in the Critical Zone (Eales, 2000; Mondal & Mathez, 2007; Maier & Barnes, 2008; Voordouw *et al.*, 2009; Eales & Costin, 2012) or (2) the existence of previously formed sulphide liquids in the Merensky magma (Lee, 1996). For Stage 2b to have occurred the density of the injecting magma must have been higher than that of the resident magma, which is likely if it was charged with a significant amount of chromite (Scoon & Teigler, 1994; Rice & Eales, 1995).

We suggest that the driving force for emplacement of magma into a mid- to upper-crustal staging chamber is linked to inflation, either by roof uplift or floor depression, followed by collapse of the system with magma displaced along the TML (Fig. 21). Elements of this model are broadly consistent with mechanisms linked to the emplacement of granitic magmas in the upper crust (e.g. Cruden & McCaffrey, 2001; Grocott & Taylor,

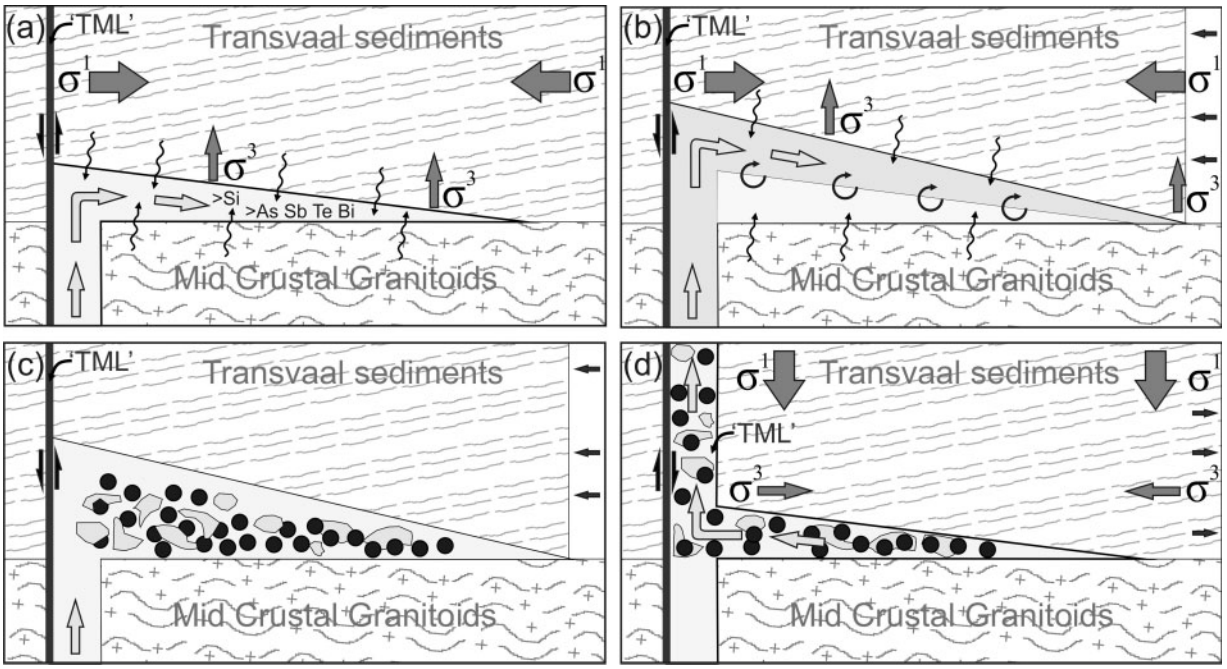

Fig. 21. Conceptual model for the emplacement of magma in a mid- to upper-crustal staging chamber that leads to the formation of chromite (black circles) and sulphide melt (grey shaded shapes), from which PGM crystallize. Collapse of the staging chamber results in displacement of the magma along the TML.

2002). Magma pumping mechanisms, such as the one proposed here, may explain how mafic magmas are able to ascend to the surface despite being denser than typical mid- to upper crust composed of granitiods, granite–gneiss and sediments. As noted in the Introduction, the TML is a major crustal suture zone at the northern margin of the Kaapvaal Craton that was active prior to, syn- and post-emplacement of the Bushveld (McCourt & Vearncombe, 1987; Kruger, 1995; Good & de Wit, 1997). The TML has also been implicated by a number of researchers as a major feeder for the Bushveld magma (e.g. Eales *et al.*, 1988; Maier & Eales, 1994; Kruger, 2005*a*, 2005*b*; Clarke *et al.*, 2009). Our emplacement mechanism may have conceptual parallels to other Earth systems. For example, Rice & Eales (1995) stressed that large volumes of material can be transported significant distances almost instantaneously (e.g. pyroclastic density currents, turbidites, mudflows).

Reinterpretation of regional PGM assemblage variations

Broad differences in the types of PGM in the chromitites and silicates are recognized from the Merensky Reef. The chromitites are dominated by PtPd-sulphides, arsenides, tellurides and alloys, and Ru-sulphides (laurite), whereas the silicate portions of the reef include various PtPd-tellurides, bismuthides and bismuthotellurides (e.g. Stumpfl & Tarkian, 1976; Mostert *et al.*, 1982; Von Gruenewaldt *et al.*, 1986; Merkle, 1987; Kinloch & Peyerl, 1990; Verryn & Merkle, 1994; Lee, 1996; Schouwstra *et al.*, 2000; Cawthorn *et al.*, 2002; Prichard *et al.*, 2004*a*; Godel *et al.*, 2007; Osbahr *et al.*, 2013). However, in detail, the PGM assemblages in the chromitites vary around the complex, with some areas, particularly north of Impala, containing abundant Pt-alloys and Pd-alloys (e.g. Cawthorn *et al.*, 2002). In general, three distinct PGM categories were recognized by Cawthorn *et al.* (2002) from the Merensky Reef: Pt and Pd sulfides, tellurides and arsenides, and alloys and metals. Their interpretations for the observed variation in the types of PGM in different localities in the Bushveld include 'secondary processes related to cooling, local changes in $f(S_2)$ in the crystallization environment, and subsolidus re-equilibration' and that the different assemblages formed by overprinting of pre-existing PGM by volatile fluids (Schiffries, 1982). Cawthorn *et al.* (2002) noted that local variation in PGM, particularly for Pt-alloys, is controlled by proximity to potholes and 'discordant ultramafic bodies' (as also recognized by Peyerl, 1982; Kinloch & Peyerl, 1990; Lee, 1996; Viljoen, 1999). However, it has also been recognized that the proportion of PGE alloys decreases southwards towards Impala in the Western Bushveld, after which alloys are a relatively minor component of the overall PGM assemblage (e.g. Lee, 1996; Cawthorn *et al.*, 2002). Only one alloy (Pt_3Fe) out of several hundred PGM is represented in our assemblages (Table 1). Within the scope of our model, two possible mechanisms could explain the observed regional control on the distribution of PGM assemblages: (1) magmatic erosion leading to removal of previously more widespread occurrences; (2) deposition of PGM from magmas flowing from north to south that did not extend much beyond Impala, particularly for the alloy-dominant assemblage.

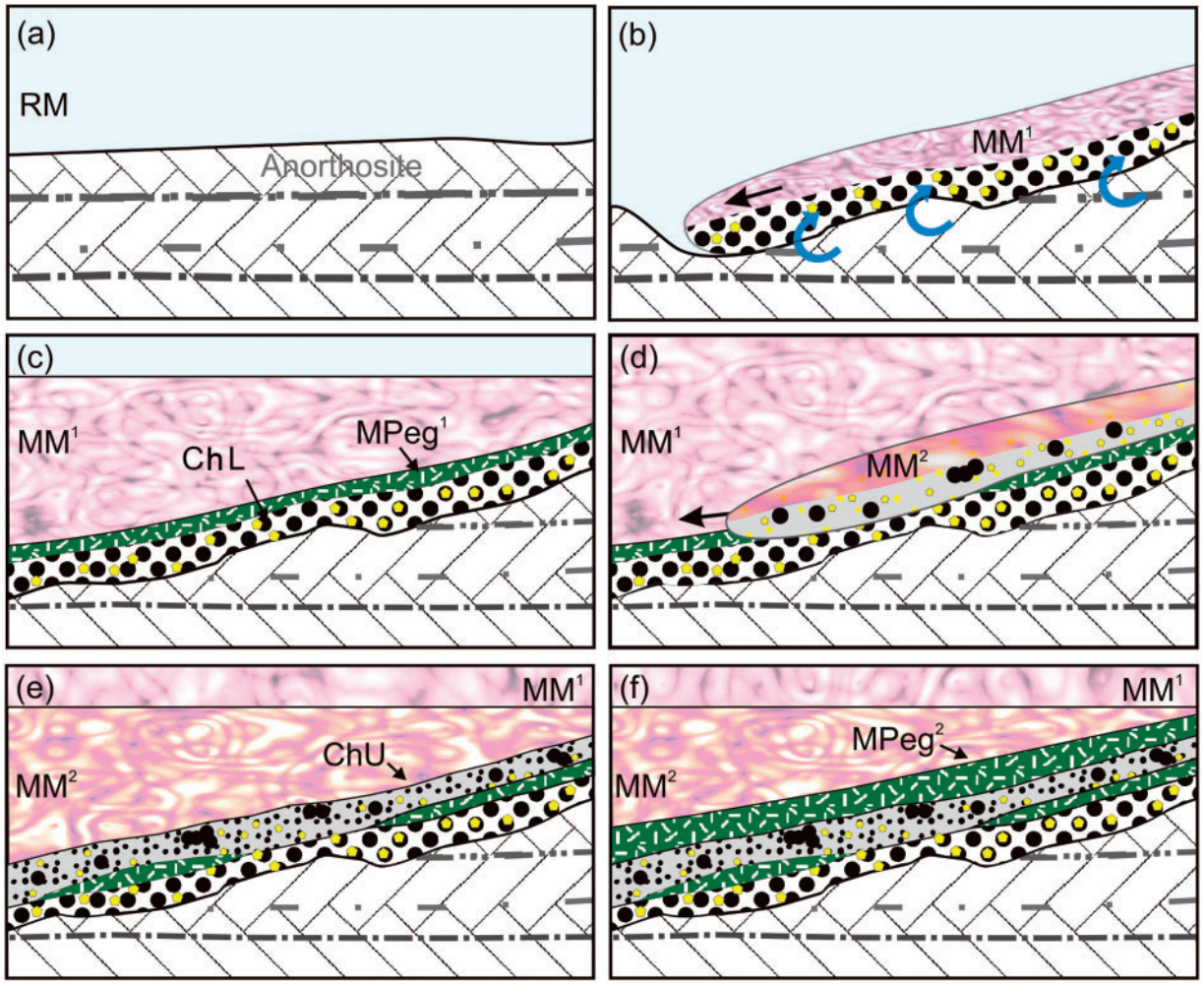

Fig. 22. Merensky Reef emplacement model. (a) Pre-Merensky with resident magma (RM) above anorthosite; (b) injection of first Merensky magma (MM^1) leads to erosion of the footwall and deposition of chromite, sulphides and PGM (ChL); (c) development of pegmatite above basal chromitite ($MPeg^1$); (d) new injection of magma (MM^2) leads to erosion and partial removal of pre-existing layers; (e) crystallization of chromite leads to upper chromitite formation (ChU); (f) development of pegmatite above upper chromitite ($MPeg^2$). RM, resident magma; MM^1, Merensky magma^1; $MPeg^1$, Merensky pegmatite^1; ChL, lower chromitite; ChU, upper chromitite; MM^2, Merensky magma^2; $MPeg^2$, Merensky pegmatite^2.

The latter situation is consistent with an inferred southerly flow direction of magma from a major feeder zone located to the north (e.g. Eales *et al.*, 1988; Maier & Eales, 1994; Kruger, 2005*a*, 2005*b*; Clarke *et al.*, 2009).

Although elevated PGE contents are commonly associated with chromitites (e.g. Scoon & Teigler, 1994; Maier & Barnes, 1999; Cawthorn *et al.*, 2002), PGE can also be enriched in the silicate rocks (e.g. Mathez, 1995; Maier & Barnes, 1999; Cawthorn *et al.*, 2002); for example, in pyroxenite at Winnaarshoek and at the contact between the basal pyroxenite and the pegmatitic pyroxenite at Lebowa (Mossom, 1986; Mathez, 1995; Cawthorn *et al.*, 2002; Cawthorn & Boerst, 2006). These could represent influxes of magma carrying sulphide and PGM without chromite.

Models of reef formation

The above discussion leads to the following petrogenic model for the formation of the Merensky Reef at BRPM (Fig. 22). Crucially, this model can be extrapolated to explain features found elsewhere in the Bushveld Complex (Fig. 23). The initial Merensky magma (MM^1, Fig. 21b) emplaced into the Bushveld Complex contained a basal load of chromite with some PGM-bearing sulphide. This formed the lower chromitite ('ChL') with a PGM assemblage dominated by Pt-minerals (cooperite–braggite–vysotskite series) and Ru- and Ir-minerals (laurite and hollingworthite–irarsite). As observed elsewhere, a coarse-grained melanorite or pegmatitic pyroxenite developed above the basal chromitite ($MPeg^1$, Fig. 22c) (e.g. Nicholson & Mathez, 1991; Barnes & Maier, 2002*a*; Cawthorn & Boerst, 2006; Godel *et al.*, 2007). Cawthorn & Boerst (2006) suggested that such pegmatites form in response to injection of superheated melts that 'permitted prolonged interaction with the crystal mush at the crystal–liquid interface', leading to the recrystallization of smaller cumulus crystals into larger grains. Naldrett *et al.* (2009) also argued that the pegmatites formed as a consequence of magma

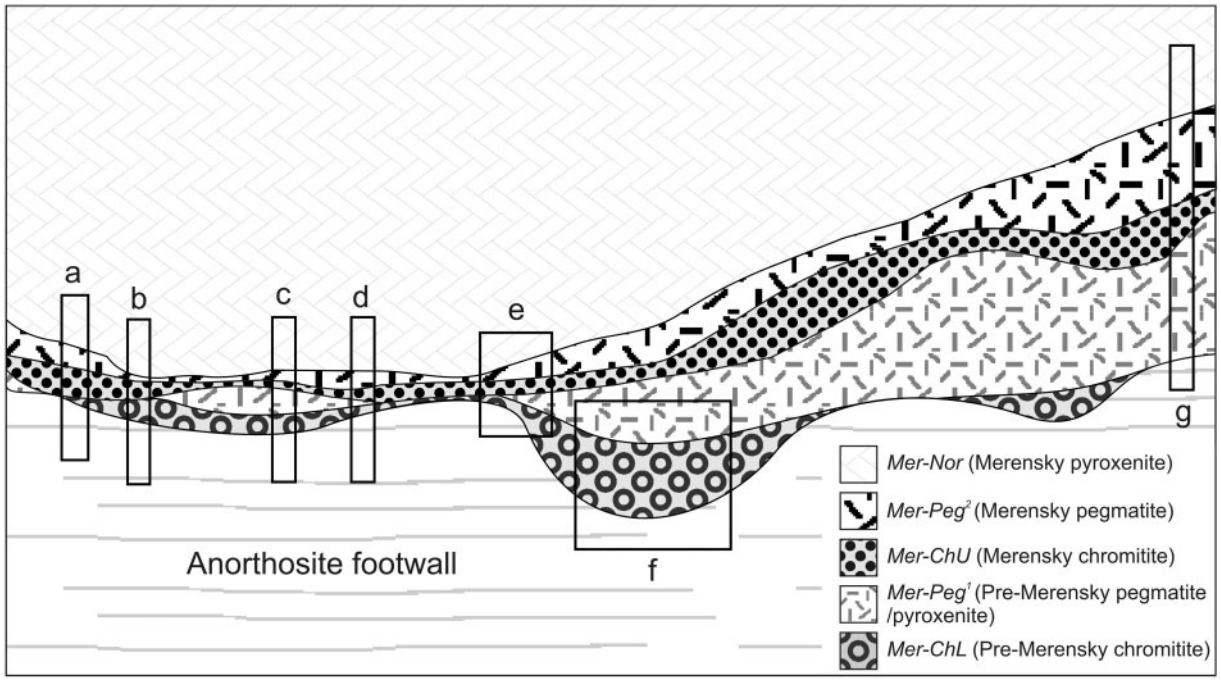

Fig. 23. Conceptual model to explain the variation in Merensky stratigraphy observed in different parts of the Western and Eastern Bushveld. The names of the layers used in this study are compared with those of Naldrett *et al.* (2009). Letters represent locations where various relationships are observed: a, BRPM ('contact reef': this study); b, Impala ('contact reef': this study); c, Impala and Siphumelele 2 Shaft, formerly Brakspruit Shaft ('thin reef' and 'normal reef': Ballhaus & Stumpfl, 1986; Nicholson & Mathez, 1991; Barnes & Maier, 2002*a*); d, RPM ('thin reef': Vukmanovic *et al.*, 2013); e, Khuseleka 1 Shaft, formerly Townlands Shaft ('contact and thin reef': Naldrett *et al.*, 2009); f, BRPM (this study; Fig. 5c). It should be noted that the first appearance of chromitite can occur above the anorthosite–pyroxenite contact in some areas (e.g. at 'g') as observed at Lebowa (Atok) and Winnaarshoek (Mathez, 1995; Mathez *et al.*, 1997; Cawthorn *et al.*, 2002; Cawthorn & Boerst, 2006; Mitchell & Scoon, 2007).

emplacement and they stressed the importance of the trace-element evidence presented by Cawthorn & Boerst (2006). Introduction of superheated melts into the Bushveld magma chamber may have triggered the partial melting and recrystallization of plagioclase and pyroxene trapped in the basal chromitite, and may also explain the clots of intercumulus quartz and feldspar with symplectitic textures in the pegmatite.

At BRPM the injection of a new Merensky Magma (MM^2) into the magma chamber led to the removal of pegmatite $MPeg^1$ and in places the partial removal the lower chromitite 'ChL' (Fig. 22d). A similar conclusion was reached by Naldrett *et al.* (2009). MM^2 introduced a new PGM assemblage that contained significant sperrylite and platarsite. Within-chamber crystallization of chromite led to development of the upper chromitite 'ChU' (Fig. 22e). This may have been initiated by mixing of the new and resident magmas, as proposed by Naldrett *et al.* (2009). Merensky pegmatite ($MPeg^2$, Fig. 22f) formed above the upper chromitite, as observed at BRPM and in many other areas of the Merensky Reef (e.g. Wagner, 1929; Ballhaus & Stumpfl, 1986; Nicholson & Mathez, 1991; Barnes & Maier, 2002*a*; Cawthorn & Boerst, 2006). In our Impala sample this pegmatite layer is barely a few grains thick (Fig. 4c) and in some areas is missing altogether; for example, in parts of Impala particularly towards the northern end of the mine (Leeb-du Toit, 1986; Viljoen, 1999; Cawthorn *et al.*, 2002; Cawthorn & Boerst, 2006). Within the scope of our model this pegmatite has been partially or wholly removed due to subsequent magma influxes.

Added complexity not shown in this model comes from the presence of additional chromitite layers in some parts of the Merensky Reef (e.g. Lee, 1996; Cawthorn & Boerst, 2006).

Extrapolation of the petrogenic model to other regions of the complex

The variation across the Merensky Reef in layer thicknesses, relative stratigraphic positions, and the presence or absence of particular layers (i.e. chromitites, pegmatites, pyroxenites and melanorites) can be explained as a function of varying degrees of erosion by, and deposition from, successive magma emplacement events (Fig. 23), as broadly suggested by Eales *et al.* (1990), Cawthorn & Walraven (1998), Cawthorn & Boerst (2006), Naldrett *et al.* (2009) and Cawthorn (2010).

The similarity of our BRPM and Impala samples (Fig. 4) implies that emplacement of Merensky magma MM^2 resulted in erosion to the level of the lower chromitite. This is consistent with the findings of Naldrett *et al.* (2009), who concluded that the erosion level in the west of the Bushveld Complex is more or less constant, but noted that small-scale variations can occur on a local scale ('500 m or less').

Can these models explain other PGE-enriched chromitite layers?

The Critical Zone of the Bushveld contains large numbers of chromitite layers (Fig. 2) and most are enriched in PGE (e.g. Scoon & Teigler, 1994; Maier & Barnes, 1999; Cawthorn *et al.*, 2002). An intriguing comparison with the work of Naldrett *et al.* (2009) revealed that our lower chromitite could be equivalent to their 'Pre-Merensky chromitite', whereas our upper chromitite would be equivalent to their 'Merensky chromitite'. This would require broadly similar processes of PGM mineralization in two temporally unrelated chromitite layers. A number of similarities also exist between the Merensky chromitites and UG-2; for example: (1) disconformable relationships at the reef contact with their respective footwall lithologies (e.g. Feringa, 1959; Viljoen *et al.*, 1986*a*, 1986*b*; Eales *et al.*, 1988; Hahn & Ovendale, 1994; Lomberg *et al.*, 1999; Kruger, 2005b; Naldrett *et al.*, 2009); (2) broad similarities in PGM types (e.g. Kinloch, 1982; Verryn & Merkle, 1994; Lee, 1996); (3) the observation that most, if not all, of the chromitites in the Critical Zone are enriched in PGE (Wagner, 1929; Hiemstra, 1979, 1985, 1986; McLaren & de Villiers, 1982; Scoon & Teigler, 1994; Maier & Barnes, 1999); (4) the presence of pothole structures (e.g. Viljoen & Hieber, 1986; Carr *et al.*, 1994, 1999; Hahn & Ovendale, 1994; Viljoen & Schürmann, 1998; Lomberg *et al.*, 1999; Hoffmann, 2010); (5) the presence of poikilitic textures involving silicates enclosing chromite (Voordouw *et al.*, 2009); (6) the presence of recrystallized and coarsened silicates above the chromitites (Merensky: Nicholson & Mathez, 1991; Mathez, 1995; Barnes & Maier, 2002*b*; Cawthorn & Boerst, 2006; Naldrett *et al.*, 2009; UG-2: Mondal & Mathez, 2007).

The Merensky Reef, therefore, forms part of the broader framework of chromitite-associated Ni–Cu–PGE mineralization that characterizes the Upper Critical Zone of the Bushveld, rather than forming as a result of any unique event or process.

CONCLUSIONS

At least four magmatic events are recorded in a highly compressed interval in a hand sample of Merensky Reef from BRPM. In addition, some of the stratigraphy noted from other regions of the Bushveld Complex is missing. Each of the recognizable layers in the BRPM sample preserves a characteristic sulphide and PGM assemblage that has remained largely in its original depositional position, albeit with some localized redistribution and recrystallization on a sub-centimetre scale. The boundaries between the two chromitite layers are demonstrably textural rather than chemical and their extreme enrichment in PGE is attributed to physical concentration of particulate Pt- and Ru-dominated PGM. The presence of similar Ni–Cu–PGE mineralization in our two chromitites requires broadly similar processes of formation that involve a staging chamber in which magmas interacted with Transvaal sediments. Rather than a fire-fountain type feeder model (e.g. Scoon & Teigler, 1994; Kruger & Schoenberg, 1998; Schoenberg *et al.*, 1999) we argue for sustained, high-energy, lateral injections driven by periodic collapse of mid- to upper-crustal level staging chambers.

Variations in the number and relative positions of the chromitites, pegmatite and melanorite layers in the Merensky Reef are a result of thermo-mechanical erosion together with the deposition, or non-deposition, of layers in response to successive magma influxes.

The Platreef and Merensky magmas appear broadly similar in terms of geochemistry and mineralogy (e.g. Kruger, 2005*a*, 2005*b*, 2010). Both formed from multiple emplacement events (Platreef: Kinnaird, 2005; Manyeruke *et al.*, 2005; Merensky Reef: Eales *et al.*, 1990; Cawthorn & Walraven, 1998; Cawthorn & Boerst, 2006; Naldrett *et al.*, 2009; Cawthorn, 2010). Both are linked by contamination with As, Sb, Te and Bi derived from Transvaal sediments that promote the formation of PGM from sulphide liquids. Consequently, the Merensky Reef and Platreef are linked by two key processes: (1) formation of PGM and removal of PGE from the sulphide liquids; (2) physical concentration of PGM. In the case of the Merensky Reef, PGM concentration was significantly more efficient than in the Platreef owing to the timing of PGM formation prior to magma emplacement (in the Platreef this occurred predominantly post-emplacement). In the Platreef, the degree of PGE extraction from the sulphide liquids was more efficient owing to the presence of higher concentrations of As, Sb, Te and Bi (i.e. higher levels of contamination). On this evidence it is considered unlikely that the Merensky and Platreef magmas were present in the same staging chamber (Merensky located largely within Transvaal sediments; Platreef largely within Archaean granitoids), unless the staging chamber was large enough to be compartmentalized (e.g. Roelofse & Ashwal, 2012).

Although the mechanisms outlined above operated in magmatic environments, sedimentary-style processes explain many of the features over large and small scales. These include the deposition of dense particulate phases (chromite, sulphide and PGM) and the mechanical erosion of pre-existing layers as a consequence of magma emplacement.

ACKNOWLEDGEMENTS

Professor Tony Crawford and Dr Iain McDonald are thanked for reviewing the paper prior to submission. We would also like to thank Rais Latypov, Ed Mathez and two anonymous reviewers who prompted a thorough revision of the original version of the paper. The data presented in this paper were obtained from several different analytical facilities. At the University of Tasmania, special thanks go to Leonid Danyushevsky, Sarah Gilbert and Iain Little, who together run the laser facility within the Department of Earth Sciences. We also thank Karsten Gömann and Sandrin Feig from the

Central Science Laboratories, who run the microprobe and SEM facility; Marcus Burnham and Merilla Clement at the OGS labs in Canada for their analytical services on the Merensky samples; Steve Barnes and Belinda Godel at CSIRO for their collaboration in running the X-ray CT on the Merensky chromitite. Anglo Platinum is thanked for logistical support, particularly in gaining access to geochemical data and samples from a number of drill-cores.

FUNDING

This work was supported by a joint Anglo American Plc and Anglo American Platinum Limited research project on Tweefontein.

SUPPLEMENTARY DATA

Supplementary data for this paper are available at *Journal of Petrology* online.

REFERENCES

Arndt, N., Jenner, G., Ohnenstetter, M., Deloule, E. & Wilson, A. H. (2005). Trace elements in the Merensky Reef and adjacent norites, Bushveld Complex, South Africa. *Mineralium Deposita* **40**, 550–575.

Ashwal, L. D., Webb, S. J. & Knoper, M. W. (2005). Magmatic stratigraphy in the Bushveld Northern Lobe: continuous geophysical and mineralogical data from the 2950 m Bellevue drillcore. *South African Journal of Geology* **108**, 109–232.

Ballhaus, C. G. & Stumpfl, E. F. (1986). Sulfide and platinum mineralisation in the Merensky Reef: evidence from hydrous silicates and fluid inclusions. *Contributions to Mineralogy and Petrology* **94**, 193–204.

Ballhaus, C. G. & Sylvester, P. (2000). Noble metal enrichment processes in the Merensky Reef, Bushveld Complex. *Journal of Petrology* **41**, 545–561.

Barnes, S.-J. & Maier, W. D. (2002a). Platinum-group elements and microstructures of normal Merensky Reef from Impala Platinum Mines, Bushveld Complex. *Journal of Petrology* **43**, 103–128.

Barnes, S.-J. & Maier, W. D. (2002b). Platinum-group element distribution in the Rustenburg Layered Suite of the Bushveld Complex, South Africa. In: Cabri, L. J. (ed.) *The Geology, Geochemistry, Mineralogy and Beneficiation of Platinum-Group Elements. Canadian Institute of Mining, Metallurgy and Petroleum, Special Volume* **54**, 553–580.

Barnes, S. J., Boyd, R., Korneliussen, L.-P. & Nilsson, M. O. (1988). The use of mantle normalization and metal ratios in discriminating between the effects of partial melting, crystal fractionation and sulphide segregation on platinum-group elements, gold, nickel and copper: examples from Norway. In: Prichard, H. M., Potts, P. J., Bowles, J. F. W. & Cribb, S. J. (eds) *Geo-Platinum 87*. Barking: Elsevier, pp. 113–143.

Barnes, S.-J., Makovicky, E., Makovicky, M., Hansen, J. R. & Moller, S. K. (1997). Partition coefficients for Ni, Cu, Pd, Pt, Rh and Ir between monosulfide solid solution and sulfide liquid and the formation of compositionally zoned Ni–Cu sulfide bodies by fractional crystallisation of sulfide liquid. *Canadian Journal of Earth Science* **34**, 366–374.

Barton, J. M., Cawthorn, R. G. & White, J. (1986). The role of contamination in the evolution of the Platreef of the Bushveld Complex. *Economic Geology* **81**, 1096–1104.

Beath, C. B., Westwood, R. J. & Cousins, C. A. (1961). Platinum mining at Rustenburg. The development of operating methods. *Platinum Metals Review* **5**, 102–108.

Boudreau, A. E. (1986). The role of fluids in the petrogenesis of platinum-group element deposits in the Stillwater Complex, Montana. PhD dissertation, University of Washington.

Boudreau, A. E. (1988). Investigations of the Stillwater Complex. IV. The role of volatiles in the petrogenesis of the J-M reef, Minneapolis adit section. *Canadian Mineralogist* **26**, 193–208.

Boudreau, A. E. (2008). Modeling the Merensky Reef, Bushveld Complex, Republic of South Africa. *Contributions to Mineralogy and Petrology* **156**, 431–437.

Boudreau, A. E. & Meurer, W. P. (1999). Chromatographic separation of the platinum-group elements, gold, base metals and sulfur during degassing of a compacting and solidifying igneous crystal pile. *Contributions to Mineralogy and Petrology* **134**, 174–185.

Boudreau, A. E., Mathez, E. A. & McCallum, I. S. (1986). Halogen geochemistry of the Stillwater and Bushveld Complexes: evidence for transport of the platinum-group elements by Cl-rich fluids. *Journal of Petrology* **27**, 967–986.

Buchanan, D. L. (1976). The sulphide and oxide assemblage in the Bushveld Complex rocks of the Bethal area. *Transactions of the Geological Society of South Africa* **39**, 76–80.

Buchanan, D. L., Nolan, J., Suddaby, P., Rouse, J. E., Viljoen, M. J. & Davenport, W. J. (1981). The genesis of sulfide mineralisation in a portion of the Potgietersrus Limb of the Bushveld Complex. *Economic Geology* **76**, 568–479.

Buchanan, P. C., Reimold, W. U., Koeberl, C. & Kruger, F. J. (2004). Rb–Sr and Sm–Nd isotopic compositions of the Rooiberg Group, South Africa: early Bushveld-related volcanism. *Lithos* **29**, 373–388.

Cameron, E. N. (1977). Chromite in the central sector, eastern Bushveld Complex, South Africa. *American Mineralogist* **62**, 1082–1096.

Cameron, E. N. & Desborough, G. A. (1969). Occurrence and characteristics of chromite deposits—eastern Bushveld Complex. In: Wilson, H. D. B. (ed.) *Magmatic Ore Deposits*. The Economic Geology Publishing Company, New Haven, Connecticut, 23–40.

Campbell, I. H. (1986). A fluid dynamic model for the potholes of the Merensky Reef. *Economic Geology* **81**, 1118–1125.

Campbell, I. H., Naldrett, A. J. & Barnes, S.-J. (1983). A model for the origin of the platinum-rich sulfide horizons in the Bushveld and Stillwater complexes. *Journal of Petrology* **24**, 133–165.

Carr, H. W., Groves, D. I. & Cawthorn, R. G. (1994). The importance of synmagmatic deformation in the formation of Merensky Reef potholes in the Bushveld Complex. *Economic Geology* **89**, 1398–1410.

Carr, H. W., Kruger, F. J., Groves, D. I. & Cawthorn, R. G. (1999). The petrogenesis of Merensky Reef potholes at the Western Platinum Mine, Bushveld Complex: Sr isotopic evidence for synmagmatic deformation. *Mineralium Deposita* **34**, 335–347.

Cawthorn, R. G. (1999a). The platinum and palladium resources of the Bushveld Complex. *South African Journal of Science* **95**, 481–489.

Cawthorn, R. G. (1999b). Permeability of the footwall cumulates to the Merensky Reef, Bushveld Complex. *South African Journal of Geology* **102**, 293–302.

Cawthorn, R. G. (1999c). Platinum-group element mineralization in the Bushveld Complex—a critical assessment of geochemical models. *South African Journal of Geology* **102**, 268–281.

Cawthorn, R. G. (2004). Origin of variation of Pt/Pd values in the UG-2 chromitite layer, Bushveld Complex. Geoscience Africa Abstract Volume, University of the Witwatersrand, pp. 110–113.

Cawthorn, R. G. (2005). Pressure fluctuations and the formation of the PGE-rich Merensky and chromitite reefs, Bushveld Complex. *Mineralium Deposita* **40**, 231–235.

Cawthorn, R. G. (2006). The centenary of the discovery of platinum in the Bushveld Complex (10th November, 1906). *Journal of the Southern African Institute of Mining and Metallurgy* **107**, 1–4.

Cawthorn, R. G. (2010). Geological interpretations from the PGE distribution in the Bushveld Merensky and UG2 chromitite reefs. *The 4th International Platinum Conference, Platinum in transition 'Boom or Bust'*. The Southern African Institute of Mining and Metallurgy, pp. 57–70.

Cawthorn, R. G. (2013). The Residual or Roof Zone of the Bushveld Complex, South Africa. *Journal of Petrology* **54**, 1875–1900.

Cawthorn, R. G. & Boerst, K. (2006). Origin of the pegmatitic pyroxenite in the Merensky Unit, Bushveld Complex, South Africa. *Journal of Petrology* **47**, 1509–1530.

Cawthorn, R. G. & Lee, C. (1998). Field Excursion Guide to the Bushveld Complex. In: *8th International Platinum Symposium*. Geological Society of South Africa and the South African Institute of Mining and Metallurgy, 113 pp.

Cawthorn, R. G. & Luvhimbe, C. (2009). Suspected presence of hibbingite in olivine pyroxenite adjacent to the UG-2 chromitite, Bushveld Complex, South Africa. *Canadian Mineralogist* **47**, 1075–1085.

Cawthorn, R. G. & Walraven, F. (1998). Emplacement and crystallisation time for the Bushveld Complex. *Journal of Petrology* **39**, 1669–1687.

Cawthorn, R. G. & Webb, S. J. (2001). Connectivity between the western and eastern limbs of the Bushveld Complex. *Tectonophysics* **330**, 195–209.

Cawthorn, R. G., Barton, J. M. & Viljoen, M. J. (1985). Interaction of floor rocks with the Platreef on Overysel, Potgietersrus, Northern Transvaal. *Economic Geology* **80**, 988–1006.

Cawthorn, R. G., Lee, C. A., Schouwstra, R. & Mellowship, P. (2002). Relations between PGE and PGM in the Bushveld Complex. *Canadian Mineralogist* **40**, 311–328.

Coetzee, H. & Kruger, F. J. (1989). The geochronology and Sr- and Pb-isotope geochemistry of the Losberg Complex and the southern limit of Bushveld Complex magmatism. *South African Journal of Geology* **92**, 37–41.

Coggon, J. A., Nowell, G. M., Pearson, D. G., Oberthür, T., Lorand, J.-P., Melcher, F. & Parman, S. W. (2012). The ^{190}Pt–^{186}Os decay system applied to dating platinum-group element mineralization of the Bushveld Complex, South Africa. *Chemical Geology* **302–303**, 48–60.

Cousins, C. A. & Feringa, G. (1964). The chromite deposits of the western belt of the Bushveld Complex. In: Haughton, S. H. (ed.) *The Geology of some Ore Deposits in Southern Africa. Geological Society of South Africa, Special Publication* **2**, 183–202.

Clarke, B., Uken, R. & Reinhardt, J. (2009). Structural and compositional constraints on the emplacement of the Bushveld Complex, South Africa. *Lithos* **111**, 21–36.

Cruden, A. R. & McCaffrey, K. J. W. (2001). Growth of plutons by floor subsidence: implications for rates of emplacement, intrusion spacing and melt-extraction mechanisms. *Physics and Chemistry of the Earth, Part A: Solid Earth and Geodesy* **26**, 303–315.

Czamanske, G. K., Kunilov, V. Y., Zientek, M. L., Cabri, L. J., Likhachev, A. P., Calk, L. C. & Oscarson, R. L. (1992). A proton-microprobe study of magmatic sulfide ores from the Noril'sk–Talnakh district, Siberia. *Canadian Mineralogist* **30**, 249–287.

Daly, R. A. & Molengraaff, G. A. F. (1924). Structural relations of the Bushveld Igneous Complex, Transvaal. *Journal of Geology* **32**, 1–35.

Danyushevsky, L. V., Robinson, P., Gilbert, S., Norman, M., Large, R., McGoldrick, P. & Shelley, J. M. G. (2011). Routine quantitative multi-element analysis of sulphide minerals by laser ablation ICP-MS: Standard development and consideration of matrix effects. *Geochemistry: Exploration, Environment, Analysis* **11**, 51–60.

Dare, S. A. S., Barnes, S.-J., Prichard, H. M. & Fisher, P. C. (2010) The timing and formation of platinum-group minerals from the Creighton Ni–Cu–platinum-group element sulfide deposit, Sudbury, Canada: early crystallization of PGE-rich sulfarsenides. *Economic Geology* **105**, 1071–1096.

De Waal, S. A., Maier, W. D., Armstrong, R. A. & Gauert, C. D. K. (2001). Parental magma and emplacement of the stratiform Uitkomst Complex, South Africa. *Canadian Mineralogist* **39**, 557–571.

Distler, V. V., Malevsky, A. Y. & Laputina, I. P. (1977). Distribution of platinoids between pyrrhotite and pentlandite in crystallization of a sulphide melt. *Geochimica International* **14**, 30–40.

Dutrizac, J. E. (1976). Reactions in cubanite and chalcopyrite. *Canadian Mineralogist* **14**, 172–181.

Eales, H. V. (2000). Implications of the chromium budget of the Western Limb of the Bushveld Complex. *South African Journal of Geology* **103**, 141–150.

Eales, H. V. & Cawthorn, R. G. (1996). The Bushveld Complex. In: Cawthorn, R. G. (ed.) *Layered Intrusions*. Amsterdam: Elsevier, pp. 181–230.

Eales, W. E. & Costin, G. (2012). Crustally contaminated komatiite: primary source of the chromitites and Marginal, Lower, and Critical Zone magmas in a staging chamber beneath the Bushveld Complex. *Economic Geology* **107**, 645–665.

Eales, H. V., Field, M., De Klerk, W. J. & Scoon, R. N. (1988). Regional trends of chemical variation and thermal erosion in the Upper Critical Zone, Western Bushveld Complex. *Mineralogical Magazine* **52**, 63–79.

Eales, H. V., De Klerk, W. J. & Teigler, B. (1990). Evidence for magma mixing processes within the Critical and Lower Zones of the northwestern Bushveld Complex, South Africa. *Chemical Geology* **88**, 261–278.

Ertel, W., O'Neill, H. St. C., Sylvester, P. J. & Dingwell, D. B. (1999). Solubilities of Pt and Rh in a haplobasaltic silicate melt at 1300°C. *Geochimica et Cosmochimica Acta* **63**, 2439–2449.

Ferguson, J. & Botha, E. (1963). Some aspects of igneous layering in the basic zones of the Bushveld Complex. *Transactions of the Geological Society of South Africa* **66**, 259–278.

Feringa, G. (1959). The geological succession in a portion of the north-western Bushveld (Union Section) and its interpretation. *Transactions of the Geological Society of South Africa* **62**, 219–238.

Finnigan, C. S., Brenan, J. M., Mungall, J. E. & McDonough, W. F. (2008). Experiments and models bearing on the role of chromite as a collector of platinum group minerals by local reduction. *Journal of Petrology* **49**, 1647–1665.

Fleet, M. E., Chryssoulis, S. L., Stone, W. E. & Weisener, C. G. (1993). Partitioning of platinum-group elements and Au in the Fe–Ni–Cu–S system: experiments on the fractional crystallization of sulfide melt. *Contributions to Mineralogy and Petrology* **115**, 36–44.

Fleet, M. E., Crocket, J. H., Liu, M. & Stone, W. E. (1999). Laboratory partitioning of platinum-group elements (PGE) and gold with application of magmatic sulfide–PGE deposits. *Lithos* **47**, 127–142.

Foster, J. & Hutchinson, D. (2010). The location and distribution of the PGE in magmatic sulfides: implications for genesis and mineral processing. Abstract Volume: 11th International Platinum symposium, Sudbury.

French, W. J. & Cameron, E. P. (1981). Calculation of the temperature of crystallisation of silicates from basaltic melts. *Mineralogical Magazine* **44**, 19–26.

Gain, S. B. (1985). The geologic setting of the platiniferous UG2 chromitite layer on the farm Maandagshoek, eastern Bushveld Complex. *Economic Geology* **80**, 925–943.

Gain, S. B. & Mostert, A. B. (1982). The geological setting of the platinoid and base metal sulfide mineralisation in the Platreef of the Bushveld Complex in Drenthe, north of Potgietersrus. *Economic Geology* **77**, 1395–1404.

Gilbert, S., Danyushevsky, L., Robinson, P., Wohlgemuth-Ueberwasser, C., Pearson, N., Savard, D., Norman, M. & Hanley, J. (2013). A comparative study of five reference materials and the Lombard Meteorite for the determination of the platinum-group elements and gold by LA-ICP-MS. *Geostandards and Geoanalytical Research* **37**, 51–64.

Glotov, A. I., Polyakov, G. V., Akimtzev, V., Hoa, T. T., Balykin, P. A., Akimtsev, V. A., Krivenko, A. P., Tolstykh, N. D., Phuong, N. T., Thanh, H. H., Hung, T. Q. & Petroa, T. E. (2001). The Ban Phuc Ni–Cu–PGE deposit related to the Phanerozoic komatiite–basaltic association in the Song Da rift, northwestern Vietnam. *Canadian Mineralogist* **39**, 573–589.

Godel, B., Barnes, S.-J. & Maier, W. D. (2006). 3-D distribution of sulphide minerals in the Merensky Reef (Bushveld Complex, South Africa) and the J-M Reef (Stillwater Complex, USA) and their relationship to microstructures using X-ray computed tomography. *Journal of Petrology* **47**, 1853–1872.

Godel, B., Barnes, S.-J. & Maier, W. D. (2007). Platinum-group elements in sulphide minerals, platinum-group minerals, and whole-rocks of the Merensky Reef (Bushveld Complex, South Africa): implications for the formation of the reef. *Journal of Petrology* **48**, 1569–1604.

Godel, B., Barnes, S. J., Barnes, S.-J. & Maier, W. D. (2010). Platinum ore in three dimensions: Insights from high-resolution X-ray computed tomography. *Geology* **38**, 1127–1130.

Good, N. & de Wit, M. J. (1997). The Thabazimbi–Murchison Lineament of the Kaapvaal Craton, South Africa: 2700 Ma of episodic deformation. *Journal of the Geological Society, London* **154**, 93–97.

Gray, J. M. N. T., Shearer, M. & Thornton, A. R. (2006). Time-dependent solutions for particle-size segregation in shallow granular avalanches. *Proceedings of the Royal Society of London, Series A* **462**, 947–972.

Grocott, J. & Taylor, G. K. (2002). Magmatic arc fault systems, deformation partitioning and emplacement of granitic complexes in the Coastal Cordillera, north Chilean Andes (25°30′S to 27°00′S). *Journal of the Geological Society, London* **159**, 425–442.

Guillong, M., Meier, D., Allan, M., Heinrich, C. & Yardley, B. (2008). Sillsa: A Matlab based program for the reduction of laser ablation ICP-MS data of homogeneous materials and inclusions. In: *Mineralogical Association of Canada, Short Course Series* **40**, 328–333.

Hahn, U. F. & Ovendale, B. (1994). Chromitite layer potholes at Wildebeestfontein North Mine, Impala Platinum Limited. In: *Proceedings from XVth CMMI Congress, SAIMM* **3**, pp. 195–200.

Hall, A. L. (1932). *The Bushveld Igneous Complex of the central Transvaal*. Pretoria: Geological Survey of South Africa, Government Printer, 560 pp.

Hamilton, J. (1977). Isotope and trace element studies of the Great Dike and Bushveld mafic phase. *Journal of Petrology* **18**, 24–52.

Hamlyn, P. R. & Keays, R. R. (1986). Sulfur saturation and second-stage melts: Application to the Bushveld platinum metal deposits. *Economic Geology* **81**, 1431–1445.

Harmer, R. E., Auret, J. M. & Eglington, B. M. (1995). Lead isotope variations within the Bushveld Complex, southern Africa: a reconnaissance study. *Journal of African Earth Sciences* **21**, 595–606.

Harris, C. & Chaumba, J. B. (2001). Crustal contamination and fluid–rock interaction during the formation of the Platreef, Northern Limb of the Bushveld Complex. *South African Journal of Geology* **42**, 1321–1347.

Harris, C., Pronost, J. J. M., Ashwal, L. D. & Cawthorn, R. G. (2005). Oxygen and hydrogen isotope stratigraphy of the Rustenberg Layered Suite, Bushveld Complex: Constraints on crustal contamination. *Journal of Petrology* **46**, 579–601.

Hatton, C. J. (1984). The effect of pressure, temperature and composition on the distribution of Fe and Mg between olivine, orthopyroxene and liquid; an appraisal of the reversal in the normal fractionation trend in the Bushveld Complex. *Contributions to Mineralogy and Petrology* **86**, 45–53.

Hatton, C. J. (1995). Mantle plume origin for the Bushveld and Ventersdorp provinces. *Journal of African Earth Sciences* **21**, 571–577.

Hatton, C. J. & Schweitzer, J. K. (1995). Evidence for synchronous extrusive and intrusive Bushveld magmatism. *Journal of African Earth Sciences* **21**, 579–594.

Hatton, C. J. & Von Gruenewaldt, G. (1989). The geological setting and petrogenesis of the Bushveld chromitite layers. In: Stowe, C. W. (ed.) *Chromite Deposits through Time. International Geological Congress, Washington*, pp. 109–142.

Haughton, D. R., Roeder, P. L. & Skinner, B. L. (1974). Solubility of sulfur in mafic magmas. *Economic Geology* **69**, 451–467.

Hiemstra, S. A. (1979). The role of collectors in the formation of the platinum deposits in the Bushveld Complex. *Canadian Mineralogist* **17**, 469–482.

Hiemstra, S. A. (1985). The distribution of some platinum-group elements in the UG-2 chromitite layer of the Bushveld Complex. *Economic Geology* **80**, 944–957.

Hiemstra, S. A. (1986). The distribution of chalcophile and platinum-group elements in the UG-2 chromitite layer of the Bushveld Complex. *Economic Geology* **81**, 1080–1086.

Hoffmann, D. (2010). Statistical size analysis of potholes: an attempt to estimate geological losses ahead of mining at Lonmin's Marikana mining district. The 4th International Platinum Conference, Platinum in Transition 'Boom or Bust', Southern African Institute of Mining and Metallurgy, pp. 97–104.

Holwell, D. A. & Jordaan, A. (2006). Three-dimensional mapping of the Platreef at the Zwartfontein South mine: implications for the timing of magmatic events in the Northern Limb of the Bushveld Complex, South Africa. *Transactions of the Institution of Mining and Metallurgy* **115**, 41–48.

Holwell, D. A. & McDonald, I. (2006). Petrology, geochemistry and the mechanisms determining the distribution of platinum-group element and base metal sulphide mineralisation in the Platreef at Overysel, northern Bushveld Complex, South Africa. *Mineralium Deposita* **41**, 575–598.

Holwell, D. A. & McDonald, I. (2007). Distribution of platinum-group elements in the Platreef at Overysel, northern Bushveld Complex: a combined PGM and LA-ICP-MS study. *Contributions to Mineralogy and Petrology* **154**, 171–190.

Holwell, D. A., McDonald, I. & Armitage, P. E. B. (2006). Platinum-group mineral assemblages in the Platreef at the Sandsloot Mine, northern Bushveld Complex, South Africa. *Mineralogical Magazine* **70**, 83–101.

Holwell, D. A., Boyce, A. J. & McDonald, I. (2007). Sulfur isotope variations within the Platreef: genetic implications for the

origin of sulphide mineralisation. *Economic Geology* **102**, 1091–1110.

Holwell, D. A., McDonald, I. & Butler, I. B. (2011). Precious metal enrichment in the Platreef, Bushveld Complex, South Africa: evidence from homogenized magmatic sulfide melt inclusions. *Contributions to Mineralogy and Petrology* **161**, 1011–1026.

Hulbert, L. J. & Von Gruenewaldt, G. (1985). Textural and compositional features of chromite in the lower and critical zones of the Bushveld Complex south of Potgietersrus. *Economic Geology* **80**, 872–895.

Huminicki, M. A. E., Cabri, L., Sylvester, P. J. & Tubreet, M. N. (2004). Determinations of Platinum-Group Element (PGE) distributions using whole-rock, SEM, EMPA, image analysis, and LA-ICPMS techniques in the Kelly Lake Ni–Cu–PGE Deposit, Sudbury. *EOS Transactions, American Geophysical Union* **85**, 17.

Hutchinson, D. & Foster, J. (2009). The Merensky Reef Ni–Cu–PGE mineralisation: unlocking the processes (a forensic approach using laser mapping). In: Williams, P. J., *et al.* (eds) *Smart Science for Exploration and Mining. Proceedings of the Tenth Biennial SGA Meeting*, pp. 170–172.

Hutchinson, D. & Foster, J. (2010a). The Merensky Reef: An example of sedimentary-style magmatic deposition within a large layered mafic–ultramafic complex. Abstracts, International Association of the Genesis of Ore Deposits (IAGOD) Symposium, Brisbane.

Hutchinson, D. & Foster, J. (2010b). Why is the Merensky Reef so enriched in precious metals compared to the Platreef? Magmatic processing efficiency, plain and simple. Abstracts, 11th International Platinum Symposium, Sudbury.

Hutchinson, D. & Foster, J. (2012). Effect of contamination on PGE-hosted sulphides. Abstracts, 34th International Geological Congress, Brisbane.

Hutchinson, D. & Kinnaird, J. A. (2005). Complex multi-stage genesis for the Ni–Cu–PGE mineralisation in the southern region of the Platreef, Bushveld Complex, RSA. *Transactions of the Institution of Mining and Metallurgy* **114**, 208–224.

Hutchinson, D. & McDonald, I. (2008). Laser ablation ICP-MS study of platinum-group elements in sulphides from the Platreef at Turfspruit, northern limb of the Bushveld Complex, South Africa. *Mineralium Deposita* **43**, 695–711.

Irvine, T. N. (1975). Crystallisation sequences in the Muskox intrusion and other layered intrusions—II. Origin of chromitite layers and similar deposits of other magmatic ores. *Geochimica et Cosmochimica Acta* **39**, 991–1020.

Irvine, T. N. (1977a). Origin of chromitite layers in the Muskox intrusion and other stratiform intrusions: a new interpretation. *Geology* **5**, 273–277.

Irvine, T. N. (1977b). Chromite crystallization in the join Mg_2SiO_4–$CaMgSi_2O_6$–$CaAl_2Si_2O_8$–$MgCr_2O_4$–SiO_2. *Carnegie Institution of Washington Yearbook* **76**, 465–472.

Irvine, T. N., Keith, D. W. & Todd, S. G. (1983). The J-M Platinum–Palladium Reef of the Stillwater Complex, Montana. *Economic Geology* **78**, 1287–1334.

Jarosewich, E., Nelen, J. A. & Norberg, J. A. (1980). Reference samples for electron microprobe analysis. *Geostandards Newsletter* **4**, 43–48.

Keays, R. R. & Campbell, I. H. (1981). Precious metals in the Jimberlana Intrusion, Western Australia: implications for the genesis of platiniferous ores in layered intrusions. *Economic Geology* **76**, 1118–1141.

Keays, R. R., Ross, J. R. & Woolrich, P. (1981). Precious metals in volcanic peridotite associated nickel sulphide deposits in western Australia II: Distribution within the ores and host rocks at Kambalda. *Economic Geology* **76**, 645–1274.

Kerr, A. & Leitch, A. M. (2005). Self-destructive sulfide segregation systems and the formation of high-grade magmatic ore deposits. *Economic Geology* **100**, 311–332.

Kinloch, E. D. (1982). Regional trends in the platinum-group mineralogy of the Critical Zone of the Bushveld Complex, South Africa. *Economic Geology* **77**, 1328–1347.

Kinloch, E. D. & Peyerl, W. (1990). Platinum-group minerals in various rock types of the Merensky Reef: genetic implications. *Economic Geology* **85**, 537–555.

Kinnaird, J. A. (2005). Geochemical evidence for multiphase emplacement in the southern Platreef. *Transactions of the Institution of Mining and Metallurgy* **114**, 225–242.

Kinnaird, J. A. & McDonald, I. (2005). An introduction to mineralisation in the northern limb of the Bushveld Complex. *Transactions of the Institution of Mining and Metallurgy* **114**, 194–198.

Kinnaird, J. A., Kruger, F. J., Nex, P. A. M. & Cawthorn, R. G. (2002). Chromitite formation—a key to understanding processes of platinum enrichment. *Transactions of the Institution of Mining and Metallurgy* **111**, 23–35.

Kruger, F. J. (1992). The origin of the Merensky cyclic unit: Sr-isotopic and mineralogical evidence for an alternative orthomagmatic model. *Australian Journal of Earth Sciences* **39**, 255–261.

Kruger, F. J. (1994). The Sr-isotopic stratigraphy of the western Bushveld Complex. *South African Journal of Geology* **97**, 393–398.

Kruger, F. J. (2005a). The Main Zone of the Bushveld Complex: source of the Merensky Reef and the Platreef. In: Törmänen, T. O. & Alapieti, T. T. (eds) *10th International Platinum Symposum, Extended Abstracts*, pp. 468–471.

Kruger, F. J. (2005b). Filling the Bushveld Complex magma chamber: lateral expansion, roof and floor interaction, magmatic unconformities, and the formation of giant chromitite, PGE and Ti–V-magnetitite deposits. *Mineralium Deposita* **40**, 451–472.

Kruger, F. J. (2010). The Merensky and Bastard cyclic units and the Platreef of the Bushveld Complex: consequences of Main Zone magma influxes and dynamics. The 4th International Platinum Conference, Platinum in Transition 'Boom or Bust', Southern African Institute of Mining and Metallurgy, pp. 43–46.

Kruger, F. J. & Marsh, J. S. (1982). Significance of $^{87}Sr/^{86}Sr$ ratios in the Merensky cyclic unit of the Bushveld Complex. *Nature* **298**, 53–55.

Kruger, F. J. & Marsh, J. S. (1985). The mineralogy, petrology and origin of the Merensky Cyclic Unit in the western Bushveld Complex. *Economic Geology* **80**, 958–974.

Kruger, F. J. & Schoenberg, R. (1998). Isotope evidence for the origin of PGE rich Bushveld chromitites and the Merensky Reef by felsic magma mixing. In: *Proceedings of the Eighth International Platinum Symposium Abstracts. GSSA/SAIMM Symposium Series* **18**, 185–188.

Large, R., Danyushevsky, L., Hollit, C., Maslennekov, V., Meffre, S., Gilbert, S., Bull, S., Scott, R., Emsbo, P., Thomas, H. & Foster, J. (2009). Gold and trace element zonation in pyrite using a laser imaging technique; implications for the timing of gold in orogenic and Carlin-style sediment-hosted deposits. *Economic Geology* **104**, 635–668.

Lassiter, J. C. & DePaolo, D. J. (1997). Plume/lithosphere interaction in the generation of continental and oceanic flood basalts: chemical and isotopic constraints. In: Mahoney, J. J. & Coffin, M. F. (eds) *Large Igneous Provinces: Continental, Oceanic, and Planetary Flood Volcanism. American Geophysical Union, Geophysical Monograph Series* **100**.

Latypov, R. M., O'Driscoll, B. & Lavrenchuk, A. (2013). Towards a model for in situ origin of PGE reefs in layered intrusions: insights from chromitite seams of the Rum Eastern Layered

Intrusion, Scotland. *Contributions to Mineralogy and Petrology* **166**, 309–327.
Lauder, W. R. (1970). Origin of the Merensky Reef. *Nature* **227**, 365–366.
Lee, C. A. (1996). A review of mineralisation in the Bushveld Complex and some other layered intrusions. In: Cawthorn, R. G. (ed.) Layered Intrusions. *Amsterdam: Elsevier*, pp. 103–145.
Lee, C. A. & Butcher, A. R. (1990). Cyclicity in the Sr isotope stratigraphy through the Merensky and Bastard Reefs, Atok Section, eastern Bushveld Complex. *Economic Geology* **85**, 877–883.
Leeb-Du Toit, A. (1986): The Impala Platinum Mines. In: Anhaeusser, C. R. & Maske, S. (eds) *Mineral Deposits of Southern Africa, II. Geological Society of South Africa, Special Publication* **2**, 1091–1106.
Li, C., Ripley, E. M., Maier, W. D. & Gomwe, T. E. S. (2002). Olivine and sulfur isotopic compositions of the Uitkomst Ni–Cu sulfide ore-bearing complex, South Africa: evidence for sulfur contamination and multiple magma emplacements. *Chemical Geology* **188**, 149–159.
Li, C., Ripley, E. M., Sarkar, A., Shin, D. & Maier, W. D. (2005). Origin of phlogopite–orthopyroxene inclusions in chromites from the Merensky Reef of the Bushveld Complex, South Africa. *Contributions to Mineralogy and Petrology* **150**, 119–130.
Lipin, B. R. (1993). Pressure increases in the formation of chromite seams and the development of the ultramafic series in the Stillwater complex, Montana. *Journal of Petrology* **34**, 955–976.
Lomberg, K. G., Martin, E. S., Patterson, M. A. & Venter, J. E. (1999). The morphology of potholes in the UG-2 chromitite layer and Merensky Reef (pothole reef facies) at Union Section, Rustenburg Platinum Mines. *South African Journal of Geology* **102**, 209–220.
Longrich, H., Jackson, S. & Gunther, D. (1996). Laser ablation inductively coupled plasma mass spectrometric transient signal data acquisition and analyte concentration calculation. *Journal of Analytical Atomic Spectrometry* **11**, 899–904.
Maier, W. D. & Barnes, S.-J. (1999). Platinum-group elements in silicate rocks of the Lower, Critical and Main Zones at Union Section, Western Bushveld Complex. *Journal of Petrology* **40**, 1647–1671.
Maier, W. D. & Barnes, S.-J. (2008). Platinum-group elements in the UG1 and UG-2 chromitites, and the Bastard Reef, at Impala platinum mine, western Bushveld Complex, South Africa: evidence for late magmatic cumulate instability and reef constitution. *South African Journal of Geology* **111**, 159–176.
Maier, W. D. & Eales, H. V. (1994). A facies model for the interval between the UG-2 and Merensky Reef, Western Bushveld Complex. *Transactions of the Institution of Mining and Metallurgy* **103**, 22–30.
Maier, W. D., Arndt, N. T. & Curl, E. A. (2000). Progressive crustal contamination of the Bushveld Complex: evidence from Nd isotopic analyses of the cumulate rocks. *Contributions to Mineralogy and Petrology* **140**, 316–327.
Maier, W. D., Gomwe, T., Barnes, S.-J., Li, C. & Theart, H. (2004). Platinum group elements in the Uitkomst Complex, South Africa. *Economic Geology* **99**, 499–516.
Maier, W. D., Barnes, S.-J. & Groves, D. I. (2013). The Bushveld Complex, South Africa: formation of platinum–palladium, chrome- and vanadium-rich layers via hydrodynamic sorting of a mobilized cumulate slurry in a large, relatively slowly cooling, subsiding magma chamber. *Mineralium Deposita* **48**, 1–56.
Makovicky, M., Makovicky, E. & Rose-Hansen, J. (1986). Experimental studies on the solubility and distribution of platinum group elements in base-metal sulphides in platinum deposits. In: Gallagher, M. J., Ixer, R. A., Neary, C. R. & Prichard, H. M. (eds) *Metallogeny of Basic and Ultrabasic Rocks*. Basildon: Institution of Mining and Metallurgy, pp. 415–425.
Manyeruke, T. D., Maier, W. D. & Barnes, S.-J. (2005). Major and trace element geochemistry of the Platreef on the farm Townlands, northern Bushveld Complex. *South African Journal of Geology* **108**, 381–396.
Marsh, B. (2004). A magmatic mush column rosetta stone: the McMurdo Dry Valleys of Antarctica. *EOS Transactions, American Geophysical Union* **85**, 497–502.
Mathez, E. A. (1976). Sulfur solubility and magmatic sulfides in submarine basalt glass. *Journal of Geophysical Research* **81**, 4269–4276.
Mathez, E. A. (1995). Magmatic metasomatism and formation of the Merensky Reef, Bushveld Complex. *Contributions to Mineralogy and Petrology* **119**, 277–286.
Mathez, E. A. (1999). Factors controlling the concentrations of platinum-group elements in layered intrusions and chromitites. In: *Dynamic Processes in Magmatic Ore Deposits and their Application to Mineral Exploration. Geological Association of Canada, Short Course Notes* **13**, 251–286.
Mathez, E. A. & Kent, A. J. R. (2005). Tracing geochemical evolution of the Bushveld Complex with lead isotopes analyzed by LA-MC-ICP-MS. 2005 Goldschmidt Conference Abstracts. *Geochimica et Cosmochimica Acta* **69**, A331.
Mathez, E. A. & Waight, T. E. (2003). Lead isotopic disequilibrium between sulfide and plagioclase in the Bushveld Complex and the chemical evolution of large layered intrusions. *Geochimica et Cosmochimica Acta* **67**, 1875–1888.
Mathez, E. A., Hunter, R. H. & Kinzler, R. (1997). Petrologic evolution of partially molten cumulate: the Atok section of the Bushveld Complex. *Contributions to Mineralogy and Petrology* **129**, 20–34.
McCandless, T. E., Ruiz, J., Adair, B. I. & Freydier, C. (1999). Re–Os isotope and Pd/Ru variations in chromitites from the Critical Zone, Bushveld Complex, South Africa. *Geochimica et Cosmochimica Acta* **63**, 911–923.
McCourt, S. & Vearncombe, J. R. (1987). Shear zones bounding the central zone of the Limpopo mobile belt, southern Africa. *Journal of Structural Geology* **9**, 127–137.
McDonald, I. & Holwell, D. A. (2007). Did Lower Zone magma conduits store PGE-rich sulphides that were later supplied to the Platreef? *South African Journal of Geology* **110**, 611–616.
McDonough, W. F. & Sun, S. -s. (1995). The composition of the Earth. *Chemical Geology* **120**, 220–253.
McLaren, C. H. & De Villiers, J. P. R. (1982). The platinum-group chemistry and mineralogy of the UG-2 chromitite layer of the Bushveld Complex. *Economic Geology* **77**, 1348–1366.
Merkle, R. K. W. (1987). *Platinum-group minerals in the middle group of chromitite layers at Marikana, western Bushveld Complex—Indications for collection mechanisms and post-magmatic modification. Institute of Geological Research on the Bushveld Complex, Research Report* **66**, 32 pp.
Mitchell, A. A. & Scoon, R. N. (2007). The Merensky Reef at Winnaarshoek, Eastern Bushveld Complex: a primary magmatic hypothesis based on a wide reef facies. *Economic Geology* **102**, 971–1009.
Molyneux, T. G. (1974). A geological investigation of the Bushveld Complex in Sekhukhunelan and part of the Steelpoort Valley. *Transactions of the Geological Society of South Africa* **77**, 329–338.
Mondal, S. K. & Mathez, E. A. (2007). Origin of the UG-2 chromitite layer, Bushveld Complex. *Journal of Petrology* **48**, 495–510.

Moodley, P. (2008). Facies variation in the Merensky Reef at Bafokeng Rasimone Platinum mine. In: *3rd International Platinum Conference 'Platinum in Transformation'*. Southern African Institute of Mining and Metallurgy, pp. 87–95.

Mossom, R. J. (1986). The Atok Platinum Mine. In: Anhaeusser, C. R. & Maske, S. (eds) *Mineral Deposits of Southern Africa, II. Geological Society of South Africa, Special Publication* **2**, 1143–1154.

Mostert, A. B., Hofmeyr, P. K. & Potgieter, G. A. (1982). The platinum group mineralogy of the Merensky Reef at Impala platinum mines, Bophuthatswana. *Economic Geology* **77**, 1385–1394.

Naldrett, A. J. (1989). Stratiform PGE deposits in layered intrusions. In: Whitney, J. A. & Naldrett, A. J. (eds) *Ore Deposition Associated with Magmas. Reviews in Economic Geology* **4**, 135–166.

Naldrett, A. J. (2004). *Magmatic Sulfide Deposits: Geology, Geochemistry and Exploration*. Berlin: Springer, 728 pp.

Naldrett, A. J. & Lehmann, J. (1988). Spinel non-stoichiometry as an explanation for Ni-, Cu-, and PGE-enriched sulphides in chromitites. In: Prichard, H. M., Potts, P. J., Bowles, J. F.W. & Cribb, S. J. (eds) *Geo-Platinum 87*. Amsterdam: Elsevier, pp. 113–143.

Naldrett, A. J., Innes, D. G., Sowa, J. & Gorton, M. P. (1982). Compositional variations between five Sudbury ore deposits. *Economic Geology* **77**, 1519–1534.

Naldrett, A. J., Gasparrini, E. C., Barnes, S. J., Von Gruenewaldt, G. & Sharpe, M. R. (1986). The Upper Critical Zone of the Bushveld Complex and the origin of Merensky-type ores. *Economic Geology* **81**, 1105–1117.

Naldrett, A. J., Lehmann, J. & Auge, T. (1987). Spinel non-stoichiometry and reactions between chromite and closely associated sulphides. In: Campbell, A. (ed.) *IGCP Project 161, 5th Magmatic Sulphide Field Conference, Abstracts and Field Guide*. Harare: Geological Society of Zimbabwe, pp. 18–19.

Naldrett, A. J., Brügmann, G. E. & Wilson, A. H. (1990). Models for the concentration of PGE in layered intrusions. *Canadian Mineralogist* **28**, 389–408.

Naldrett, A. J., Wilson, A., Kinnaird, J. & Chunnett, G. (2009). PGE tenor and metal ratios within and below the Merensky Reef, Bushveld Complex: implications for its genesis. *Journal of Petrology* **50**, 625–659.

Nex, P. A. M. (2005). The structural setting of mineralisation on Tweefontein Hill, northern limb of the Bushveld Complex, South Africa. *Transactions of the Institution of Mining and Metallurgy* **114**, 243–251.

Nicholson, D. M. & Mathez, E. A. (1991). Petrogenesis of the Merensky Reef in the Rustenburg section of the Bushveld Complex. *Contributions to Mineralogy and Petrology* **107**, 293–309.

Osbahr, I., Klemd, R., Oberthür, T., Brätz, H. & Schouwstra, R. (2013). Platinum-group element distribution in base-metal sulfides of the Merensky Reef from the eastern and western Bushveld Complex, South Africa. *Mineralium Deposita* **48**, 211–232.

Page, N. J. (1971). Comments on the role of oxygen fugacity in the formation of immiscible sulfide liquids in the H chromitite zone of the Stillwater Complex, Montana. *Economic Geology* **66**, 607–610.

Palme, H. & O'Neill, H. St. C. (2004). Cosmochemical estimates of mantle composition. In: Carlson, R. W. (ed.) *The Mantle and Core. Treatise on Geochemistry, 2*. Amsterdam: Elsevier, pp. 1–38.

Peach, C. L., Mathez, E. A. & Keays, R. R. (1990). Sulfide melt–silicate melt distribution coefficients for noble metals and other chalcophile elements as deduced from MORB: implications for partial melting. *Geochimica et Cosmochimica Acta* **54**, 3379–3389.

Peyerl, W. (1982). The influence of the Driekop dunite pipe on the platinum-group mineralogy of the UG2 chromitite in its vicinity. *Economic Geology* **77**, 1432–1438.

Pitra, P. & de Waal, S. A. (2001). High-temperature, low-pressure metamorphism and development of prograde symplectites, Marble Hall Fragment, Bushveld Complex (South Africa). *Journal of Metamorphic Petrology* **19**, 311–325.

Prevec, S. A., Ashwal, L. D. & Mkaza, M. S. (2005). Mineral disequilibrium in the Merensky Reef, western Bushveld Complex, South Africa: new Sm–Nd isotopic evidence. *Contributions to Mineralogy and Petrology* **149**, 306–315.

Prichard, H. M. & Brough, C. (2009). Potential of ophiolite complexes to host PGE deposits. In: Li, C. & Ripley, E. M. (eds) *New Developments in Magmatic Ni–Cu and PGE Deposits*. Beijing: Geological Publishing House, pp. 277–290.

Prichard, H. M., Barnes, S.-J., Maier, W. D. & Fisher, P. C. (2004a). Variations in the nature of the platinum-group minerals in a cross section through the Merensky Reef at Impala platinum mines: implications for the mode of formation of the reef. *Canadian Mineralogist* **42**, 423–437.

Prichard, H. M., Hutchinson, D. & Fisher, P. C. (2004b). Petrology and crystallisation history of multi-phase sulphide droplets in a mafic dyke from Uruguay: Implications for the origin of Cu–Ni–PGE–sulphide deposits. *Economic Geology* **99**, 365–376.

Reichhardt, F. J. (1994). The Molopo Farms Complex, Botswana: history, stratigraphy, petrography, petrochemistry and Ni–Cu–PGE mineralisation. *Exploration and Mining Geology* **3**, 263–284.

Rice, A. R. & Eales, H. V. (1995). The densities of Bushveld melts: textural and hydrodynamic criteria. *Mineralogy and Petrology* **54**, 45–53.

Richardson, S. H. & Shirey, S. B. (2008). Continental mantle signature of Bushveld magmas and coeval diamonds. *Nature* **453**, 910–913.

Roberts, M. D., Reid, D. L., Miller, J. A., Bassoon, I. J., Roberts, M. & Smith, D. (2007). The significance of footwall reconstitution within normal to regional pothole reef types in the Bushveld Complex. *Mineralium Deposita* **42**, 271–292.

Roelofse, F. & Ashwal, L. D. (2012). The lower main zone in the northern limb of the Bushveld Complex - a $>$ 1*3 km thick sequence of intruded and variably contaminated crystal mushes. *Journal of Petrology* **53**, 1449–1476.

Roeder, P. L. & Reynolds, I. (1991). Crystallization of chromite and chromium solubility in basaltic melts. *Journal of Petrology* **32**, 909–934.

Sampson, E. (1932). Magmatic chromitite deposits in Southern Africa. *Economic Geology* **27**, 113–144.

Schiffries, C. M. (1982). The petrogenesis of a platiniferous dunite pipe in the Bushveld Complex: infiltration metasomatism by a chloride solution. *Economic Geology* **77**, 1439–1453.

Schiffries, C. M. & Rye, D. M. (1989). Stable isotope systematics of the Bushveld Complex: I. Constraints of magmatic processes in layered intrusions. *American Journal of Science* **289**, 841–875.

Schmidt, E. R. (1952). The structure and composition of the Merensky Reef and associated rocks on the Rustenburg platinum mine. *Transactions of the Geological Society of South Africa* **55**, 233–279.

Schoenberg, R., Kruger, F. J., Nägler, T. F., Meisel, T. & Kramers, J. D. (1999). PGE enrichment in chromitite layers and the Merensky Reef of the western Bushveld Complex; a Re–Os and Rb–Sr isotope study. *Earth and Planetary Science Letters* **172**, 49–64.

Schürmann, L. W., Grabe, P. J. & Steenkamp, C. J. (1998). Chromium. In: Wilson, M. G. C. & Anhaeusser, C. R. (eds) *Mineral Resources of South Africa,* 6th edn. *Council for Geoscience, Handbook* **16**, 90–105.

Scoates, J. S. & Friedman, R. M. (2008). Precise age of the platiniferous Merensky Reef, Bushveld Complex, South Africa, by the U–Pb zircon chemical abrasion ID-TIMS technique. *Economic Geology* **103**, 465–471.

Scoon, R. N. & Teigler, B. (1994). Platinum-group element mineralisation in the critical zone of the western Bushveld Complex; I, Sulfide poor-chromitites below the UG-2. *Economic Geology* **89**, 1094–1121.

Sharpe, M. (1985). Strontium isotope evidence for preserved density stratification in the Main Zone of the Bushveld Complex, South Africa. *Nature* **316**, 119–126.

Sharpe, M. R. & Irvine, T. N. (1983). Melting relations of two Bushveld chilled margin rocks and implications for the origin of chromitite. *Carnegie Institution of Washington Yearbook* **82**, 295–300.

Sharpe, M. R., Irvine, T. N., Mysen, B. O. & Hazen, R. M. (1983). Density and viscosity characteristics of melts of Bushveld chilled margin rocks. *Carnegie Institution of Washington Yearbook* **82**, 300–305.

Sharpe, M. R., Evensen, N. M. & Naldrett, A. J. (1986). Sm/Nd and Rb/Sr evidence for liquid mixing magma generation and contamination in the Eastern Bushveld Complex. In: *Geocongress Conference Abstract Volume, University of the Witwatersrand, Johannesburg*, pp. 621–624.

Schouwstra, R. P., Kinloch, E. D. & Lee, C. A. (2000). A short review of the Bushveld Complex. *Platinum Minerals Review* **44**, 33–39.

Stumpfl, E. F. & Tarkian, M. (1976). Platinum genesis; New mineralogical evidence. *Economic Geology* **71**, 1451–1460.

Talkington, R. W. & Watkinson, D. H. (1986). Whole rock platinum-group element trends in chromite-rich rocks in ophiolitic and stratiform igneous complexes. In: Gallagher, M. J., Ixer, R. A., Neary, C. R. & Prichard, H. M. (eds) *Metallogeny of Basic and Ultrabasic Rocks*. Basildon: Institution of Mining and Metallurgy, pp. 427–440.

Talkington, W., Watkinson, D. H., Whittaker, P. J. & Jones, P. C. (1983). Platinum-group-mineral inclusions in chromite from the Bird River Sill, Manitoba. *Mineralium Deposita* **18**, 245–255.

Teigler, B. & Eales, H. V. (1993). Correlation between chromite composition and PGE mineralisation in the Critical Zone of the western Bushveld Complex. *Mineralium Deposita* **28**, 291–302.

Treble, P. C., Chappell, J. & Shelley, J. M. G. (2005). Complex speleothem growth processes revealed by trace element mapping and scanning electron microscopy of annual layers. *Geochimica et Cosmochimica Acta* **69**, 4855–4863.

Tredoux, M., Lindsay, N. M., Davies, G. & McDonald, I. (1995). The fractionation of the platinum-group elements in magmatic systems with the suggestion of a novel causal mechanism. *South African Journal of Geology* **98**, 157–167.

Ulmer, G. C. (1969). Experimental investigations of chromite spinels. In: Wilson, H. D. (ed.) *Magmatic Ore Deposits*. The Economic Geology Publishing Company, New Haven, Connecticut. pp. 114–131.

Van der Merwe, M. J. (1976). The layered sequence of the Potgietersrus limb of the Bushveld Complex. *Economic Geology* **71**, 1337–1351.

Vermaak, C. F. (1976). The Merensky Reef—thoughts on its environment and genesis. *Economic Geology* **71**, 1270–1298.

Vermaak, C. F. (1995). *The Platinum-group Metals—a Global Perspective*. Randburg: Mintek.

Verryn, S. M. C. & Merkle, R. W. (1994). Compositional variation of cooperite, braggite, and vysotskite from the Bushveld Complex. *Mineralogical Magazine* **58**, 223–234.

Viljoen, M. J. (1999). The nature and origin of the Merensky Reef of the Western Bushveld Complex based on geological facies and geophysical data. *South African Journal of Geology* **102**, 221–239.

Viljoen, M. J. & Hieber, R. (1986). The Rustenburg Section of Rustenburg Platinum Mines Limited, with reference to the Merensky Reef. In: Anhaeusser, C. R. & Maske, S. (eds) *Mineral Deposits of South Africa. Geological Society of South Africa, Special Publication* **2**, 1107–1134.

Viljoen, M. J. & Schürmann, L. W. (1998). Platinum-group metals. In: Wilson, M. G. C. & Anhaeusser, C. R. (eds) *The Mineral Resources of South Africa. Council for Geoscience Handbook* **16**, 740 pp.

Viljoen, M. J., De Klerk, W. J., Coetzer, P. M., Hatch, N. P., Kinloch, E. & Peyerl, W. (1986a). The Union section of Rustenburg Platinum Mines Limited, with reference to the Merensky Reef. In: Anhaeusser, C. R. & Maske, S. (eds) *Mineral Deposits of Southern Africa. Geological Society of South Africa, Special Publication* **2**, 1061–1090.

Viljoen, M. J., Theron, J., Underwood, B., Walters, B. M., Weaver, J. & Peyerl, W. (1986b). The Amandelbult section of Rustenburg Platinum Mines Limited, with reference to the Merensky Reef. In: Anhaeusser, C. R. & Maske, S. (eds) *Mineral Deposits of Southern Africa. Geological Society of South Africa, Special Publication* **2**, 1041–1060.

Von Gruenewaldt, G. (1973). The main and upper zones of the Bushveld complex in the Roossenekal area, Eastern Transvaal. *Transactions of the Geological Society of South Africa* **76**, 207–227.

Von Gruenewaldt, G. (1977). The mineral resources of the Bushveld Complex. *Minerals and Mining Science and Engineering* **9**, 83–95.

Von Gruenewaldt, G., Hatton, C. A., Merkle, R. K. W. & Gain, S. B. (1986). Platinum-group element–chromitite associations in the Bushveld Complex. *Economic Geology* **81**, 1067–1079.

Von Gruenewaldt, G., Hulbert, L. J. & Naldrett, A. J. (1989). Contrasting platinum-group element concentration patterns in cumulates of the Bushveld Complex. *Mineralium Deposita* **24**, 219–229.

Voordouw, R., Gutzmer, J. & Beukes, N. J. (2009). Intrusive origin for Upper Group (UG1, UG-2) stratiform chromitite seams in the Dwars River area, Bushveld Complex, South Africa. *Mineralogy and Petrology* **97**, 75–94.

Vukmanovic, Z., Barnes, S. J., Reddy, S. M., Godel, B. & Fiorentini, M. (2013). Morphology and microstructure of chromite crystals in chromites from the Merensky Reef (Bushveld Complex, South Africa). *Contributions to Mineralogy and Petrology* **165**, 1031–1050.

Wager, L. R. & Brown, G. M. (1968). *Layered Igneous Rocks*. Edinburgh: Oliver & Boyd, 588 pp.

Wagner, P. A. (1923). The chromite of the Bushveld Igneous Complex. *South African Journal of Science* **20**, 223–235.

Wagner, P. A. (1925). The platinum deposits in the western part of the Lydenburg District, Transvaal. *South African Journal of Industries* **8**, 90–113.

Wagner, P. A. (1929). *The Platinum Deposits and Mines of South Africa*. Edinburgh: Oliver & Boyd, 326 pp.

Walraven, F., Armstrong, R. A. & Kruger, F. J. (1990). A chronostratigraphic framework for the north–central Kaapvaal craton, the Bushveld Complex and the Vredefort structure. *Tectonophysics* **171**, 23–48.

Willemse, J. (1964). A brief outline of the geology of the Bushveld Igneous Complex. In: Haughton, S. H. (ed.) *The Geology of some Ore Deposits in Southern Africa, 2*. Johannesburg: Geological Society of South Africa, pp. 91–128.

Willemse, J. (1969). The geology of the Bushveld Complex, the largest repository of magmatic ore deposits in the world. In: Wilson, H. D. B. (ed.) Economic Geology Monograph The Economic Geology Publishing Company, New Haven, Connecticut, pp. 1–22.

Willmore, C. C., Boudreau, A. E. & Kruger, F. J. (2000). The halogen geochemistry of the Bushveld Complex, Republic of South Africa: implications for chalcophile element distribution in the Lower and Critical zones. *Journal of Petrology* **41**, 1517–1539.

Wilson, A. & Chunnett, G. (2006). Trace element and platinum group element distributions and the genesis of the Merensky Reef, Western Bushveld Complex, South Africa. *Journal of Petrology* **47**, 2369–2403.